PHOTOCURABLE INORGANIC-ORGANIC HYDROGELS

FOR BIOMEDICAL APPLICATIONS

A Dissertation

by

YAPING HOU

Submitted to the Office of Graduate Studies of
Texas A&M University
in partial fulfillment of the requirements for the degree of

DOCTOR OF PHILOSOPHY

December 2009

Major Subject: Materials Science and Engineering

PHOTOCURABLE INORGANIC-ORGANIC HYDROGELS

FOR BIOMEDICAL APPLICATIONS

A Dissertation

by

YAPING HOU

Submitted to the Office of Graduate Studies of
Texas A&M University
in partial fulfillment of the requirements for the degree of

DOCTOR OF PHILOSOPHY

Approved by:

Chair of Committee,	Melissa Grunlan
Committee Members,	Arum Han
	Zoubeida Ounaies
	Christian Schwartz
Intercollegiate Faculty Chair,	Tahir Cagin

December 2009

Major Subject: Materials Science and Engineering

ABSTRACT

Photocurable Inorganic-Organic Hydrogels for Biomedical Applications.

(December 2009)

Yaping Hou, B.E. Beijing University of Aeronautics and Astronautics

Chair of Advisory Committee: Dr. Melissa A. Grunlan

There are two primary objectives of this dissertation research. The first objective was to prepare a library of inorganic-organic hydrogels from methacrylated star polydimethylsiloxane ($PDMS_{star}$-MA) and diacrylated poly(ethylene oxide) (PEO-DA) with tunable chemical and physical properties for use as tissue engineering scaffolds. These inorganic-organic hydrogels provide a useful platform to study the effect of scaffold properties on cell behavior in tissue culture.

Twenty compositionally unique hydrogels were prepared by photo-crosslinking varing molecular weights (M_n) of PEO-DA (M_n = 3.4k and 6k g/mol) and $PDMS_{star}$-MA (M_n = 1.8k, 5k and 7k g/mol) at varying weight ratios (up to 20 wt% $PDMS_{star}$-MA). Introduction of $PDMS_{star}$-MA caused formation of discrete PDMS-enriched "micro-particles" dispersed within the PEO hydrogel matrix. The swelling ratio, mechanical properties in tension and compression, non-specific protein adhesion and cytotoxicity of hydrogels were studied.

The second objective was to prepare thermoresponsive nanocomposite hydrogels, which are mechanically robust and can remove adhered cells via thermal modulation.

Such hydrogels may be useful as “self-cleaning” membranes for implanted biosensors to extend their lifetime and efficiency. These hydrogels are comprised of a poly(*N*-isopropylacrylamide) (PNIPAAm) hydrogel matrix and polysiloxane colloidal nanoparticles (~220 nm and 50 nm ave. diameter). Due to the low preparation temperature, the nanocomposite hydrogels exhibited a homogeneous morphology by SEM analysis. The volume phase transition temperature (VPTT, ~33 °C) of the nanocomposite hydrogels was not altered versus the pure PNIPAAm hydrogel, which is near body temperature. Generally, nanoparticles led to improve mechanical properties versus pure PNIPAAm hydrogels. When these nanocomposite hydrogels are heated above the VPTT, they become more hydrophobic. When they are reversibly switched from a water-swollen to a deswollen state, the change in surface properties, as well as swelling-deswelling, was effective upon the removal of adhered cells.

DEDICATION

To My Husband

I give my deepest expression of love and appreciation for the encouragement that you gave and the unconditional support you made during this graduate program

To My Parents

Thanks for your love, endless support and encouragement throughout my life

ACKNOWLEDGEMENTS

My deepest gratitude goes to my research advisor, Professor Melissa A. Grunlan, who gave me the guidance to recover when my steps faltered. Her patience and support helped me overcome hardships and finish this dissertation.

I thank Professor Mariah Hahn, who has been always there to answer my questions and give advice. I am grateful to her for the help on cell releasing and protein adsorption studies.

I would like to thank my committee members for both promotion to candidancy and dissertation guidance: Professors Arum Han, Zoubeida Ounaies, Cris Schwartz, Andreas Holzenburg, Mike McShane, Haiyan Wang and James Silas, for their help and input.

I am also thankful to E. Ann Ellis, who gave me an unconditional help on hydrogel sample preparation for both the scanning electron microscopy (SEM) and the transmission electron microscopy (TEM).

Thanks also go to my research group members for their various forms of support during my graduate study.

Finally, thanks to my mother and father for their love and encouragement through my life and making everything possible. Also thanks my husband, for his love and support.

TABLE OF CONTENTS

CHAPTER Page

LIST OF FIGURES

FIGURE Page

FIGURE Page

LIST OF TABLES

CHAPTER I

INTRODUCTION

1.1 Overview

A hydrogel is a three-dimensional (3D) polymer network in which a large amount of water is present [1-3]. In general, the amount of water is 20 to 99% of the total weight. Hydrogels are typically formed from hydrophilic polymers such as those which contain hydrophilic moieties (e.g. sulfonic ($-SO_3H$), carboxyl (-COOH), amidic (-CONH-), hydroxyl (-OH), and amino ($-NH_2$) groups). Hydrophobic polymers may be incorporated into hydrogels at low level by blending, co-polymerizing or by producing interpenetrating or semi-interpenetrating polymer networks with hydrophilic polymers. The stability (i.e. insolubility) of the hydrogel in water is due to the presence of covalent or physical crosslinks which maintain the 3D network. Hydrogels can be classified in several ways (Table 1.1).

Table 1.1 Classifications of hydrogels

Classification	Contents
Source	(1) Natural; (2) Synthetic
Component	(1) Homopolymer; (2) Copolymer; (3) Multipolymer,
Crosslink	(1) Covalent bond; (2) Intermolecular force
Preparation method	(1) From macromer; (2) From macromer
Stimuli-responsive	(1) Thermoresponsive; (2) pH-responsive; (3) Glucose-responsive

This dissertation follows the style of Biomaterials.

Hydrogels may be formed from either natural or synthetic polymers.[4] Such natural polymers include proteins (e.g. collagen, gelatin and fibrin) and carbohydrates (e.g. agarose, alginate, hyaluronic acid and heparin)[5]. Synthetic polymers used to form hydrogels include poly(ethylene glycol) (PEG), poly(hydroxyethyl methacrylate) (PHEMA), poly(vinyl alcohol) (PVA), poly(acrylamide) (PAAm), poly(acrylic acid) (PAA), and poly(lactic acid) (PLA). Depending on the number of unique polymer components, hydrogels may be classified as homopolymer, copolymer, or multipolymer hydrogels. Homopolymer, copolymer, and multipolymer hydrogels are composed of polymers with one, two or three (or more) unique monomer repeat units, respectively.

To maintain the 3D network structures, polymer chains of hydrogels are connected via chemical or physical crosslinks. Chemical crosslinks are primary covalent bonds formed by reaction of various terminal or pendant functional groups. Physical crosslinks are secondary molecular interaction, such as van der Waals interactions, ionic interactions, hydrogen bonding, or hydrophobic interactions. Hydrogels may be prepared from a reactive monomer and multifunctional crosslinker or a macromer with pendant or terminal group and optionally a multifunctional crosslinker. Crosslinking may be catalyzed by heat or UV-irradiation in the presence of a catalyst. Crosslinking may be accomplished with aqueous solution or networks soaked in H_2O following crosslinking.

Certain hydrogels are stimuli- or environmentally-responsive such that swelling behavior is dependent on the external environment. Environmentally responsive hydrogels show drastic changes in their swelling ratio due to modulation of various external stimuli, including temperature, pH, and glucose concentration.

Hydrogels are a widely studied class of biomaterials due to their unique properties including: biocompatibility, porosity, hemocompatibility and mechanical properties similar to some soft tissues. The biocompatibility of hydrogels limits the host response. Because they are porous, hydrogels provide sufficient diffusion of oxygen, nutrients, waste and permits cellular ingrowth in tissue engineering. The similar mechanical properties of hydrogels and soft tissues limit local mechanical irritation of the tissue.

One of the earliest applications of hydrogels was for contact lenses. The original material for hydrogel contact lens was poly(2-hydroxyethyl methacrylate) (PHEMA). Other hydrogel materials include methacrylic acid (MAA), 1-vinyl-2-pyrrolidone (NVP), dimethylacrylamide (DMA), poly(ethylene glycol) (PEG) and poly(*N*-isopropyl acrylamide) (PNIPAAm). Hydrogels responsive to specific molecules, such as glucose or antigens, can be used *in vitro* in drug delivery (e.g. drug delivery patch) or *in vivo* (drug delivery system). Alginate is one of the most popular natural hydrogel matrices for drug release. Hyaluronic acid derivatives are a good example of naturally occurring polymers that have been modified to control the degradation and release rates of insulin and nerve growth factor. Poly(vinyl alcohol) (PVA) is used for releasing bovine serum albumin *in vitro*. Poloxamer gels have also been used as delivery system. The poloxamers (Pluronic®) are ABA-type triblock copolymers composed of poly(ethylene oxide) (PEO)(A) and poly(propylene oxide) (PPO) (B) units. In the work, hydrogels were utilized as tissue engineering scaffolds and membranes for biosensors.

1.2 Hydrogels as Tissue Engineering

Every year, millions of Americans suffer tissue loss or organ failure[6]. Surgeons have several options to treat organ or tissue loss including: (1) Allotransplantation: organs or tissues are transplanted from a cadaveric or living-related donor into the patient. (2) Autotransplantation: organs or tissues are moved from their original location in the same patient, (3) Xenotransplantation: organs or tissues are moved from one species to a human patient, and (4) Transplantation: artificial, nonbiological materials are used to replace tissues or organs. However, there are drawbacks to each of these approaches, including lack of available healthy tissue from patient or donor, rejection of tissue or organ from donor, and host-response to artificial transplants.

Tissue engineering is an interdisciplinary field that combines the knowledge of the life sciences with engineering design principles to create novel methods to restore, maintain, or improve tissue function[7, 8]. Although the field of tissue engineering is less than 20 years old, a significant amount of progress has been made in a relatively short period of time. Nearly every tissue in the body is being investigated, including skin[9, 10], cartilage[11-13], bone[14, 15], nerves[16, 17], blood vessels[18], heart valves and heart muscle [19, 20]. Engineered skin is the first tissue engineered product to be commercially available.

Two general tissue engineering strategies have emerged: the use of acellular matrices and the use of matrices with cells. Both strategies requires a 3D porous scaffold is often used to create an environment in which living cells can attach, differentiate, proliferate and produce new extracellular matrix (ECM) (Fig. 1.1). The materials used

for scaffold are biocompatible, easily fabricated, sterilized and ideally biodegradable. The ideal scaffolds should have an extensive network of interconnecting pores so that cells can migrate, multiply and attach deep within the scaffolds.

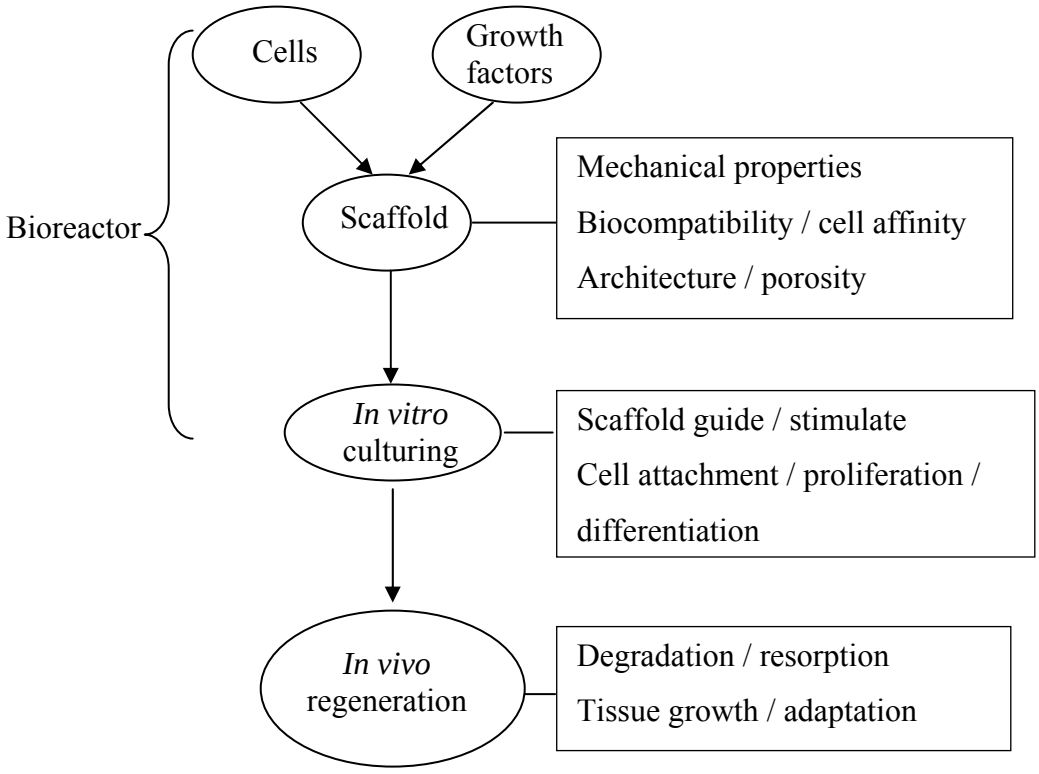

Figure 1.1. General process of tissue engineering. Adapted from [21] .

Both natural and synthetic polymers have been used to create tissue engineering scaffolds. Natural polymers used in tissue engineering are usually composed of extracellular matrix components (e.g., collagen, fibrin, glycosaminoglycans, and chitosan) or complete decellularized matrices (e.g., heart valves, small intestinal submucosa). A broad array of synthetic polymers have been used as scaffolds in tissue

engineering including: poly(glycolic acid) (PGA), poly(lactic acid) (PLA), copolymers of glycolic and lactic acids, polyurethanes, poly(hydroxyl alkanoate) (PHA), polyanhydrides and polyortho esters.

Hydrogels are of interest as scaffolds for engineering many due to their distinct advantages (Table 1.2). These advantages include: high tissue-like water content, high biocompatibility, mechanical properties that parallel the properties of soft tissues, efficient transport of nutrients and waste, powerful ability to uniformly encapsulate cells, and ability to be injected as a liquid that gels *in situ*.

Table 1.2. Advantages and disadvantages of hydrogels as tissue engineering scaffolds

Advantages
Aqueous environment can protect cells and fragile drugs
Good transport of nutrient to cells and products from cells
May be easily modified with cell adhesion ligands
Can be injected *in vivo* as a liquid that gels at body temperature
Usually biocompatible

Disadvantages
Usually mechanically weak
May be difficult to load drugs and cells and then crosslink in vitro as a prefabricated
May be difficult to sterilize

1.3 Hydrogels as Sensor Membranes

Biosensors are functional analogs based on the direct coupling of an immobilized biologically active compound with a signal transducer and an electronic amplifier. When

biomedical implants such as biosensors come in contact with physiological environments, negative interactions lead to reduced efficiency or complete failure. Biosensor failure modes may be divided into two main categories: (1) component-based failures such as lead detachment, electrical shorts, and mcembrane delamination; and (2) biocompatibility-based failures such as membrane biofouling, electrode passivation, and fibrous encapsulation. Some researchers advocate that biofouling of the membrane is the main problem. Membrane biofouling is the accumulation of proteins, cells, and other biological materials on the sensor surface.

Figure 1.2 shows an example of sequence of events which leads to formation of fibrous capsules around biosensors implanted subcutaneously. First, subcutaneous implantation causes a local injury followed by an acute inflammatory response that involves the release of fluid and plasma proteins. Leukocytes (mainly neutrophils and monocytes) migrate to the implanted device and adhere to the surface in an attempt to begin the process of phagocytosis. After the initial acute inflammatory response, chronic inflammation involves a sustained localized biological response at the implant site, including the recruitment of macrophages, monocytes, and lymphocytes. Finally, a fibrous capsule composed mainly of macrophages and collagen forms around the implanted device. For an implanted glucose sensor to work, glucose diffusion must not be interrupted. Unfortunately, the adhered proteins and cells from the physiological environment on the surface of an implanted glucose sensor or any biosensor limit glucose diffusion. This reduces the lifetime and efficiency of the biosensor and it must be removed. With membrane biofouling playing a significant role in sensor instability,

biosensors have over the years proved to be inadequate for long term *in vivo* applications.

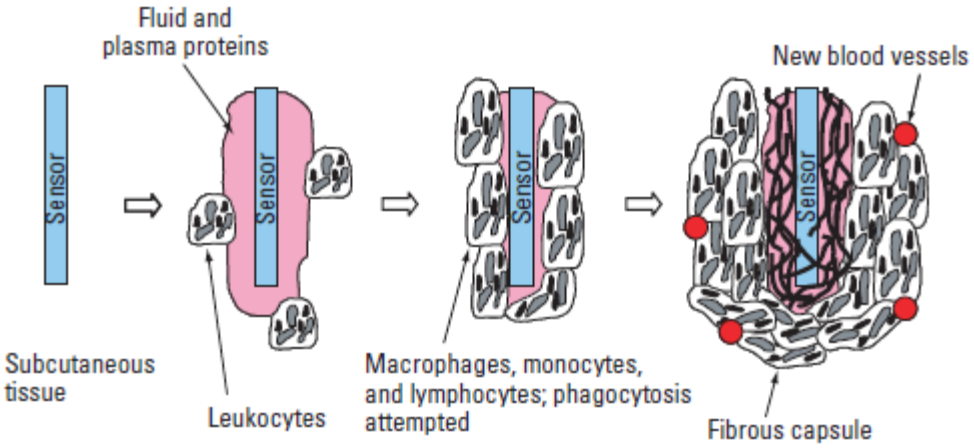

Figure 1.2. Sequence of events that leads to formation of fibrous capsules around implanted biosensors[22].

CHAPTER II

PHOTO-CROSSLINKED $PDMS_{star}$-PEG HYDROGELS: SYNTHESIS, CHARACTERIZATION, AND POTENTIAL APPLICATION FOR TISSUE ENGINEERING SCAFFOLDS

2.1 Overview

Inorganic-organic hydrogels with tunable chemical and physical properties were prepared from methacrylated star polydimethylsiloxane ($PDMS_{star}$-MA) and diacrylated poly(ethylene glycol) (PEG-DA) for use as tissue engineering scaffolds. Twenty compositionally unique hydrogels were prepared by photo-crosslinking varying weight ratios of PEO-DA and $PDMS_{star}$-MA of different molecular weights (M_n): PEG-DA (M_n = 3.4k and 6k g/mol) and $PDMS_{star}$-MA (M_n = 1.8k, 5k and 7k g/mol). Introduction of $PDMS_{star}$-MA caused formation of discrete PDMS-enriched microparticles dispersed within the PEG matrix. The swelling ratio, mechanical properties in tension and compression, non-specific protein adhesion and cytotoxicity of hydrogels were also studied. This library of inorganic-organic hydrogels with tunable properties provides a useful platform to study the effect of scaffold properties on cell behavior.

2.2 Introduction

Tissue engineering (TE) seeks to repair or replace damaged or diseased tissues and organs.[23] A three-dimensional polymeric scaffold is often used to create an environment in which living cells can attach, proliferate, differentiate, and ultimately

produce a new extracellular matrix (ECM).[5, 21, 23-30] Synthetic polymers generally provide greater control and range of chemical and physical properties compared to natural polymers.[21, 28, 31] Synthetic hydrogels have been widely studied as tissue engineering scaffolds.[4, 31, 32] Hydrogels are hydrated polymer networks comprised of hydrophilic polymers which are crosslinked via chemical bonds or physical interactions.[3, 33, 34] The utility of hydrogels as scaffolds is attributed to several factors, including superior biocompatibility which minimizes inflammation, thrombosis, and tissue damage, as well as high diffusivity and elasticity which parallels many tissues.[4, 31, 32] Compared to thermal or redox initiated crosslink mechanisms, photo-induced free radical hydrogel crosslinking produces less heat while allowing for improved spatial and temporal control. As a result, geometrically complex scaffolds may be rapidly formed *in situ* from cells suspended in aqueous solutions of monomers or macromers and may be done so *in vivo*.[30, 35-38]

Photopolymerizable poly(ethylene glycol) diacrylate (PEG-DA) based hydrogels have been extensively utilized as scaffolds for the regeneration of tissues including bone,[39, 40] cartilage,[37, 41, 42] nerve,[43] and vascular tissue.[44-48] PEG hydrogels are particularly useful for controlled studies of cell-material interactions because of their intrinsic resistance to protein absorption and cell adhesion.[49] Thus, PEG hydrogels are “biological blank slates” in which cell-material interactions may be limited to the adhesive ligands introduced.[40, 44, 50] To permit eventual replacement by the growing tissue, biodegradable PEG hydrogels have been formed by incorporation of enzymatically labile peptides[51, 52] or hydrolytically labile linear esters.[53-57]

In natural tissues, the ECM mediates critical cell function, including regeneration, via signaling cascades involving specific binding events as well as non-specific chemical and physical features.[58, 59] Thus, development of scaffolds having specific properties which guide cell behavior is critical for tissue regeneration.[60] Certain scaffold material properties have been shown to impact cell behavior.[61, 62] For instance, the chemical nature of the scaffold, in terms of bioactivity, chemical functionality, and hydrophilicity has been shown to influence cell behavior.[63-73] Physical properties such as scaffold morphology[74-80] and modulus[81-87] also affect cell behavior.

In order to guide cell behavior through cell-material interactions, scaffolds with precisely tunable chemical and physical properties are crucial. For such studies, synthetic hydrogel scaffolds with chemical and physical properties which can be finely and easily controlled are required. For PEG-DA hydrogels, crosslink density and mechanical properties may be tailored by simply varying the molecular weight and/or the concentration of PEGDA.[88] However, since PEG-DA hydrogels are single-component systems, the ability to uncouple various material properties, such as modulus and swelling, is limited.[89] Thus, hydrogels that maintain the benefits of PEG-DA while extending the ability to tune and uncouple material properties would further enhance the ability to establish relationships between cell behavior and scaffold properties.

In this study, both the chemical and physical properties of PEG-DA hydrogels were tuned by introduction of a methacrylated star polydimethylsiloxane ($PDMS_{star}$-MA)

macromer. PDMS is an inorganic polymer which is biocompatible, hydrophobic, exhibits excellent gas permeability, low glass transition temperature (T_g,-127 °C), and exceptional elasticity when lightly crosslinked.[90] Silicon-containing materials have been shown to specifically affect cell behavior. For instance, silica-calcium phosphate composite scaffolds have been shown to induce osteoblast alkaline phosphatase activity with increasing silica content.[73] Also, for siloxane-gelatin scaffolds, enhanced osteoblast alkaline phosphatase activity was observed with increasing siloxane content.[71, 72] The hydrogels reported herein are two component systems and so the average number molecular weight (M_n) and concentration of both macromers (i.e. PEG-DA and $PDMS_{star}$-MA) were used to tailor hydrogel properties. The chemical properties of the hydrogels were switched from purely organic, PEG to inorganic-organic $PDMS_{star}$-PEG by introducing increased levels of $PDMS_{star}$-MA, an inorganic polymer. In addition, the effect of hydrogel composition on physical properties, including morphology, equilibrium swelling (i.e. hydration), mechanical properties, non-specific protein adsorption, and cytoxicity were examined.

2.3 Experimental Section

Polymer Characterization

NMR. ^{1}H spectra were obtained on a Mercury 300 300-MHz spectrometer operating in the Fourier transform mode. Five percent (w/v) $CDCl_3$ solutions were used.

IR Spectroscopy. IR spectra of neat liquids on NaCl plates were recorded using a Bruker TENSOR 27 Fourier transform infrared spectrometer.

Gel Permeation Chromatography. Gel permeation chromatography (GPC) analysis was performed on a Viscotek GPC system equipped with three detectors in series: refractive index (RI), right angle laser light scattering (RALLS), and viscometer (VP). The ViscoGEL HR-Series (7.8mm x 30 cm) column packed with divinylbenzene crosslinked polystyrene was maintained at 25°C in a column oven. The eluting solvent was HPLC grade toluene at a flow rate of 1.0 mL/min. The detectors were calibrated with a polystyrene narrow standard with the following parameters: M_w (115,000 g/mol), polydispersity (1.01), intrinsic viscosity (0.519 dL/g), and dn/dc (0.185 mL/g). Data analysis was performed with Viscotek OmniSec software (Version 4.0).

Hydrogel Characterization

Morphological Characterization. For a given hydrogel, a disc (8 mm diameter, 1.5 mm thickness) was punched from a hydrogel sheet with a die. A Nile Red solution was prepared as follows: 75 μL of a Nile Red solution (20 mg per mL of methanol) was dissolved in 8 mL of double distilled water (DDW) and combined with 120 mL of PBS. Each hydrogel disc was sequentially soaked for 24 hr each in 60 mL of the aforementioned Nile Red solution and 60 mL of PBS. With each disc placed on a glass microscope slide and DDW dropped onto the disc to maintain hydration, images were captured with confocal laser scanning microscopy (CLSM) using a Leica TCS SP5 confocal microscope (Leica Microsystems, Bannockburn, IL). Images were acquired in 3-μm steps from the top to the bottom of the hydrogel and the 100 middle stack reconstructed to create a 3D images using Osirix software.

Energy Dispersive X-Ray Spectrometry (EDS). Identification of elemental

compositions of specific regions of a hydrogel was performed with a field emission scanning electron microscope and energy dispersive X-ray spectrometer (FE-SEM/EDS) (FEI Quanta 600). The hydrogel was crosslinked with ruthenium vapor, plunged into liquid nitrogen and sequentially soaked in HMDS and ethanol. The samples were sputter coated with Pt/Pd at the surface with 4 nm thickness.

Equilibrium Swelling Behavior. For a given hydrogel, three hydrogel discs (13 mm diameter, 1.5 mm thickness) were punched from a single hydrogel sheet with a die. Hydrogel equilibrium swelling ratio is defined as: s*welling ratio* = $(W_s - W_d)/W_d$, where W_s is the weight of the water-swollen hydrogel at a certain temperature and W_d is the weight of the vacuum dried hydrogel (30 in. Hg, 60 ºC, 24 h). Each disc was sealed inside a vial containing 20 mL PBS, immersed in a temperature controlled water bath for 24 h at 25 °C, removed, blotted with filter paper to remove surface water, and weighed (W_s).

Dynamic Mechanical Analysis (DMA). DMA of hydrogels were measured in the compression mode with a dynamic mechanical analyzer (TA Instruments Q800) equipped with parallel-plate compression clamp with a diameter of 40 mm (bottom) and 15 mm (top). Swollen hydrogel discs of constant dimension (13 mm diameter, 1.5 mm thickness) were punched from a hydrogel sheet and clamped between the parallel plates. Silicone oil was then placed around the exposed edges of the hydrogel to prevent dehydration. The samples were tested in a multi-frequency-strain mode (1 to 18 Hz). Results reported are based on the average of five individual specimens.

Tensile Tests. Tensile tests of hydrogels ring specimens were measured on a TA Instruments DMA Q800 operating in the tension mode. Specimens with a ring geometry were prepared by cutting a portion from a hydrogel tube produced from the double wall tubular mold (ID = 3 mm, OD = 7.5 mm). Individual rings (~3 mm width) were cut from the central portion of the appropriate hydrogel tube using a clean razor blade and sample dimensions measured with an electronic caliper. Each hydrogel ring was blotted with filter paper and loaded onto custom aluminum bars gripped directly into DMA tension clamps so that the upper and lower bars were located inside the ring. Samples were subjected to a constant strain (1 mm/min) until they broke at the center of one side of the ring. Stress was calculated from the measured force divided by the cross-sectional area of two rectangles with sides equal to the width and wall thickness of the ring. The gauge length corresponded to the outer diameter of the ring less the wall thickness. The following parameters were determined: (1) tensile modulus, (2) ultimate tensile strength (UTS), and (3) % strain at break. The tensile modulus was obtained from the slope of the linear part of the stress-strain curve. The UTS represents the maximum stress prior to failure. Strain was calculated from the measured displacement divided by the gauge length. Results reported are the average result of three specimens cut from central portion of the same hydrogel tube.

Protein Adhesion. The adhesion of Alexa Fluor 555 dye conjugate of bovine serum albumin (AF-555 BSA; MW = 66 kDa; Molecular Probes, Inc.) onto hydrogels was studied by fluorescence microscopy. For a given hydrogel, three hydrogel discs (14.5 mm diameter, 1.5 mm thickness) were punched from a single hydrogel sheet and

placed in PBS (15 min) to ensure hydration. Immediately prior to transferring to a 24 well plate, discs were gently blotted with filter paper to remove surface water. Of the three discs, two discs were each placed in wells containing 1.5 mL BSA (0.1 mg/mL) and the third disc placed in a well containing 1.5 mL of PBS. Hydrogel discs were maintained in the dark at RT for 3 h. Next, from both the top and bottom surfaces of the discs, the BSA solution was carefully removed via aspiration and both sides of the disc rinsed with fresh PBS 3 times. Each of these discs was returned to a well containing 1.5 mL of fresh PBS.

A Zeiss Axiovert 200 optical microscope equipped with a A-Plan 5x objective, Axiocam HRC Rev. 2), and filter cube (excitation filter of 546 ± 12 nm [band pass] and emission filter 575-640 nm [band pass]) was used to obtain fluorescent images on 3 randomly selected regions each hydrogel surface. The fluorescent light source was permitted to warm up for 30 min prior to image capture. Linear operation of the camera was ensured and constant exposure time used during the image collection to permit quantitative analyses of the observed fluorescent signals. The fluorescence microscopy images were analyzed using the histogram function of PhotoShop, which yielded the mean and standard deviation of the fluorescence intensity within a given image. For a given hydrogel composition, the average fluorescence intensity of the two discs exposed to AF-555 BSA was subtracted from that of the disc maintained only in PBS to ensure correction for of any fluorescence signal from the material itself. The background-corrected fluorescence intensities for each hydrogel were then used to quantify AF-555 BSA levels adsorbed by comparison against a calibration curve constructed from the

measured fluorescence intensities of AF-555 BSA standard solutions. Standard solutions were prepared at 0, 0.005, 0.01, 0.02, and 0.04 mg/mL AF-555 BSA in PBS and each placed into an individual well containing a pure PEG hydrogel discs (**H control**).

Cytotoxicity. The cytotoxicity of hydrogels was assessed by measuring lactate dehydrogenase (LDH) levels released by 10T½ SM progenitor cells at 24 and 72 h post-photoencapsulation. Cells were suspended (2 x 10^6 cells/mL) in sterile-filtered hydrogel precursor solutions prepared with HEPES buffered saline (HBS; 10 mM HEPES, 150 mM NaCl, pH = 7.4) to which was added acryloyl-PEG-RGDS (1 μmol/mL). Acryoyl-PEG-RGDS was prepared by reacting acryoyl PEG- *N*-hydroxysuccinimide (acryloyl-PEG-NHS, 3.4 kDa) with RGDS.[91] Hydrogel discs (8 per composition) were formed in the wells of a 48 well plate by the addition of 110 μL precursor solution per well and exposure to longwave UV light (UV-Transilluminator, 6 mW/cm^2, 365 nm) for 2 min. The resulting cell-containing hydrogels discs were maintained for 1 hr at 37 °C with 5% CO_2 in DMEM supplemented with 10% v/v heat-inactivated FBS and 1% v/v PSA solution. After transferring to a well of a 24 well plate, each disc was maintained in 500 μL of supplemented DMEM. The media changed every 24 h. For each composition, the LDH activity was measured on four different discs at 24 h and 72 h using a LDH cytotoxicity detection kit (Roche). After measurement of the LDH activity, the gels were digested in 0.1 N NaOH for 72 h at 37 °C and DNA levels were measured at 24 and 72 hr using a PicoGreen assay (Invitrogen). Calf thymus DNA (Sigma) was used as a standard. The average LDH activity was normalized by DNA amount in the sample.

2.4 Materials

Pt-divinyltetramethyldisiloxane complex (Karstedt's catalyst, 2 wt% in xylene), tetrakis(dimethylsiloxy)silane (tetra-SiH), and octamethylcyclotetrasiloxane (D_4) were obtained from Gelest. Allyl methacrylate, acryloyl chloride, triflic acid, 2,2-dimethyl-2-phenyl-acetophenone (DMAP), 1-vinyl-2-pyrrolidinone (NVP), triethylamine (Et_3N), $MgSO_4$, K_2CO_3, hexamethyldisilazane (HMDS), N3013 Nile Red (Nile Blue A Oxazone) and solvents were obtained from Sigma Aldrich. HPLC grade toluene and CH_2Cl_2 and NMR grade $CDCl_3$ were dried over 4Å molecular sieves. Poly(ethylene glycol) (PEG) [PEG-6000; MW = 5000-7000 g/mol and PEG-3400; MW = 3000-3700 g/mol per manufacturer's specifications] were obtained from BioChemika. The M_n of PEO-3400 (3274 g/mol) and PEO-6000 (5881 g/mol) were back-calculated from ^1H NMR end-group analysis of the corresponding diacrylated products (**L** and **H**, respectively). Phosphate buffered solution (PBS, pH = 7.4, without calcium and magnesium), HEPES, Dulbecco's Modified Eagle Medium (DMEM), fetal bovine serum (FBS), and PSA solution (10 U/mL penicillin, 10 g/L streptomycin, and 10 g/L amphotericin) were obtained from Mediatech. Peptide RGDS was obtained from American Peptide. Acryoyl PEG-*N*-hydroxysuccinimide (acryloyl-PEG-NHS, 3.4 kDa) was obtained from Nextar. Mouse smooth muscle precursor cells (10T1/2) were obtained from American Type Culture Collection (ATCC).

2.5 Synthetic Approach

Synthesis of Photo-crosslinkable Macromers

All reactions were run under a N_2 atmosphere with a Teflon-covered stir bar to agitate the reaction mixture. $PDMS_{star}$-MA (**A-C**) were prepared in two synthetic steps (Figure 2.1). First, silane-terminated star polydimethylsiloxanes ($PDMS_{star}SiH$) (**a-c**) were prepared by the acid-catalyzed equilibration of octamethylcyclotetrasiloxane (D_4) with tetrakis(dimethylsiloxy)silane (tetra-SiH).[92, 93] These reagents were combined in a 200 mL round bottom (rb) flask equipped with a rubber septum and triflic acid added via syringe. The mixture was allowed to stir for 16 h at room temperature (RT) and excess HMDS added to neutralize the mixture. The polymer mixture was precipitated three times in toluene/MeOH and the isolated polymer dried under reduced pressure. In the second step, Pt-catalyzed hydrosilylation of **a-c** each with allyl methacrylate yielded **A-C**, respectively.[94] In a 250 mL 3-neck rb flask equipped with an addition funnel and rubber septum, **a-c** were each combined with ~30 mL toluene and the mixture heated 45 °C. After dropwise addition of allyl methacrylate, the mixture was heated to 90 °C and Karstedt's catalyst added via syringe. The progress of the reaction was monitored with IR spectroscopy by the disappearance of the Si-H (~2125 cm^{-1}) absorbance. After ~12 h, an aliquot of the reaction solution was evaporated on a NaCl plate and the IR spectrum obtained. In case of an incomplete reaction, additional Karstedt's catalyst (50% of original volume) was added and the reaction continued for another ~6 h before checking the IR spectrum. This cycle was repeated until no Si-H absorbance was observed in the IR spectrum. Typically, no additional Kartstedt's catalyst was required to complete the

reaction. After removal of volatiles under reduced pressure, the catalyst was removed from the residue via flash column chromatography on silica gel with hexanes:ethyl acetate (2:1 vol:vol) and volatiles removed under reduced pressure.

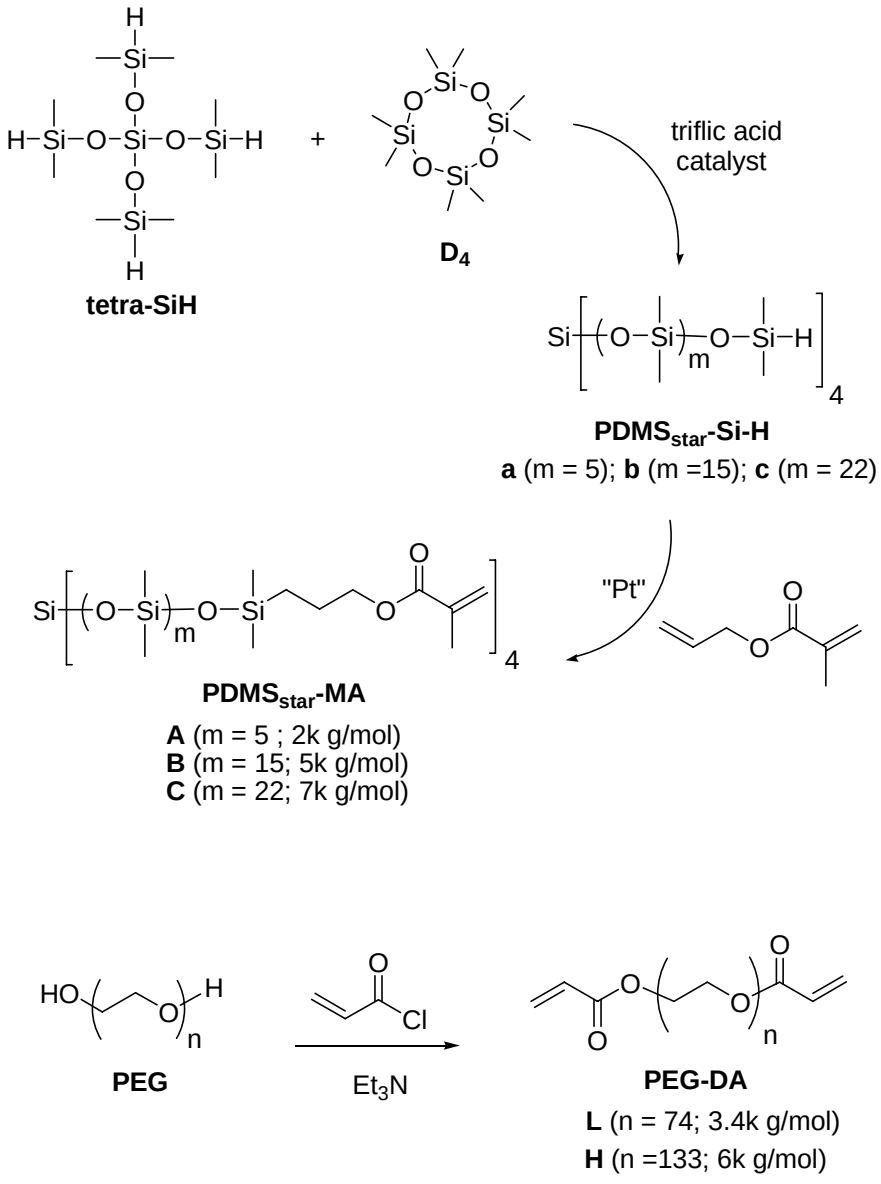

Figure 2.1. Synthesis of: (top) inorganic $PDMS_{star}$-MA (**A-C**) macromers and (bottom) organic PEG-DA (**L**, **H**) macromers.

PEG-DA (**L, H**) were prepared by acrylating the terminal hydroxyl groups of linear PEG [3.4k g/mol ("low" M_n) and 6k g/mol ("high" M_n), respectively].[95] Dry PEG was dissolved in CH_2Cl_2 in a 300 mL rb flask equipped with a rubber septum. Et_3N and acryloyl chloride were sequentially added slowly via syringe. The reaction mixture was allowed to stir at RT overnight. The mixture was transferred to a separatory funnel and washed with 2M K_2CO_3. After allowing the layers to separate overnight, the organic layer was isolated, dried with $MgSO_4$ and gravity filtered. The filtrate was precipitated in diethyl ether, vacuum filtered, washed with diethyl ether and dried under vacuum (30 in. Hg).

Synthesis of $PDMS_{star}$-SiH (a)

D_4 (30 g, 101.4 mmol), tetra-SiH (7.8 g, 23.8 mmol), triflic acid (60 μL), and HMDS (0.15 g, 0.93 mmol) were reacted as above. In this way, **a** (23.3 g, 62% yield) was obtained as a colorless liquid, M_n/M_w= 1,700/2,700 g/mol, PDI = 1.6. ^{1}H NMR (δ, ppm): 0.025-0.19 (bm, 231H, Si*CH*$_3$), 4.7 (m, 4H, Si*H*). IR (ν): 2130 cm^{-1} (Si-H).

Synthesis of $PDMS_{star}$-SiH (b)

D_4 (29.9 g, 101.0 mmol), tetra-SiH (1.7 g, 5.2 mmol), triflic acid (60 μL), and HMDS (0.15 g, 0.93 mmol) were reacted as above. In this way, **b** (23.7 g, 75% yield) was obtained as a colorless liquid, M_n/M_w= 4,800/11,200 g/mol, PDI = 2.3. ^{1}H NMR (δ, ppm): 0.010-0.175 (bm, 1038H, Si*CH*$_3$), 4.7 (m, 4H, Si*H*). IR (ν): 2130 cm^{-1} (Si-H).

Synthesis of $PDMS_{star}$-SiH (c)

D_4 (29.9 g, 101.0 mmol), tetra-SiH (1.1 g, 3.4 mmol), triflic acid (60 μL), and HMDS (0.15 g, 0.93 mmol) were reacted as above. In this way, **c** (24.4 g, 79% yield) was obtained as a colorless liquid, M_n/M_w= 6,800/17,700 g/mol, PDI= 2.6. ^{1}H NMR (δ, ppm): 0.064-0.113 (bm, 1114H, Si*CH*$_3$), 4.7 (m, 4H, Si*H*). IR (ν): 2130 cm^{-1} (Si-H).

Synthesis of $PDMS_{star}$-MA (A)

a (1.5 g, 0.88 mmol), allyl methacrylate (0.42 g, 3.33 mmol), toluene (3 mL), and Karstedt's catalyst (20 μL) were reacted as above. In this way, **A** (1.1 g, 57% yield) was obtained as a colorless liquid, M_n/M_w= 2,050/4,800 g/mol, PDI = 2.3. ^{1}H NMR (δ, ppm): 0.045-0.127 (bm, 282H, Si*CH*$_3$), 0.306 (m, 9H, Si*CH*$_3$), 0.563 (m, 8H, -Si*CH*$_2$CH$_2$CH$_2$, 1.69 (m, 8H, -SiCH$_2$*CH*$_2$CH$_2$), 1.93 (s, 12H, C(CH$_2$)*CH*$_3$), 4.10 (m, 8H, -SiCH$_2$CH-$_2$*CH*$_2$), 5.58 (m, 4H, -C(*CH*$_2$)CH$_3$), 6.11 (m, 4H, -C(*CH*$_2$)CH$_3$). IR (ν): no Si-H peak.

Synthesis of $PDMS_{star}$-MA (B)

b (20.0 g, 4.2 mmol), allyl methacrylate (1.3 g, 10.3 mmol), toluene (35 mL), and Karstedt's catalyst (100 μL) were reacted as above. In this way, **B** (20.7 g, 97% yield) was obtained as a colorless liquid, M_n/M_w = 5,000/14,450 g/mol, PDI = 2.9. ^{1}H NMR (δ, ppm): 0.007-0.204 (bm, 1670H, Si*CH*$_3$), 0.293 (m, 9H, Si*CH*$_3$), 0.587 (m, 8H, -Si*CH*$_2$-CH$_2$CH$_2$), 1.70 (m, 8H, -SiCH$_2$*CH*$_2$CH$_2$), 1.95 (s, 12H, -C(CH$_2$)*CH*$_3$), 4.11 (m, 8H, -SiCH$_2$CH$_2$*CH*$_2$), 5.60 (s, 4H, -C(*CH*$_2$)CH$_3$), 6.13 (s, 4H, -C(*CH*$_2$)CH$_3$). IR (ν): no Si-H peak.

Synthesis of $PDMS_{star}$-MA (C)

c (20.0 g, 2.9 mmol), allyl methacrylate (1.6 g, 12.7 mmol), toluene (35 mL), and Karstedt's catalyst (100 μL) were reacted as above. In this way, **C** (10.4 g, 48% yield) was obtained as a colorless liquid, M_n/M_w= 7,000/23,400 g/mol, PDI = 3.3. ^{1}H NMR (δ, ppm): 0.004-0.266 (bm, 1746H, Si*CH*$_3$), 0.571 (m, 8H, -$SiCH_2$*CH*$_2$$CH_2$), 1.69 (m, 8H, -$SiCH_2$*CH*$_2$$CH_2$), 1.95 (s, 12H, -$C(CH_2)$*CH*$_3$), 4.10 (m, 8H, -$SiCH_2CH_2$*CH*$_2$), 5.58 (s, 4H, -C(*CH*$_2$)$CH_3$), 6.15 (s, 4H, -C(*CH*$_2$)$CH_3$). IR (ν): no Si-H peak.

Synthesis of PEG-DA (L)

PEG-3350 (23.5 g, 7.0 mmol), Et_3N (1.95 mL, 14.0 mmol) and acryloyl chloride (2.27 mL, 28.0 mmol) were reacted as above. In this way, **L** (18.3 g, 76% yield) was obtained. ^{1}H NMR (δ, ppm): 3.62 (s, 296H, -O*CH*$_2$*CH*$_2$), 5.81 (dd, 2H, *J* = 10.2 and 1.5 Hz, -CH=C*H*$_2$), 6.12 (dd, 2H, *J* = 17.3 and 10.5 Hz, -C*H*=CH_2), 6.40 (dd, 2H, *J* = 17.3 and 1.5 Hz, -CH=C*H*$_2$). By ^{1}H NMR end-group analysis, M_n of **L** was determined to be 3382 g/mol (~3400 g/mol).

Synthesis of PEG-DA (H)

PEG-6000 (24.0 g, 4.0 mmol), Et_3N (1.12 mL, 8.0 mmol) and acryloyl chloride (1.3 mL, 16.0 mmol) were reacted as above. In this way, **H** (17.9 g, 75% yield) was obtained. ^{1}H NMR (δ, ppm): 3.61 (s, 533H, -O*CH*$_2$*CH*$_2$), 5.81 (dd, 2H, *J* = 10.2 and 1.5 Hz, -CH=C*H*$_2$), 6.12 (dd, 2H, *J* = 17.1 and 10.5 Hz, -C*H*=CH_2), 6.39 (dd, 2H, *J* = 17.3

and 1.5 Hz, -CH=CH_2). By ^{1}H NMR end-group analysis, M_n of **H** was determined to be 5989 g/mol (~6000 g/mol).

2.6 Hydrogel Preparation

Hydrogels were prepared by the photopolymerization of aqueous mixtures of $PDMS_{star}$-MA **(A-C)** and PEG-DA **(L, H)** macromers. Aqueous precursor solutions were prepared at concentrations of 10 mg/mL (10 wt %). 10 μL of photoinitiator solution (30 wt% solution of DMAP in NVP) was added per one mL of the aqueous solution. The $PDMS_{star}$-MA and photoinitiator solution were sequentially added to an aqueous solution of PEG-DA and vortexed for 1 min after each component was added. Solutions prepared with **A**-**C** were hazy but did not separate into layers. Hydrogels were prepared with the following wt% ratios of **A**, **B**, or **C** to **L** or **H**: 0:100, 1:99, 10:90 and 20:80 (**Table 2.1**).

Planar hydrogel sheets (1.5 mm thick) were prepared by pipetting the precursor solution between two clamped microscope slides (75 x 50 mm) separated by polycarbonate spacers and exposing the mold to longwave UV light (UV-Transilluminator, 6 mW/cm2, 365 nm) for 80 sec. After removal from the mold, the hydrogel sheet was rinsed with DI water and then soaked in PBS for 2 days with daily PBS changes to remove impurities. Hydrogel sheets prepared in this way were used for morphological, swelling, compression, protein adhesion, and cytotoxicity tests.

Table 2.1. Hydrogel Composition and Notation

		$PDMS_{star}$-MA		
PEG-DA	**Wt% ratio of A-C to L**	**A** (M_n = 2k g/mol)	**B** (M_n = 5k g/mol)	**C** (M_n = 7k g/mol)
	0:100		**L control**	
L	1:99	**A_1 L_{99}**	**B_1 L_{99}**	**C_1 L_{99}**
(M_n = 3.4k	10:90	**A_{10} L_{90}**	**B_{10} L_{90}**	**C_{10} L_{90}**
g/mol)	20:80	**A_{20} L_{80}**	**B_{20} L_{80}**	**C_{20} L_{80}**

		$PDMS_{star}$-MA		
PEG-DA	**Wt% ratio of A-C to H**	**A** (M_n = 2k g/mol)	**B** (M_n = 5k g/mol)	**C** (M_n = 7k g/mol)
	0:100		**H control**	
H	1:99	**A_1 H_{99}**	**B_1 H_{99}**	**C_1 H_{99}**
(M_n = 6k	10:90	**A_{10} H_{90}**	**B_{10} H_{90}**	**C_{10} H_{90}**
g/mol)	20:80	**A_{20} H_{80}**	**B_{20} H_{80}**	**C_{20} H_{80}**

For tensile tests, hydrogels were prepared with a "ring" geometry. First, hydrogels were prepared in a hollow tube geometry with a double walled tubular mold composed of an inner glass mandrel (diameter = 3 mm) and an outer glass cylinder (diameter = 7.5 mm). The tubular mold was filled with a precursor solution and cured as above but with constant rotation such that each surface point of the mold received equal UV intensity and exposure time. The hydrogel tube was removed from the mold and similarly purified as above by rinsing and soaking in PBS. Ring specimens were obtained but cutting ~3 mm wide pieces from the central portion of the hydrogel tube.

2.7 Results and Discussion

Synthesis of $PDMS_{star}$-MA (A-C)

Acid-catalyzed equilibration is useful to convert cyclosiloxanes and a suitable disiloxane to linear polymer.[96] Here, Si-H-terminated star polydimethylsiloxanes ($PDMS_{star}SiH$, **a-c**) were prepared by acid-catalyzed equilibration of D_4 with tetra-SiH.[92, 93] The molecular weight was controlled by the ratio of D_4 and tetra-SiH. Because equilibration reactions generate a mixture of linear and cyclic species, the resulting mixture was precipitated to isolate the higher molecular weight materials. The lack of cyclic materials is confirmed by GPC of **a-c.** Si-H terminal groups of **a-c** were subsequently converted to photo-sensitive methacrylate groups by Pt-catalyzed hydrosilylation of each with allyl methacrylate to yield **A-C**, respectively.[94] The chemical reaction was confirmed by the disappearance of the Si-H peak (~ 4.5 ppm) in the ^1H NMR spectra and Si-H absorbance (~2125 cm^{-1}) in the FT- IR spectra of **A-C**.

Hydrogel Morphology and Chemical Composition

It is known that hydrogel morphology impacts cell behavior by changing cell alignment, proximity, and cell-cell interactions.[74-80] The morphology of PEG-DA hydrogels cannot be visualized using techniques such as scanning electron microscopy (SEM).[97] Instead, CLSM was used herein to image hydrogels which were treated with a hydrophobic dye (Nile Red) to stain PDMS-enriched regions and while maintaining hydrogel hydration. Because of the water-insolubility of PDMS, aqueous precursor solutions prepared with **A-C** were visibly hazy but did not separate into layers. Thus, photochemical cure effectively trapped the liquid microphase separation in the resulting

hydrogel. The CLSM images revealed that the morphology of the resulting $PDMS_{star}$-PEG hydrogels was heterogeneous and consisted of stained PDMS-enriched microparticles surrounded by a PEG-enriched matrix (Figure 2.2).

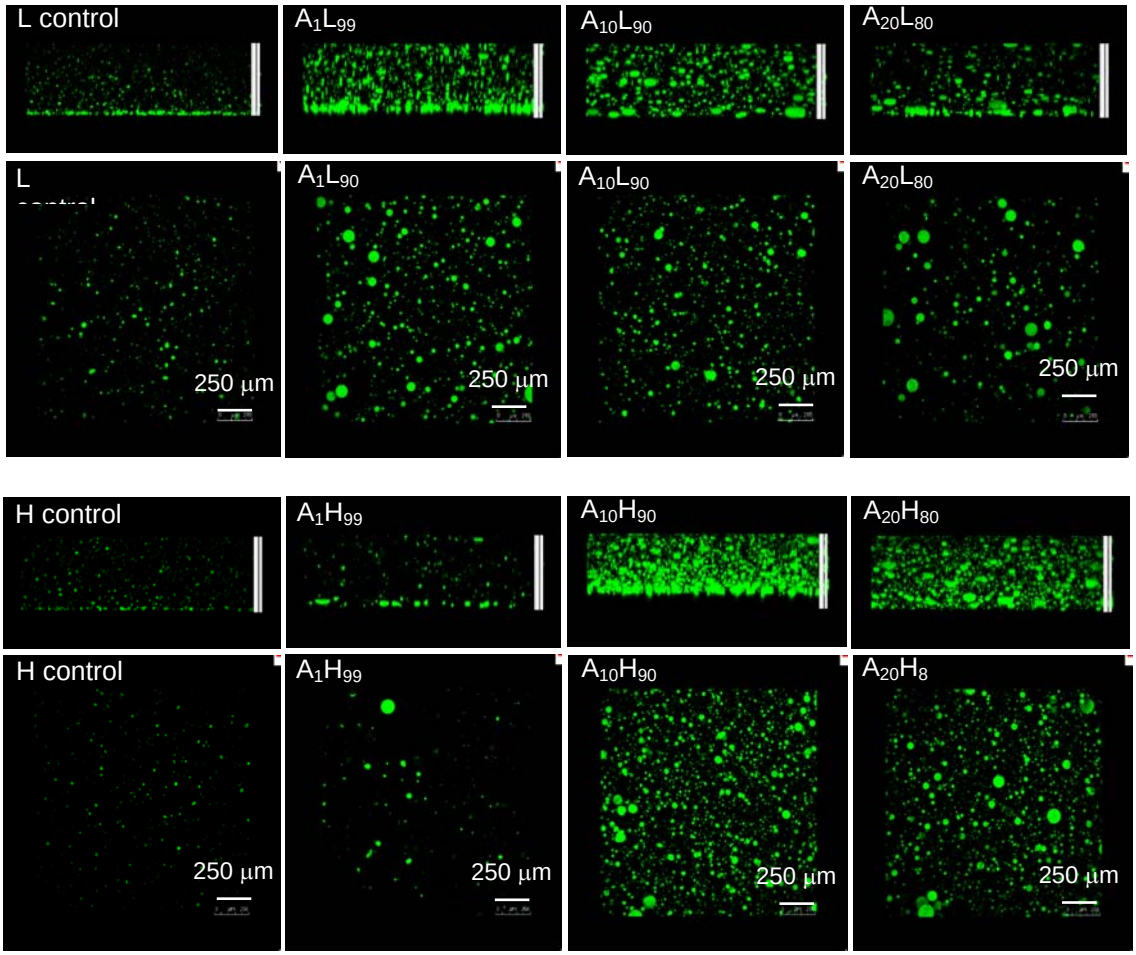

Figure 2.2. CLSM images of hydrated hydrogels stained with Nile Red. Cross-sectional view (top rows) and top view (bottom rows). The hydrophobic dye stained hydrophobic PDMS-enriched microparticles

Some staining occurred for the **L control** and **H control** due to the hydrophobic photoinitiator. FE-SEM/EDS confirmed the presence of silicon (Si) in the microparticles

and its absence in the surrounding matrix (Appendix A). The chemical nature of the hydrogels was systematically changed from a purely organic to increasingly inorganic with higher levels of $PDMS_{star}$-MA (**A-C**). However, for all hydrogels, the general morphological features were maintained. These discrete PDMS-enriched microparticles are expected to have an impact on cell behavior.[71-73] Thus, these hydrogels provide controlled alteration of hydrogel morphology and chemical composition.

Hydrogel Hydration and Mechanical Properties

Both hydration and mechanical properties of hydrogel scaffolds influence cell behavior.[81-85] These properties are coupled in PEG-DA and other hydrogels in that the degree of hydrogel swelling is directly related to its mechanical properties and hydrogels become more rigid and stronger with decreased water content.[98] It is therefore critical to maintain hydrogel hydration during mechanical tests to achieve accurate results.[99] Tensile testing of flat, rectangular hydrogel specimens with ends secured in tension grips is often complicated by sample slippage from or breakage at the grip. Thus, specimens with a ring geometry were employed to minimize slippage/breakage for improved accuracy.[48] Ring specimens also allowed their rapid mounting on tensile bars so that testing was completed before significant water loss. During dynamic compression tests, silicone oil was placed around the hydrogel disc specimen sandwiched between two compression clamps to inhibit water loss.

Hydrogel swelling and mechanical properties are summarized in Table 2.2 and Figures 2.3-2.5. Hydrogels based on **H** (PEG-DA, 6k g/mol) exhibited higher swelling

than that of hydrogels based on **L** (PEG-DA, 3.4k g/mol) because of the formers lower crosslink density. However, for a given hydrogel series based on **L** or **H**, the swelling ratio of $PDMS_{star}$-PEG hydrogels were not substantially different from one another or the corresponding pure PEG-DA hydrogel (**L** and **H controls**), particularly for those based on **H**. The lack of change in hydration with hydrophobic **A-C** may be explained by the fact that it formed PDMS-enriched particles which does not perturb the surrounding PEG matrix (Figure 2.2). The tensile strength and elongation at break of $PDMS_{star}$-PEG hydrogels were not considerably changed versus the pure PEG hydrogels.

Table 2.2. Hydrogel swelling ratio, tensile strength (TS), % elongation at break (%EL), and adsorption of BSA protein.

	Swelling Ratio	Tensile Strength (kPa)	% EL	mg BSA absorbed per cm^2 (x 10^{-4})*
L control	**7.0 ± 0.01**	**34.2 ± 3.0**	**40.5 ± 4.0**	**5.2 ± 1.2**
A_1L_{99}	6.5 ± 0.03	34.5 ± 4.2	49.2 ± 4.9	3.6 ± 0.6
$A_{10}L_{90}$	6.2 ± 0.04	27.5 ± 3.4	48.5 ± 4.1	13.5 ± 3.5
$A_{20}L_{80}$	6.7 ± 0.05	22.3 ± 2.9	49.2 ± 7.2	25.7 ± 4.9
B_1L_{99}	6.6 ± 0.15	34.4 ± 5.2	48.8 ± 7.0	9.4 ± 1.7
$B_{10}L_{90}$	6.6 ± 0.12	26.0 ± 2.9	48.2 ± 5.0	14.5 ± 1.5
$B_{20}L_{80}$	7.1 ± 0.10	20.0 ± 2.7	45.2 ± 4.9	28.7 ± 6.4
C_1L_{99}	6.7 ± 0.14	40.6 ± 9.4	55.0 ± 9.0	14.1 ± 6.4
$C_{10}L_{90}$	6.8 ± 0.05	29.0 ± 3.5	53.6 ± 6.3	5.7 ± 2.6
$C_{20}L_{80}$	7.3 ± 0.08	24.5 ± 1.8	53.4 ± 4.4	19.0 ± 1.6
H control	**8.0 ± 0.06**	**39.7 ± 7.7**	**61.0 ± 9.3**	**12.4 ± 4.7**
A_1H_{99}	8.0 ± 0.06	35.5 ± 2.4	64.0 ± 3.3	10.1 ± 1.8
$A_{10}H_{90}$	8.0 ± 0.11	48.1 ± 5.0	82.9 ± 7.4	16.0 ± 4.3
$A_{20}H_{80}$	7.9 ± 0.11	37.1 ± 6.7	77.4 ± 9.9	10.2 ± 1.9
B_1H_{99}	8.0 ± 0.18	39.7 ± 5.3	65.9 ± 5.4	5.3 ± 2.1
$B_{10}H_{90}$	8.1 ± 0.09	46.0 ± 4.3	79.2 ± 4.8	15.0 ± 9.9
$B_{20}H_{80}$	8.1 ± 0.08	26.8 ± 6.8	59.6 ± 10.8	8.6 ± 1.1
C_1H_{99}	8.0 ± 0.01	33.4 ± 5.9	58.5 ± 6.5	15.0 ± 1.6
$C_{10}H_{90}$	8.1 ± 0.23	25.6 ± 4.3	51.1 ± 5.1	12.8 ± 3.1
$C_{20}H_{80}$	8.4 ± 0.16	33.6 ± 4.5	73.6 ± 6.2	10.0 ± 1.3

*After 3 hr exposure to BSA (0.1 mg/mL PBS)

For hydrogels based on **L**, increased levels of $PDMS_{star}$-MA (**A-C**) systematically decreased tensile modulus (Figure 2.3). A similar but less substantial decrease in tensile modulus was observed for hydrogels based on **H** (Figure 2.4). Although the weight percent of **A-C** impacted tensile modulus of $PDMS_{star}$-PEO hydrogels, the M_n of **A-C** did not. The dynamic storage modulus (G') of the hydrogels was also measured in compression as a function of frequency (Figure 2.5). Based on the tensile test results, the hydrogels with 1 wt% **A-C** showed characteristics intermediate of the corresponding pure PEG-DA hydrogel and those containing 10 wt% **A-C**. Therefore, compression tests were not conducted on hydrogel compositions with 1 wt% **A-C** due to the limited additional information that would be obtained. Over the low strain conditions examined, G' values exhibited values similar to the corresponding tensile modulus and likewise generally decreased with higher levels of **A-C**. The PDMS particles, although they do not significantly alter swelling, apparently change the manner in which the surrounding PEG-DA hydrogel network deforms under applied stress. Thus, these $PDMS_{star}$-PEO hydrogels are particularly useful to examine scaffold mechanical properties on cell behavior as modulus may be tuned independent of swelling.

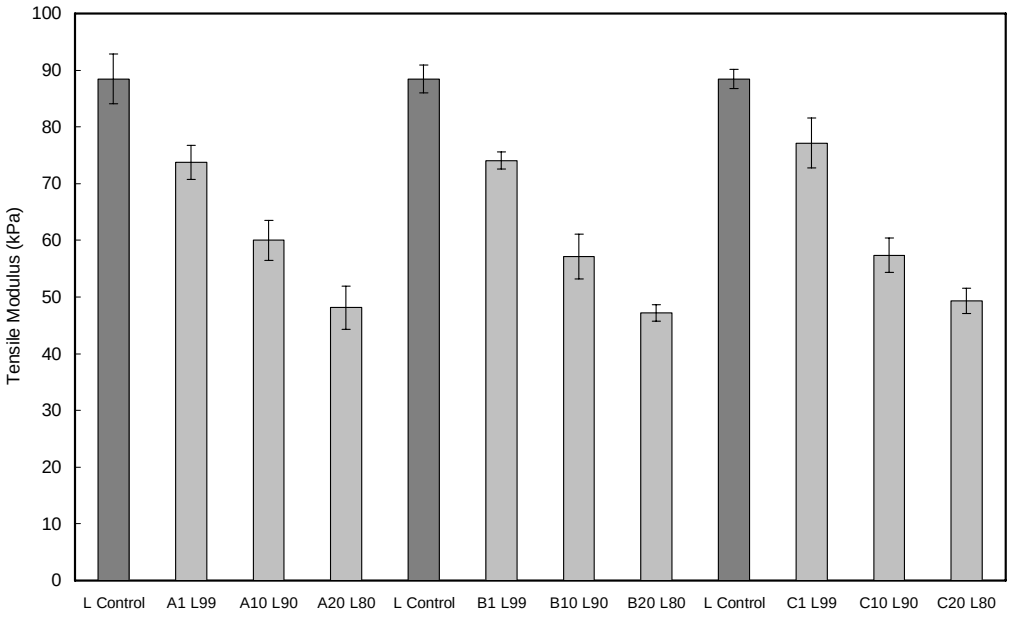

Figure 2.3. Tensile modulus of hydrogels based on **L**. Statistical significance within a given series (i.e. A, B and C) was determined by one-way analysis of variance (Holm-Sidak method where $p \leq 0.05$.) For a given series, all are statistically different versus the control and other compositions.

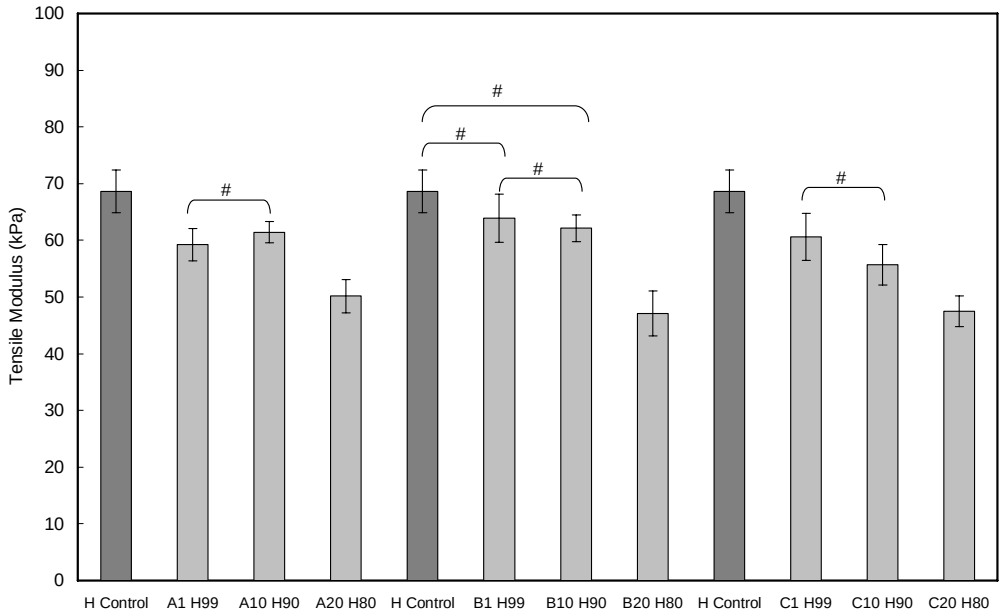

Figure 2.4. Tensile modulus of hydrogels based on **H**. Statistical significance within a given series (i.e. **A**, **B** and **C**) was determined by one-way analysis of variance (Holm-Sidak method where $p \leq 0.05$, unless otherwise noted. [#] indicates $p > 0.05$).

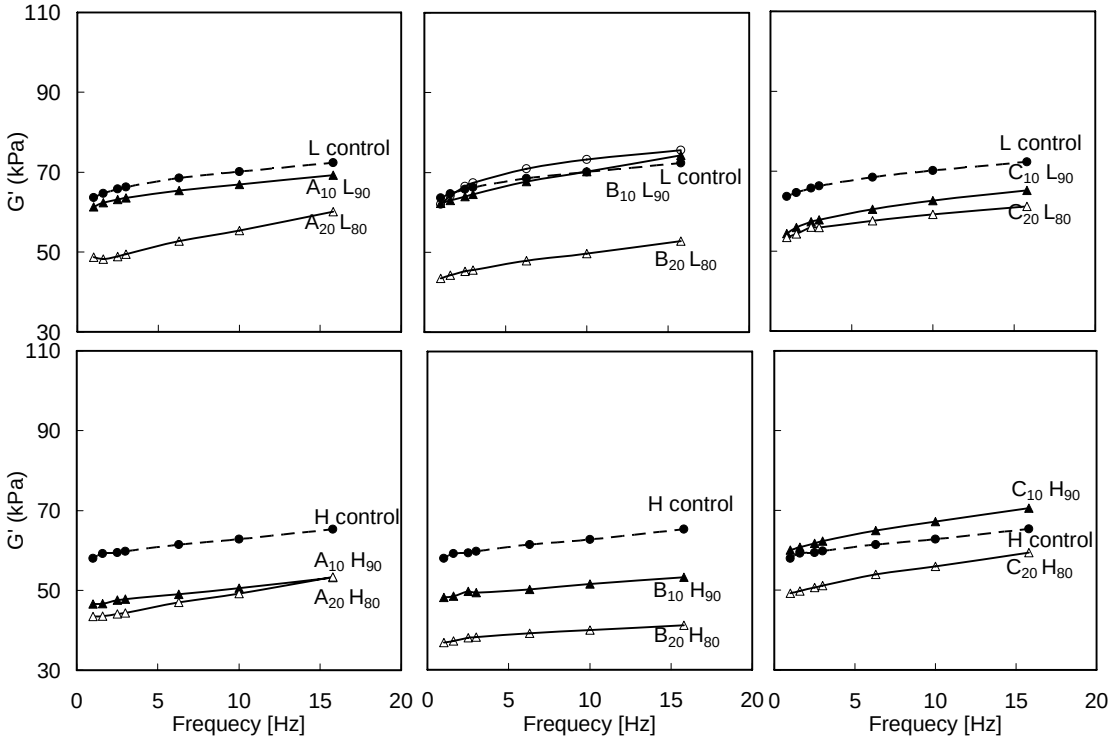

Figure 2.5. Storage modulus (G') of hydrogels measured in compression.

Non-specific Protein Adhesion

Proteins which are non-specifically adsorbed from serum or plasma as well as specifically introduced to the scaffold are known to alter cell behavior.[44, 50, 63] Thus, to study cell behavior in response to specific, isolated scaffold properties, the protein resistant nature of PEG-DA hydrogels must be maintained. The adhesion of BSA to $PDMS_{star}$-PEG hydrogels was compared to that of the corresponding PEG-DA hydrogels (**L** and **H controls**) (Table 2.2). Aside from $\mathbf{A_{20}L_{80}}$ and $\mathbf{B_{20}L_{80}}$, BSA adsorption levels by $PDMS_{star}$-PEG hydrogels were generally similar to each other and to the PEG-DA hydrogels. PDMS has been shown to be highly adhesive to proteins due to its hydrophobicity [100]. Despite the presence of PDMS, $PDMS_{star}$-PEG hydrogels exhibit

protein resistance similar to PEG-DA hydrogels. It has been previously shown that BSA adsorption on PEG-DA hydrogels is intimately linked to its hydrophilicity.[101] Because of the similar swelling of the series of $PDMS_{star}$-PEG hydrogels based on **L** or **H**, it is reasonable that protein adsorption is also similar. For all hydrogels, protein adsorption levels were within the range reported for PEG-DA hydrogels.[101] Retention of the low protein adsorption property of PEG-DA hydrogels by these $PDMS_{star}$-PEG hydrogels is useful to extend their utility as scaffolds in tissue engineering.

Cytotoxicity

Low cytotoxicity of $PDMS_{star}$-PEG hydrogels is critical for their utility as tissue engineering scaffolds. LDH is a soluble cytosolic enzyme that is released into the culture medium following membrane damage due to apoptosis or necrosis.[102] Differences in the normalized levels of exogenous LDH across cell-laden hydrogels therefore indicate difference in the extent of cell death induced by various formulations. To assess the cytocompatibility of $PDMS_{star}$-PEG gels, LDH activity assays were conducted on hydrogels based on **H** and **C** macromers (Figure 2.6). Although the exogenous LDH activity at 24 h was higher the hydrogel containing 20 wt % **C** versus the corresponding pure PEG-DA hydrogel (**H control**), the hydrogels containing 1 wt% and 10 wt% of **C** demonstrated similar cytocompatibility. At 72 h, all formulations showed similar levels of exogenous LDH activity. Thus, $PDMS_{star}$-PEG hydrogels appear to maintain the low cytotoxicity of PEG-DA hydrogels over a range of PDMS levels.

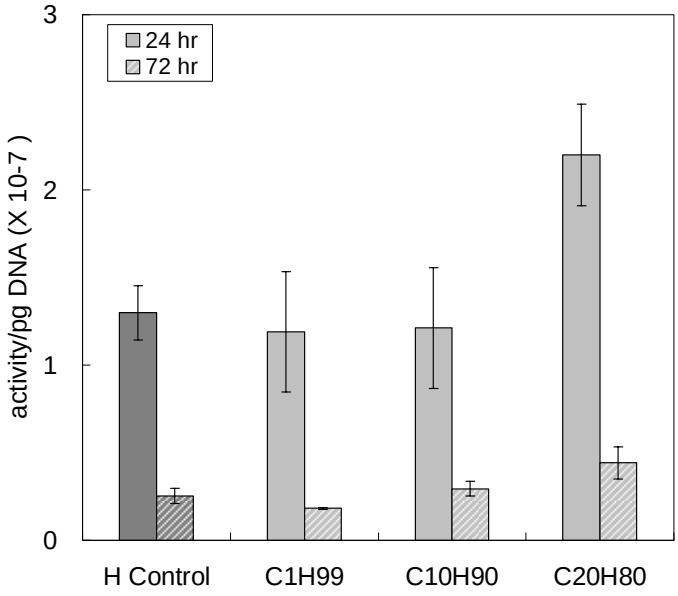

Figure 2.6. LDH activity at 24h (left columns) and 72 h (right columns).

2.8 Conclusion

A library of 18 unique $PDMS_{star}$-PEG hydrogels were formed by the rapid photocrosslinking of 10 wt% aqueous precursor solutions containing varying weight ratios of $PDMS_{star}$-MA (**A-C**: 1.8k, 5k and 7k g/mol, respectively) and PEG-DA (**L** and **H**: 3.4k and 6k g/mol, respectively): 0:100, 1:99, 10:90 and 20:80, respectively. PEG-DA hydrogels are single-component systems in which only two compositional variables (e.g. PEG-DA M_n and concentration) may be utilized to alter hydrogel properties. These $PDMS_{star}$-PEG hydrogels are two-component systems in which four compositional variables (e.g. PEG-DA and $PDMS_{star}$-MA M_n and concentration) may be altered to tune physical and additionally chemical properties. The chemical properties of the hydrogels were switched from a purely organic, PEG to inorganic-organic with increased levels of **A-C**. Hydrogel morphology consisted of spherical PDMS-enriched microparticles

dispersed throughout a PEG matrix. Although not demonstrated here, filtration of the precursor solution prior to crosslinking produces a finer dispersion of PDMS particles in the PEG matrix to further control the morphology and chemical composition of the hydrogel. For hydrogels based on **L**, increased levels of **A-C** systematically decreased tensile modulus and a similar but less substantial decrease was observed for hydrogels based on **H**. At the same weight ratio, the M_n of **A-C** did not significantly impact mechanical properties. For a given hydrogel series based on **L** or **H**, the equilibrium swelling did not differ substantially across hydrogel formulations relative to that of the corresponding pure PEG-DA hydrogel (**L** and **H controls**). Thus, for a given hydrogel series, modulus was decoupled from equilibrium swelling. These hydrogels therefore permit the evaluation of the effect of scaffold modulus apart from hydration. The resistance to non-specific protein adsorption as well of low cytotoxicity of PEG-DA hydrogels was maintained for the $PDMS_{star}$-PEG hydrogels. Thus, these inorganic-organic hydrogels with tunable chemical and physical properties should prove useful in elucidating cell-material interactions.

CHAPTER III

THERMORESPONSIVE NANOCOMPOSITE HYDROGELS WITH CELL-RELEASING BEHAVIOR

3.1 Overview

Poly(*N*-isopropylacrylamide) (PNIPAAm) hydrogels become more hydrophobic when they reversibly switch from a water-swollen to a deswollen state above the volume phase transition temperature (VPTT, ~ 33 °C) which has been used to modulate cell adhesion. In the current work, we prepared novel thermoresponsive nanocomposite hydrogels comprised of a PNIPAAm hydrogel matrix and polysiloxane colloidal nanoparticles (~220 nm ave. diameter) via *in situ* photopolymerization of aqueous solutions of NIPAAm monomer, *N,N'*-methylenebisacrylamide (BIS, crosslinker), photoinitiator and polysiloxane nanoparticles (0.5 to 2.0 wt% based on solution weight) at ~7 °C. The VPTT of the nanocomposite hydrogels is not altered versus the pure PNIPAAm hydrogel. Dynamic mechanical analysis and tensile tests revealed that higher nanoparticle content generally produced improved hydrogel mechanical properties. Surfaces of nanocomposite hydrogels became increasingly more hydrophobic at all temperatures between 10 and 40 °C as the amount of hydrophobic polysiloxane nanoparticles was increased. When cooled from 37 °C to 25 °C, mouse smooth muscle precursor cells (10T1/2) were effectively detached from nanocomposite hydrogel surfaces. The utility of photopatterning to create surface micropillars comprised of nanocomposite hydrogels was demonstrated.

3.2 Introduction

Materials which reversibly switch from a hydrophilic to hydrophobic state in aqueous media in response to an external stimulus are of interest for creating "smart" or "intelligent" biomedical materials [103]. Thermoresponsive hydrogels are crosslinked, three dimensional polymer networks that reversibly swell with and then expel aqueous media in response to temperature changes. Thermoresponsive hydrogels may be prepared by crosslinking polymers which exhibit a lower critical solubility temperature (LCST) [103, 104]. Most widely studied is poly(*N*-isopropylacrylamide) (PNIPAAm) (LCST, ~32 °C) which is soluble in water below the LCST and reversibly insoluble above the LCST [105]. Crosslinked PNIPAAm hydrogels undergo a reversible volume phase transition in water from a swollen state to a deswollen state above their volume phase transition temperature (VPTT; ~33 °C) [106, 107]. Thus, surfaces of PNIPAAm hydrogels [108-110] as well as those comprised of covalently grafted PNIPAAm chains [110-112] undergo a large discontinuous change from a hydrophilic to a hydrophobic state when heated above the phase transition temperature.

The thermal modulation of hydrophilic/hydrophobic surface properties of PNIPAAm systems is useful for the controlled detachment of cultured cells [113, 114]. In this way, confluent cell sheets useful for tissue engineering may be detached from culture without enzymes or chelating agents known to damage cells [115]. Cells generally adhere and proliferate more readily on polymeric materials with hydrophobic surfaces rather than hydrophilic surfaces [2, 116-124]. Often characterized by contact angle measurements, polymer surfaces displaying water contact angles greater than 90°

are generally considered to be hydrophobic [125]. Several studies have shown that cell adhesion is maximized on moderately hydrophobic surfaces displaying a water contact angle between 40 and 70° [2, 120-124]. Thus, at ~ 37 °C (above the LCST), PNIPAAm-grafted surfaces are relatively hydrophobic and various types of cells grow well. However, upon cooling below 32 °C (below the LCST), they become more hydrophilic and cells spontaneously detach without damaging the cells [126-130]. Similarly, cells may be detached from the surfaces of PNIPAAm hydrogels after cooling below the VPTT [131, 132].

Extending the utility of PNIPAAm hydrogels as robust cell-releasing materials for tissue culture substrates [113, 114], anti-fouling coatings [133-135], or "self-cleaning" implanted sensor membranes [136, 137] requires improvement of their poor mechanical properties as well as tailoring the changes in surface hydrophilicity/hydrophobicity. Hybrid materials prepared from inorganic and organic components have attracted interest to yield properties superior to that of parent materials [138-142]. For targeted biomedical applications, the proximity of the VPTT to room temperature and body temperature is desirable to maintain. However, the VPTT of PNIPAAm hydrogels (and LCST of aqueous solutions of linear PNIPAAm) are typically altered upon copolymerization with a second monomer. For instance, the VPTT of PNIPAAm-based hydrogels is generally decreased by incorporation of hydrophobic comonomers [143, 144] or increased with hydrophilic comonomers [144, 145]. On the other hand, the VPTT of PNIPAAm hydrogels is not usually altered if the second component is incorporated as chemically independent phase. For instance,

interpenetrating polymer networks (IPNs) and semi-IPNs have been prepared with chemically independent PNIPAAm and poly(dimethylsiloxane) (PDMS) (a hydrophobic, inorganic polymer) components without altering the VPTT but improving mechanical strength [146-148]. Hybrid composites comprised of an organic PNIPAAm matrix and silica (SiO_2) particles (an inorganic glass) have also been studied to improve mechanical properties. For instance, PNIPAAm hydrogels covalently bonded to silica particles may be formed by *in situ* copolymerization of NIPAAm with 3-methacryloxypropyl-trimethoxysilane (MPTMOS) or ethylene triethoxysilane (ETEOS) followed by sol-gel condensation which leads to a decrease in the VPTT with increased silane content [149-151]. However, the VPTT was not changed for PNIPAAm hydrogels containing but not covalently bonded to silica particles as formed by *in situ* polymerization of NIPAAm and *N,N'*-methylenebisacrylamide (BIS) or high molecular weight PNIPAAm each with tetramethoxysilane (TMOS) followed by sol-gel condensation [152, 153].

In this paper, thermoresponsive nanocomposite hydrogels were prepared consisting of an organic PNIPAAm hydrogel matrix and variable levels of inorganic polysiloxane nanoparticles. Nanoparticles are classically defined as colloidal systems with a diameter smaller than 1000 nm [154, 155]. Here, polysiloxane nanoparticles (diameter = 106 – 531 nm) were prepared from cationic emulsion polymerization of octamethylcyclotetrasiloxane (D_4) and 1,3,5,7-tetramethyl-1,3,5,7-tetravinylcyclotetra-siloxane (D_4^{Vi}). The resulting nanoparticles were subsequently stabilized by free radical crosslinking the copoly(dimethylsiloxane/methylvinylsiloxane) chains inside the nanoparticles. Crosslinked polysiloxane nanoparticles (0.5 – 2.0 wt%) were introduced

into aqueous solutions of NIPAAm, BIS (crosslinker), and photoinitiator and subsequently photopolymerized at low temperatures (~ 7 °C) to yield thermoresponsive nanocomposite hydrogels. The effect of polysiloxane nanoparticle content on hydrogel morphology, VPTT, mechanical properties as well as temperature-dependent swelling behavior, surface properties, and cell release behavior are presented. Furthermore, we demonstrated the successful photopatterning of nanocomposite hydrogels which may extend their utility in applications such as cell co-culture [156, 157] and microfluidics [158, 159].

3.3 Experimental Section

Preparation of Crosslinked Polysiloxane Colloidal Nanoparticles

Polysiloxane colloidal particles were prepared by cationic emulsion polymerization of D_4 and D_4^{Vi} (Fig. 3.1) [160]. Into a 500 mL water-jacketed polymerization vessel equipped with a mechanical stirrer and Teflon stirring paddle, reflux condenser, and addition funnel, DBSA (0.5 g, 1.53 mmol) was dissolved in deionized (DI) water (200 g). A mixture of D_4 (39.6 g, 133.8 mmol) and D_4^{Vi} (9.9 g, 28.8 mmol) was added dropwise via the addition funnel to the DBSA aqueous solution with constant stirring (300 rpm). The resulting stable emulsion was then heated to 75 °C for 24 h with constant stirring (280 rpm). The final emulsion was cooled, filtered through a 10 μm filter bag, and the pH adjusted to 7 with aq. NH_4OH (25 wt%). The solid content of the emulsion was determined by weight loss from an aliquot after drying (115 °C, 8 h). Emulsion solid content: 17.4% (87 % conversion).

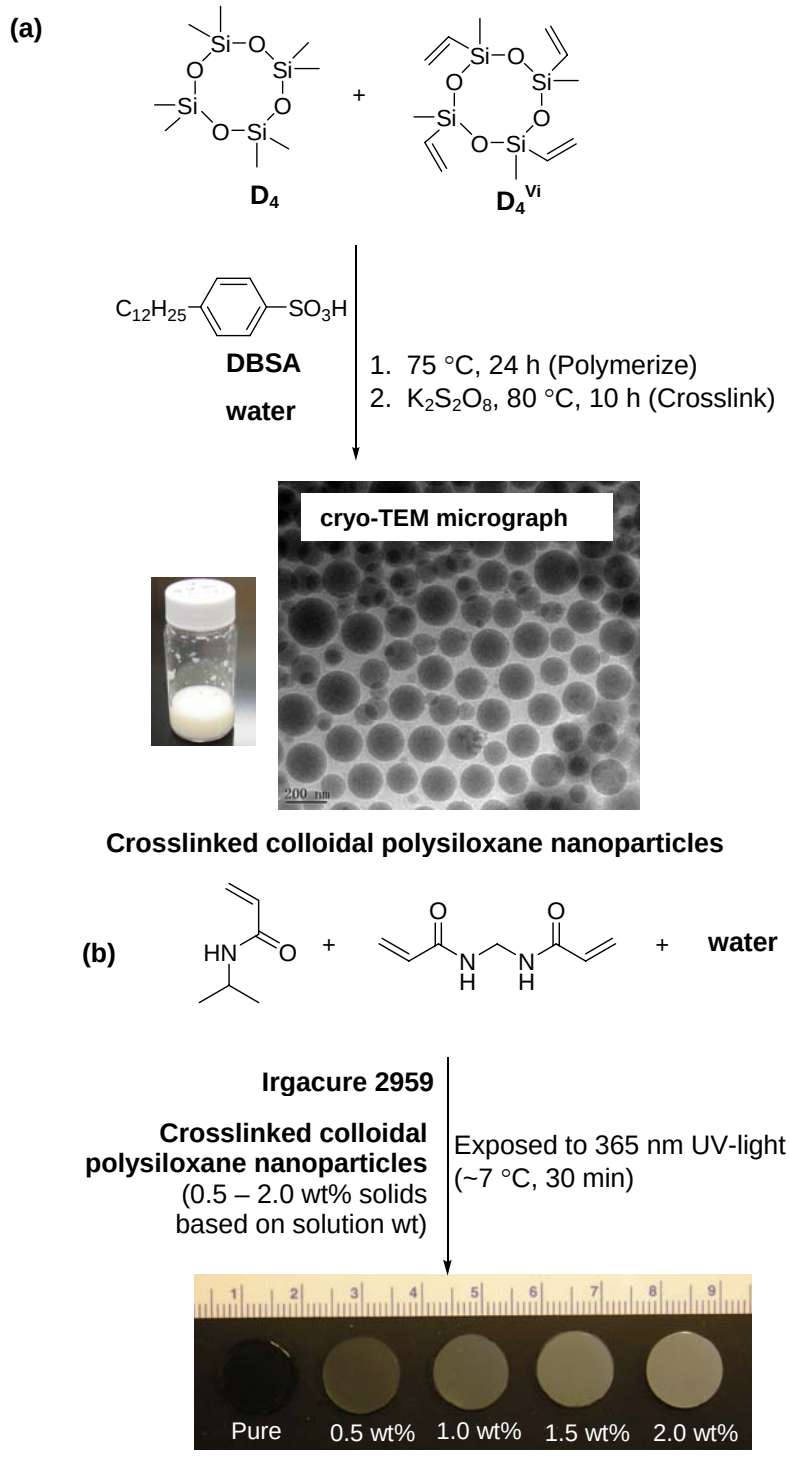

Figure 3.1. **(a)** Preparation of colloidal polysiloxane nanoparticles via emulsion polymerization and subsequent crosslinking and **(b)** preparation of thermoresponsive nanocomposite hydrogels with variable wt% nanoparticles (based on total solution weight).

Linear copoly(dimethylsiloxane/methylvinylsiloxane) was isolated from the aforementioned colloidal nanoparticles for subsequent characterization. A portion of the final emulsion was precipitated into ethanol, centrifuged, and the isolated clear oil dried under vacuum. ^{1}H NMR δ (ppm): 0.1 (bs, Si-C*H*$_3$), 5.7-6.0 (m, Si-C*H*=C*H*$_2$); ratio of 12:1. Gel permeation chromatography (GPC): M_w/M_n = 67,200/36,500 g/mol, PDI = 1.84.

These colloidal nanoparticles were subsequently stabilized by crosslinking of the copoly(dimethylsiloxane/methylvinylsiloxane) chains within the nanoparticles via their vinyl groups (Fig. 3.1) [161]. The above final emulsion (50 g) was added to a 3-neck round bottom (rb) flask equipped with a Teflon-covered stir bar, reflux condenser, and nitrogen (N_2) inlet. After the addition of $K_2S_2O_8$ (0.5 g), the mixture was reacted at 80 ºC for 10 h under N_2. The emulsion was cooled and filtered through a 10 μm filter bag. The resulting colloidal nanoparticles were purified via dialysis (Slide-A-Lyzer ® Dialysis Cassette, MWCO = 10,000, Pierce Chemical Co.) against daily changes of DI water for 3 days. Emulsion solid content: 8.5%. Dynamic light scattering (DLS): 219 nm (average diameter) and 0.10 (polydispersity, PD) with particles ranging in size from 106 to 531 nm.

Characterization of Polysiloxane Colloidal Nanoparticles

Particle size of colloidal nanoparticles was determined by dynamic light scattering (DLS) (Malvern Zetasizer® Nano S) with a detection angle of 90 º. Measurements were carried out at 25 °C. One μL of the designated emulsion was

diluted with ~ 20 mL filtered DI water just prior to measurement in order to rule out interaction and multiple scattering effects.

Cryogenic transmission electron microscopy (Cryo-TEM) was used to visualize the nanoparticles and confirm their lack of aggregation in water. A JEOL 1210 TEM, operated at 120 kV and equipped with a Gatan 626 cryo holder, was used for imaging. Further details on sample preparation and imaging analysis were previously described [162].

GPC analysis of the isolated linear copoly(dimethylsiloxane/methylvinyl-siloxane) was performed on a Viscotek GPC system equipped with three detectors in series: refractive index (RI), right angle laser light scattering (RALLS), and viscometer (VP). The ViscoGEL™ HR-Series (7.8 mm x 30 cm) column packed with divinylbenzene crosslinked polystyrene (SDVB) was maintained at 25 °C in a column oven. The eluting solvent was HPLC grade toluene at a flow rate of 1.0 mL/min. The detectors were calibrated with a polystyrene (PS) narrow standard with the following parameters: MW (66K), polydispersity (1.03), intrinsic viscosity (0.845 dL/g), and dn/dc (0.112 mL/g). Data analysis was performed with Viscotek OmniSec software (Version 4.0).

^{1}H NMR spectrum of a 5% (w/v) $CDCl_3$ solution of isolated linear copoly(dimethylsiloxane/methylvinylsiloxane) was obtained on a Mercury 300 300-MHz spectrometer operating in the Fourier transform mode. Residual $CDCl_3$ served as an internal standard.

Extent of Crosslinking

The amount of uncrosslinked material in select hydrogels was determined by weight loss following Soxhlet extraction. For a given hydrogel, three hydrogel discs (13 mm diameter, 1.5 mm thickness) were punched from a single hydrogel sheet with a die and immediately dried in a vacuum oven (30 in. Hg, 60 ºC, 24 h) and weighed. The dried discs were extracted with dichloromethane in a Soxhlet apparatus for 12 hr and weighed after similarly drying in a vacuum oven. The percentage of uncrosslinked material was calculated as the average weight difference of the extracted versus unextracted weight divided by the unextracted weight.

Morphological Characterization

The morphology of hydrogels was studied by scanning electron microscopy (SEM). To retain their morphology, swollen hydrogel specimens were freeze dried in lyophilizer (Labconco CentriVap Gel Dryer System) for 6 h at -40 °C. Cross-sections of the freeze-dried gels were subjected to Pt-sputter coating and viewed with a field emission SEM (Zeiss 1530 VP FE-SEM) at accelerated electron energy of 5 keV and 15 keV.

Equilibrium Swelling

For equilibrium swelling measurements, three hydrogel discs of constant dimension (13 mm diameter, 1.5 mm thickness) were prepared as above. Hydrogel equilibrium swelling ratio is defined as: s*welling ratio* $= (W_s - W_d)/W_d$, where W_s is the

weight of the water-swollen hydrogel at a certain temperature and W_d is the weight of the vacuum dried hydrogel (30 in. Hg, 60 ºC, 24 h). Each disc was sealed inside a vial containing 20 mL DI water, immersed in a temperature controlled water bath for 24 h at the designated temperature (10 to 50 °C), removed, blotted with filter paper to remove surface water, and weighed (W_s).

Volume Phase Transition Temperature (VPTT)

VPTT of swollen hydrogels were determined by differential scanning calorimetry (DSC, TA Instruments Q100). Water-swollen hydrogels were blotted with filter paper and a small piece sealed in a hermetic pan. After cooling to -50 °C, the temperature was increased to 50 ºC at a rate of 3 ºC/min for 2 cycles. The resulting exothermic phase transition peak is characterized by the initial temperature at which the exotherm starts (T_o), the peak temperature of the exotherm (T_{max}) and the enthalpy change (ΔH) of the phase transition. Data reported is from the 2nd cycle.

Dynamic Mechanical Analysis (DMA)

DMA of hydrogels were measured in the compression mode with a dynamic mechanical analyzer (TA Instruments Q800) equipped with parallel-plate compression clamp with a diameter of 40 mm (bottom) and 15 mm (top). Swollen hydrogel discs of constant dimension (13 mm diameter, 1.5 mm thickness) were punched from a hydrogel sheet and clamped between the parallel plates. Silicone oil was then placed around the exposed edges of the hydrogel to prevent dehydration. Following equilibration at the 25

°C (5 min), the samples were tested in a multi-frequency-strain mode (1 to 100 Hz) at the temperature of 25 °C (below the VPTT). Results reported are based on the average of five individual specimens.

Tensile Test

Tensile tests of hydrogels ring specimens were measured on a TA Instruments DMA Q800 operating in the tension mode. Specimens with a ring geometry were prepared by cutting a portion from a hydrogel tube produced from the double wall tubular mold (ID = 3 mm, OD = 7.5 mm). Individual rings (~3 mm width) were cut from the central portion of the appropriate hydrogel tube using a clean razor blade and sample dimensions measured with an electronic caliper. Each hydrogel ring was blotted with filter paper and loaded onto custom aluminum bars gripped directly into DMA tension clamps so that the upper and lower bars were located inside the ring. Samples were subjected to a constant strain (1 mm/min) until they broke at the center of one side of the ring. Stress was calculated from the measured force divided by the cross-sectional area of two rectangles with sides equal to the width and wall thickness of the ring. The gauge length corresponded to the outer diameter of the ring less the wall thickness. The following parameters were determined: (1) tensile modulus, (2) ultimate tensile strength (UTS), and (3) % strain at break. The tensile modulus was obtained from the slope of the linear part of the stress-strain curve. The UTS represents the maximum stress prior to failure. Strain was calculated from the measured displacement divided by the gauge

length. Results reported are the average result of three specimens cut from central portion of the same hydrogel tube.

Contact Angle Measurements

The temperature-dependent surface properties of the hydrogels were determined by measuring static contact angles (θ_{static}) of sessile of distilled/DI water droplets (10 μL) with a KSV Instruments CAM-200 contact angle measurement system equipped with an autodispenser, video camera, and KSV CAM drop-shape analysis software. θ_{static} was measured at 10 and 25 °C (below VPTT) and at 40 °C (above VPTT). Hydrogel sheets (1.5 mm thick) were immersed in a temperature controlled water bath and equilibrated at the designated temperature (~30 min). The hydrogel was removed from the water bath, gently blotted with Kim Wipes to remove surface water, and placed on a pre-set thermostatted stage to maintain the designated temperature during the measurements. After every measurement, the hydrogel was re-immersed in the water bath for 30 min and the process repeated. Values were obtained 1 min after deposition of the water droplet. The reported θ_{static} value is the average of ~6 measurements.

Temperature-dependent Cell Release

Hydrogel sheets **(a-e)** were prepared as above under sterile conditions. A "PEO-RGDS" hydrogel was prepared from poly(ethylene oxide)-diacrylate (PEO-DA, M_n = 6000 g/mol) containing the acrylate-derivatized cell adhesion peptide RGDS (acryoyl-PEO-RGDS). Preparation of PEO-DA and acryloyl-PEO-RGDS are described elsewhere

[95]. Photoinitiator solution (10 μL of 30 wt% solution of DMAP in NVP) was added for every one mL of aqueous solution containing 10 wt% PEO-DA macromers and 1 μmol/mL acryoyl-PEO-RGDS in PBS. The PEO-DA and PNIPAAm-based precursor solutions were each cured between two glass sheets separated by 0.5 mm polycarbonate spacers by exposure to 365 nm UV light (UV-Transilluminator, 6 mW/cm^2) for 2 min. All hydrogel formulations were permitted to swell for two days in phosphate-buffered saline (PBS; pH = 7.4) with daily PBS changes to remove hydrogel impurities. Swollen hydrogel discs of constant dimension (9 mm diameter, 0.5 mm thickness) were punched from each hydrogel sheet and transferred to a 24 well plate containing media in each well. The plate was then incubated at 37 °C (above VPTT) for 2 h to force PNIPAAm-based hydrogels (**a-e**) into a deswollen, hydrophobic state and to equilibrate the hydrogels with the cell culture media. Mouse smooth muscle precursor cells (10T1/2) were seeded onto each hydrogel surfaces at 25,000 cells/cm^2. After incubation at 37 °C for 4 h, the 24 well plate was transferred to a Zeiss Axiovert A200 microscope and air-cooled to 25 °C (below VPTT) at a rate of ~ 2 ºC/min thereby causing **a-e** to swell. The well plate was then transferred back to a 37 °C incubator for 4 h and a second cooling cycle was similarly performed. For each cooling cycle, images were captured at two second intervals.

Photo-patterning

Microscope glass slide onto which hydrogel micropatterns are formed was cleaned by soaking in Piranha solution (H_2O_2 and concentrated H_2SO_4; 1:3 vol:vol) for

10 min, followed by thorough washing with DI water and blow drying with N_2 gas. Another glass slide working as a cover was cleaned with acetone and isopropanol followed by thoroughly washing with DI water. Aqueous precursor solutions for pure PNIPAAm hydrogel (**a**) and for nanocomposite hydrogel **c** (containing 1 wt% nanoparticles) were each pipetted in between the two cleaned glass slides separated by a 100 μm thick spacer. A mask with 100 or 200 μm diameter circular patterns was placed on top of the Piranha cleaned glass slide of the sandwiched structure. The entire structure was immersed into an ice water bath (~7 °C) and exposed to longwave UV light (Omnicure Series 1000, 15 mW/cm^2, 365 nm) for 40 sec. After removing the slide and mask from one side of the sandwich structure, unpolymerized solution was carefully washed out with DI water. SEM images of the glass-bound hydrogel micropillars (**a**, **c**) were captured following air-drying and Pt-sputter coating (Zeiss 1530 VP FE-SEM, accelerated electron energy of 5 keV).

3.4 Materials

Octamethylcyclotetrasiloxane (D_4), 1,3,5,7-tetramethyl-1,3,5,7-tetravinylcyclo-tetrasiloxane (D_4^{Vi}), and silicone oil (trimethylsiloxy terminated PDMS; viscosity = 1000 cSt.) were purchased from Gelest Inc. Dodecylbenzensulfonic acid (DBSA, BIO-SOFT® S-101) was received from Stepan Co.. Potassium persulfate ($K_2S_2O_8$), *N*-isopropyl-acrylamide (NIPAAm, 97%), 2,2-dimethyl-2-phenyl-acetophenone (DMAP), *N*-vinyl-pyrrolidone (NVP) were purchased from Aldrich. *N,N'*-methylenebisacrylamide (BIS, 99%) was obtained from Acros Organics. 1-[4-(2-Hydroxyethoxy)-phenyl]-2-hydroxy-2-

methyl-1-propane-1-one (Irgacure® 2959) was obtained from Ciba. All reagents were used as received. Mouse smooth muscle precursor cells (10T1/2) were obtained from American Type Culture Collection (ATCC).

3.5 Preparation of Nanocomposite Hydrogels

Nanocomposite hydrogels were prepared by *in situ* photopolymerization of aqueous precursor solutions containing NIPAAm monomer, BIS crosslinker, Irgacure-2959 photoinitiator, and crosslinked polysiloxane nanoparticles (Fig. 3.1). In a 50 mL rb flask equipped with a Teflon-covered stir bar, NIPAAm (1.0 g, 8.84 mmol), BIS (0.02 g, 0.13 mmol), and Irgacure-2959 (0.08 g, 0.36 mmol) were dissolved in DI water (the total volume equal to 7 mL including the volume of water introduced later by the nanoparticle emulsion) and the solution stirred under N_2 for 15 min. Finally, the appropriate amount of emulsion containing crosslinked colloidal nanoparticles was added and the mixture stirred for 10 min under N_2. In total, four different hydrogel compositions were prepared with varying amounts of colloidal nanoparticles: **(a)** pure NIPAAm (no nanoparticles; a control), **(b)** 0.5 wt%, **(c)** 1.0 wt%, **(d)** 1.5 wt%, and **(e)** 2.0 wt% (wt % solids of nanoparticles with respect to total precursor solution wt).

Hydrogel sheets (1.5 or 0.5 mm thick) were prepared by first pipetting a precursor solution between two clamped glass microscope slides (75 x 50 mm) separated by polycarbonate spacers of appropriate thickness. The mold was submerged in an ice water bath (~7 °C) and exposed to longwave UV light (UV-Transilluminator, 6 mW/cm^2, 365 nm) for 30 min. After removal from the mold, the hydrogel sheet was

rinsed with DI water and then soaked in DI water for 2 days with daily water changes to remove impurities. Hydrogel sheets (1.5 mm thick) were used to prepare samples for morphological, VPTT, swelling, mechanical, and contact angle studies. Hydrogel sheets (0.5 mm thick) were used for cell-release studies.

For tensile tests, hydrogels were prepared with a "ring" geometry. First, hydrogels were prepared in a hollow tube geometry with a double walled tubular mold composed of an inner glass mandrel (diameter = 3 mm) and an outer glass cylinder (diameter = 7.9 mm). The tubular mold was filled with a precursor solution and cured while submerged in an ice water bath (~7 °C) for 30 min under constant rotation such that each surface point of the mold received equal UV intensity and exposure time. The hydrogel tube was removed from the mold and similarly purified as above by rinsing and soaking in DI water. Cutting the resulting hydrogel tube into ~3 mm wide pieces afforded hydrogel ring specimens.

3.6 Results and Discussion

Preparation of Crosslinked Polysiloxane Colloidal Nanoparticles

Polysiloxane colloidal nanoparticles were prepared by cationic ring-opening emulsion polymerization of D_4 and D_4^{Vi} using DBSA as an inisurf (i.e. an initiator and surfactant) (Fig. 3.1) [160]. From the non-crosslinked nanoparticles was isolated linear copoly(dimethylsiloxane/methylvinylsiloxane) (M_w/M_n = 67,200/36,500 g/mol). Based on ^{1}H NMR analysis, the ratio of dimethylsiloxane and methyvinylsiloxane repeat units is 4 to 1. The colloidal nanoparticles were subsequently crosslinked via free radical

reaction between of the vinyl groups. Surfactant and other reaction impurities were removed from the resultant emulsion via dialysis. This process yielded polysiloxane colloidal nanoparticles having an average diameter of 219 nm (PD = 0.10) with particles ranging in size from 106 to 531 nm.

Preparation of Nanocomposite Hydrogels: Crosslinking and Morphology

Nanocomposite hydrogels (**b-e**) were prepared by photopolymerization aqueous mixtures of NIPAAm monomer, BIS crosslinker, Irgacure-2959 photoinitiator, and crosslinked colloidal polysiloxane nanoparticles ~7 °C for 30 min (Fig. 3.1). PNIPAAm hydrogels are typically formed by the free radical crosslinking copolymerization of aqueous solutions of NIPAAm and BIS using redox initiators which typically relies inert environments, elevated temperatures, and/or long reaction times [108, 163-166]. Thus, photopolymerization was utilized herein to prepare PNIPAAm nanocomposite hydrogels more rapidly with a 30 min cure time [167-169]. Although NIPAAm may be photocrosslinked in the absence of a crosslinker (e.g. BIS), it may produce elevated sol content [170]. With increasing PDMS nanoparticle content, the aqueous precursor solutions became increasingly opaque which may block the transmission of UV-light and diminish extent of crosslinking. However, following Soxhlet extraction, hydrogels containing 2 wt% nanoparticles (**d**) and pure PNIPAAm hydrogel **(a)** both exhibited no detectable weight loss (<0.1 wt%). Thus, photopolymerization effectively produced nanocomposite hydrogels without significant amounts of non-reacted NIPAAm.

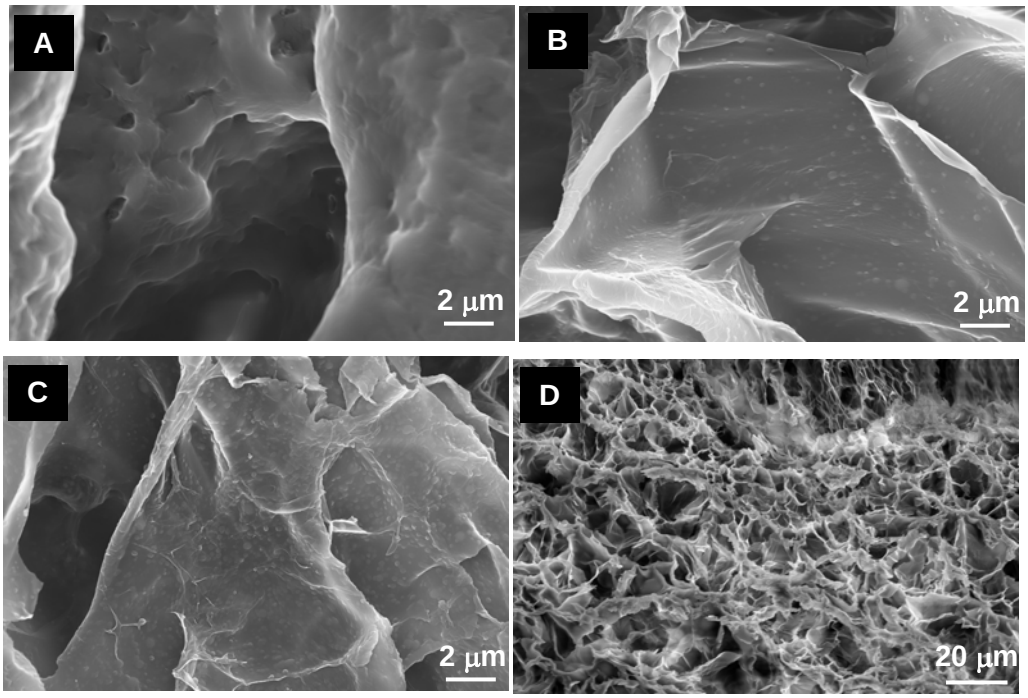

Figure 3.2. SEM micrographs of **(A)** pure PNIPAAm hydrogel **a**; **(B)** nanocomposite hydrogel **b** (containing 0.5 wt% nanoparticles); **(C)** nanocomposite hydrogel **e** (containing 2.0 wt% nanoparticles); **(D)** nanocomposite hydrogel **b**.

The preparation temperatures (T_{prep}) at which PNIPAAm hydrogels are formed has been shown to impact their chemical and physical properties by altering hydrogel morphology [171-176]. PNIPAAm hydrogels formed at T_{prep} < 20 °C are morphologically homogeneous whereas those formed at higher temperatures are heterogeneous. At T_{prep} > ~ 20 °C, newly formed insoluble PNIPAAm chains phase separate such that subsequent crosslinking leads to the formation of a macroscopic network of loosely interconnected highly crosslinked polymer rich domains and lightly crosslinked polymer poor domains. As a result, heterogeneous PNIPAAm hydrogels are opaque whereas homogeneous hydrogels are transparent. Heterogeneous PNIPAAm hydrogels display higher swelling ratios but are mechanically weaker compared to the

corresponding homogeneous hydrogel [174-176]. Thus, to optimize mechanical strength of the nanocomposite hydrogels, photopolymerization was conducted at ~7 °C to obtain nanocomposite hydrogels consisting of a homogeneous PNIPAAm matrix with embedded nanoparticles. The homogeneity of the PNIPAAm hydrogel matrix is confirmed by the optically transparent nature of the pure PNIPAAm hydrogel (**a**, no nanoparticles). Freeze-drying (i.e. lyophilization) is known to preserve the structure and volume of swollen hydrogels even after all (or almost all) solvent is removed [177]. SEM micrographs of lyophilized nanocomposite hydrogels revealed that all demonstrated a uniform porous morphology characteristic of homogeneous PNIPAAm hydrogels. Representative SEM images are shown in Fig. 3.2 [176].

Equilibrium Swelling

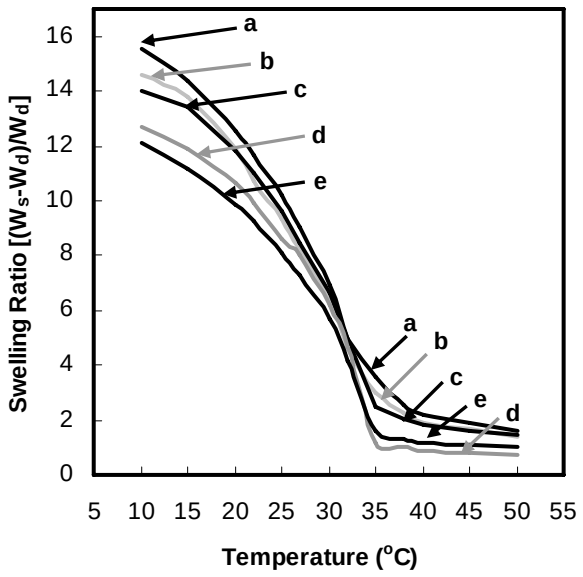

Figure 3.3. Equilibrium swelling ratio of nanocomposite hydrogels containing 0.5-2.0 wt% nanoparticles (**b-e**) and pure PNIPAAm hydrogel control (**a**).

Equilibrium swelling of the hydrogels (**a-e**) was measured gravimetrically from 10 to 50 °C to determine temperature sensitivity. The shift from a water swollen to a deswollen state occurs at ~ 33-35 °C for all hydrogels (**a-e**) (Fig. 3.3). Thus, the presence of hydrophobic polysiloxane nanoparticles did not alter the VPTT of nanocomposite hydrogels (**b-e**) versus the pure PNIPAAm hydrogel (**a**) because of their chemically independent nature within the PNIPAAm matrix. The magnitude of change from a swollen to deswollen state of the hydrogels decreased with increased levels of polysiloxane nanoparticles in the order: **a** (0 wt%) > **b** (0.5 wt%) > **c** (1.0 wt%) > **d** (1.5wt%) > **e** (2.0 wt%). Below the VPTT, increased levels of polysiloxane nanoparticles produced a decrease in equilibrium swelling. However, above the VPTT, increased levels of nanoparticles led to slightly more deswelling. Similar observations were made for PNIPAAm/PDMS semi-IPNs as the PDMS content increased [148] or for PNIPAAm/silica hydrogel composites as silica content increased [149-151]. The reduced swelling of nanocomposite hydrogels may be attributed to their increased hydrophobicity and subsequent reduced water uptake caused by incorporation of hydrophophobic polysiloxane nanoparticles.

Volume Phase Transition Temperature (VPTT)

PNIPAAm hydrogels exhibit a significant endothermic effect during the volume phase transition due to breaking of hydrogen bonds between water molecules surrounding hydrophobic moieties on the polymer [166, 178]. The VPTT is typically designated by either the onset (T_o) or maximum temperature (T_{max}) of the endothermic peak [167, 179-181].

Table 3.1. Thermal transition properties of nanocomposite hydrogels (**b-e**) and pure PNIPAAm hydrogel control (**a**).

	Composition	Volume Phase Transition Temperature (VPTT)		
Hydrogel	Solid wt% nanoparticles	T_o (°C)	T_{max} (°C)	ΔH (J/g)
a	0	33.3	35.7	3.96
b	0.5	33.2	35.7	3.83
c	1.0	33.3	35.8	4.14
d	1.5	33.3	35.8	3.79
e	2.0	33.5	36.0	3.71

Table 3.2. Surface properties of nanocomposite hydrogels (**b-e**) and pure PNIPAAm hydrogel control (**a**).

	Composition	Static Contact Angle		
Hydrogel	Solid wt% nanoparticles	θ_{static} (°) @ 10 °C	θ_{static} (°) @ 25 °C	θ_{static} (°) @ 40 °C
a	0	50.6 ± 0.4	61.1 ± 3.1	69.2 ± 2.0
b	0.5	53.1 ± 1.9	60.7 ± 1.5	72.4 ± 1.2
c	1.0	54.0 ± 1.7	62.8 ± 1.5	75.7 ± 0.2
d	1.5	57.3 ± 0.4	68.1 ± 0.6	75.8 ± 2.0
e	2.0	60.7 ± 1.1	69.7 ± 1.4	77.7 ± 0.7

The VPTT and transition enthalpy (ΔH) values of the nanocomposite hydrogels (**b-e**) and PNIPAAm control (**a**) were determined by their respective DSC thermograms of swollen hydrogel specimens (Fig. 3.4, Table 3.1 and 3.2). T_o values were determined from the intersecting point between two tangent lines from the baseline and slope of the endothermic peak [180]. The VPTT (T_{max} or T_o) of nanocomposite hydrogels (**b-e**) remained essentially unchanged relative to that of the pure PNIPAAm hydrogel (**a**). Similarly, the ΔH values of nanocomposite hydrogels were similar to that of the pure PNIPPAm hydrogel. This indicates that polysiloxane nanoparticles do not interfere with dissociation of water molecules from hydrophobic groups when heated above the VPTT

(Table 3.2). The endothermic peak of the nanocomposite hydrogels slightly broadened with increased polysiloxane particle content. Broadening of the endothermic peak of PNIPAAm-based hydrogels is an indicator of more gradual deswelling above the VPTT [151, 182].

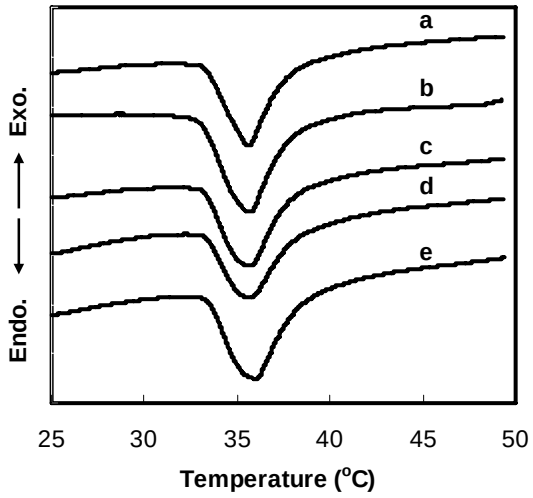

Figure 3.4. DSC thermograms for nanocomposite hydrogels (**b-e**) and pure PNIPAAm hydrogel (**a**).

Dynamic Mechanical and Tensile Properties

The mechanical properties of biomaterials such as hydrogels directly affect their utility and performance. Because of their frequent use to measure hydrogel mechanical properties, both dynamic mechanical analysis (DMA) and tensile tests were utilized in this study [98, 183, 184]. Mechanical properties of hydrogels in a swollen state are most relevant to their end-use applications. However, mechanical testing of swollen hydrogels is challenging because the difficulty maintaining hydration and their high water content/low polymer mass to unit volume make them mechanically weak and difficult to

handle. Thus, during DMA, silicone oil was placed around the hydrogel disc specimen sandwiched between two compression clamps to inhibit water loss. Tensile testing of flat, rectangular hydrogel specimens with ends secured in tension grips is often complicated by sample slippage from or breakage at the grip. Thus, specimens with a ring geometry were employed to minimize slippage/breakage for improved accuracy [48]. Ring specimens also allowed their rapid mounting on tensile bars so that testing was completed before significant water loss occurred.

In DMA, the measured storage modulus (G') is related to a materials stiffness or resistance to deformation [185]. At all frequencies (1 -100 Hz), the G' of the nanocomposite hydrogels (**b-e**) were higher than that of the pure PNIPAAm hydrogel (**a**) and increased with higher levels of polysiloxane nanoparticles (Fig. 3.5). These differences in G' became more pronounced as the frequency was increased. Nanocomposite hydrogels (**b-e**) also generally showed an increase in tensile modulus and ultimate tensile strength (UTS) with increased polysiloxane nanoparticles content (Table 3.3). The degree of hydrogel swelling is directly related to its mechanical properties and many methods to improve mechanical strength are designed to reduce swelling [98]. Thus, the increase in nanocomposite hydrogel G', tensile modulus, and UTS with increasing amounts of nanoparticles is at least partially attributed to reduced water content at 25 °C (Fig. 3.3). For PNIPAAm and other hydrogels, lower water content levels typically also results in a reduction in % strain at break [186]. However, percent strain at break was observed to generally increase with nanoparticle levels. Higher % strain at break values coupled with higher tensile modulus and UTS values of

nanocomposite hydrogels indicate the enhanced mechanical properties is due in part to the reinforcement of PNIPAAm matrix by the polysiloxane nanoparticles.

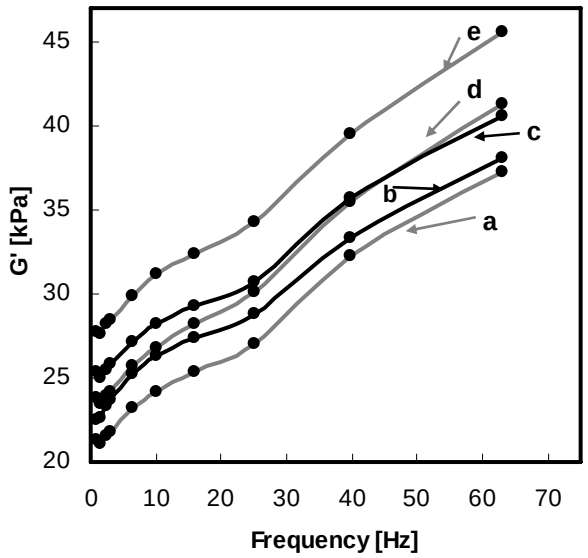

Figure 3.5. Storage modulus (G') of nanocomposite hydrogels (**b-e**) and pure PNIPAAm hydrogel (**a**) measured in the compression mode.

Table 3.3. Tensile properties of nanocomposite hydrogels (**b-e**) and pure PNIPAAm hydrogel control (**a**).

	Composition	**Tensile Properties**		
Hydrogel	**Solid wt% nanoparticles**	Modulus (kPa)	UTS (kPa)	% strain at break
a	0	14.5 ± 1.6	6.7 ± 1.5	50.4 ± 7.7
b	0.5	16.5 ± 1.0	9.8 ± 1.2	62.1 ± 3.7
c	1.0	15.6 ± 0.6	9.5 ± 0.5	64.3 ± 1.9
d	1.5	15.1 ± 2.1	10.9 ± 1.5	75.1 ± 4.5
e	2.0	17.4 ± 1.5	10.8 ± 1.3	69.6 ± 3.7

Temperature-dependent Surface Properties

Contact angle values of PNIPAAm surfaces vary according to the specimen preparation and goniometric technique used with most studies reported conducted on surface-grafted PNIPAAm [187, 188]. Herein, hydrogel sheets were carefully equilibrated in a water bath at the designated temperature for 30 min before each measurement and surface water removed by gentle blotting with filter paper. This process was designed to prevent inconsistency in hydrogel hydration and temperature which could lead to erroneous measurements. Surfaces of plasma polymerized PNIPAAm hydrogel thin films on silicon surfaces exhibited a dramatic increase in hydrophobicity when the temperature was increased from ~10 to ~25 °C, well before the VPTT [189]. Thus, we measured θ_{static} of water droplets at 10 and 25 °C (below VPTT) and at 40 °C (above VPTT) (Table 3.2). As expected, for a given composition, hydrogel surface hydrophobicity increased (i.e. θ_{static} increased) as the temperature increased. Surface hydrophobicity significantly increased between 25 and 40 °C as well as between 10 and 25 °C. As the amount of hydrophobic polysiloxane nanoparticles was increased, surface hydrophobicity of **b-e** increased at all temperatures. The average increase in θ_{static} was ~18 ° for all hydrogels when heated from 10 to 40 °C.

Temperature-Dependent Cell Release Behavior

The ability of nanocomposite hydrogels to release mouse smooth muscle precursor cells (10T1/2) from their surfaces was assessed by examining cell morphology before and after thermal cooling. A PEO-RGDS hydrogel served as a control as it is non-

thermoresponsive but cell-adhesive [190]. Since cells grow well on more hydrophobic surfaces, cells were cultured on hydrogels at 37 °C (above the VPTT). It was observed that more cells adhered to the nanocomposite hydrogels (**b-e**) compared to the pure PNIPAAm hydrogel (**a**) which may be explained by the higher hydrophobicity of **b-e** (Table 3.2). Cooling from 37 °C (above VPTT) to 25 °C (below VPTT) forced the PNIPAAm-based hydrogels (**a-e**) to swell and become more hydrophilic (Table 3.2). The media within each well containing the hydrogel disc provided water for the swelling process. After the first cooling cycle, a round cell morphology indicative of end stages of cell detachment was observed for cells on **a-e**. Time-lapsed images of cell detachment from nanocomposite hydrogel **e** (containing 2 wt% nanoparticles) are shown in Fig. 3.6. In contrast, cells on the PEO-RGDS hydrogel control maintained an extended morphology indicative of cell adhesion and spreading. Following a subsequent second heating-cooling cycle, the round morphology was even more pronounced on **a-e** (Fig. 3.7).

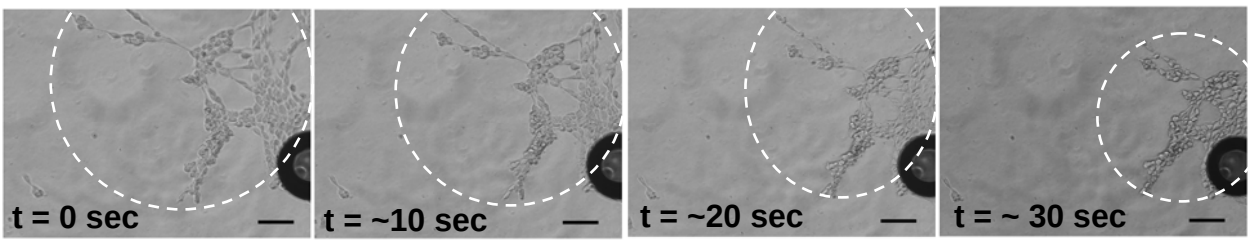

Figure 3.6. Time-lapsed images of a mouse smooth muscle precursor cells (10T1/2) on hydrogel **e** (containing 2 wt% nanoparticles) during first cooling cycle from 37 °C to 25 °C. The cell cluster collapses as individual cells switch from an extended morphology to a round morphology as they detach during the hydrogel swelling induced by cooling. All scale bars are 100 μm. Dashed white line encircles cell cluster. Dark circle is a bubble.

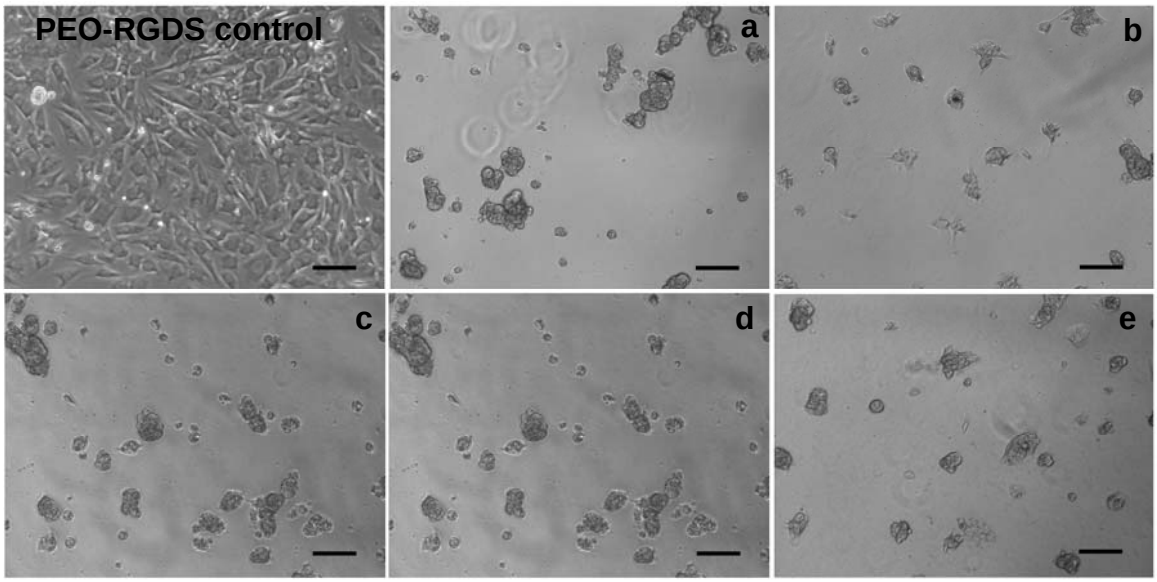

Figure 3.7. Mouse smooth muscle precursor (10T1/2) cells displayed a rounded morphology indicative of detachment on hydrogels **a-e** following two cycles of thermal cooling from 37 °C to 25 °C. A PEO-RGDS hydrogel served as a cell-adhesive but non-thermoresponsive control. All scale bars are 100 μm.

Photopatterning

Given the interest in photopatterning of PNIPAAm hydrogels, we evaluated the utility of this technique for nanocomposite hydrogels. Direct photopolymerization with a photolithography mask having 100 or 200 μm diameter circular patterns successfully produced surface micropillars of nanocomposite hydrogel **c** (containing 1 wt% nanoparticles) and the pure PNIPAAm hydrogel control (**a**) (Fig. 3.8). Because the samples were dried for SEM, the micropillars exhibit diameters of less than 100 μm and 200 μm respectively. This initial study demonstrates the utility of photopatterning to prepare microstructures with nanocomposite hydrogels for targeted applications.

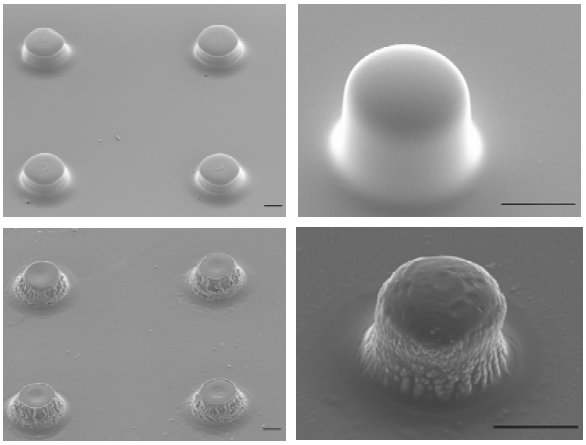

Figure 3.8. SEM micrographs of micropillar structures of pure PNIPAAm hydrogel (**a**) [top row] and nanocomposite hydrogel (**c**, containing 1.0 wt% nanoparticles) [bottom row]. Micropillars were prepared by direct photopolymerization with a photolithography mask having 200 μm circular patterns [left column] and 100 μm circular patterns [right column]. All scale bars are 50 μm.

3.7 Conclusions

Novel thermoresponsive composite hydrogels comprised of a PNIPAAm hydrogel matrix and polysiloxane colloidal nanoparticles (~220 nm ave. diameter) were prepared via *in situ* photopolymerization of aqueous solutions of NIPAAm monomer, BIS crosslinker, photoinitiator and polysiloxane nanoparticles (0.5 to 2.0 wt% based on solution weight) at ~7 °C. Due to the low preparation temperature, the nanocomposite hydrogels exhibited a homogeneous morphology confirmed by SEM analysis. The equilibrium swelling of nanocomposite hydrogels was reduced with increased levels of polysiloxane nanoparticles. Because the nanoparticles exist as a chemically independent phase, the VPTT of the nanocomposite hydrogels is not altered compared to pure PNIPAAm hydrogels. Increasing the nanoparticle content generally led to an increase in storage modulus (G'), tensile modulus, ultimate tensile strength (UTS), and % strain at

break of the nanocomposite hydrogels. An increase in surface hydrophobicity was marked by an increase of θ_{static} by ~18 ° upon heating from 10 °C (below VPTT) to 40 °C (above VPTT) for nanocomposite hydrogels (**b-e**) and pure PNIPAAm hydrogel (**a**). Nanocomposite hydrogels became increasingly more hydrophobic at all temperatures as the amount of hydrophobic polysiloxane nanoparticles was increased. When cooled from 37 °C to 25 °C, mouse smooth muscle precursor (10T1/2) cells were shown to effectively detach from nanocomposite hydrogel surfaces. Finally, the ability for these nanocomposite hydrogel formulations to be photopatterned was demonstrated.

CHAPTER IV

TRANSPARENT THERMORESPONSIVE NANOCOMPOSITE HYDROGELS WITH CELL-RELEASING BEHAVIOR

4.1 Overview

Poly(*N*-isopropylacrylamide) (PNIPAAm) hydrogels become more hydrophobic when they reversibly switch from a water-swollen to a deswollen state above the volume phase transition temperature (VPTT, ~ 33 °C) which has been used to modulate cell adhesion. In the current work, we prepared novel transparent thermoresponsive nanocomposite hydrogels comprised of a PNIPAAm hydrogel matrix and polysiloxane colloidal nanoparticles (~54 nm ave. diameter) via *in situ* photopolymerization of aqueous solutions of NIPAAm monomer, *N,N'*-methylenebisacrylamide (BIS, crosslinker), photoinitiator and polysiloxane nanoparticles (0.5 to 4.0 wt% based on solution weight) at ~7 °C. Compared to previous studies of similar hydrogels containing larger polysiloxane nanoparticles (219 nm ave. diameter), these hydrogels were optically clear. The VPTT of the nanocomposite hydrogels is not altered versus the pure PNIPAAm hydrogel. When cooled from 37 °C to 25 °C, mouse smooth muscle precursor cells (10T1/2) were effectively detached from nanocomposite hydrogel surfaces due to hydrogel swelling.

4.2 Introduction

Hydrogels which reversibly switch from a hydrophilic/swollen to hydrophobic/deswollen state in response to an external stimulus are of interest for creating "smart" or "intelligent" biomedical materials [103]. Thermoresponsive hydrogels are crosslinked, three dimensional polymer networks that reversibly swell with and then expel aqueous media in response to temperature changes. Thermoresponsive hydrogels may be prepared by crosslinking polymers which exhibit a lower critical solubility temperature (LCST) [103, 104]. Most widely studied is poly(*N*-isopropylacrylamide) (PNIPAAm) (LCST, ~32 °C) which is soluble in water below the LCST and reversibly insoluble above the LCST [105]. Crosslinked PNIPAAm hydrogels undergo a reversible volume phase transition in water from a swollen state to a deswollen state above their volume phase transition temperature (VPTT; ~33 °C) [106, 107]. Thus, surfaces of PNIPAAm hydrogels [108-110] as well as those comprised of covalently grafted PNIPAAm chains [110-112] undergo a large discontinuous change from a hydrophilic to a hydrophobic state when heated above the phase transition temperature.

The thermal modulation of PNIPAAm hydrogels has been shown to be useful for the controlled detachment of cultured cells *in vitro* [113, 114]. In this way, confluent cell sheets useful for tissue engineering may be detached from culture without enzymes or chelating agents known to damage cells [115]. Cell adhesion is diminished not only by physical changes of the surface (i.e. swelling/deswelling) but also by changes in surface properties. Often characterized by contact angle measurements, polymer surfaces

displaying water contact angles greater than 90° are generally considered to be hydrophobic [125]. Several studies have shown that cell adhesion is maximized on moderately hydrophobic surfaces displaying a water contact angle between 40 and 70° [2, 120-124]. Thus, at ~ 37 °C (above the LCST), PNIPAAm-grafted surfaces are relatively hydrophobic and various types of cells grow well. However, upon cooling below 32 °C (below the LCST), they become more hydrophilic and cells spontaneously detach without damaging the cells [126-130]. Similarly, cells may be detached from the surfaces of PNIPAAm hydrogels after cooling below the VPTT [131, 132].

The focus of this work herein is extending the utility of PNIPAAm hydrogels as robust "self-cleaning" implanted sensor membranes [136, 137]. Membrane biofouling is considered to be a leading cause of sensor failure as adhered proteins and cells diminish the diffusion of the target analyte (e.g. glucose) to the sensor [22]. Because sensors are often based on optical or fluorescent signals, a membrane which is also transparent is desirable. Our concept of a self-cleaning sensor membrane prepared from a thermoresponsive nanocomposite hydrogel material is depicted in Fig. 4.1. The nanocomposite hydrogel sensor membrane will remove cells that accumulate on its surface via periodic thermal modulation. In this figure, the "self-cleaning" mechanism is accomplished through deswelling although cells may also be released via swelling as demonstrated herein. This "self-cleaning" membrane will enable a glucose biosensor to remain implanted for longer periods of time without compromising glucose-sensing sensitivity.

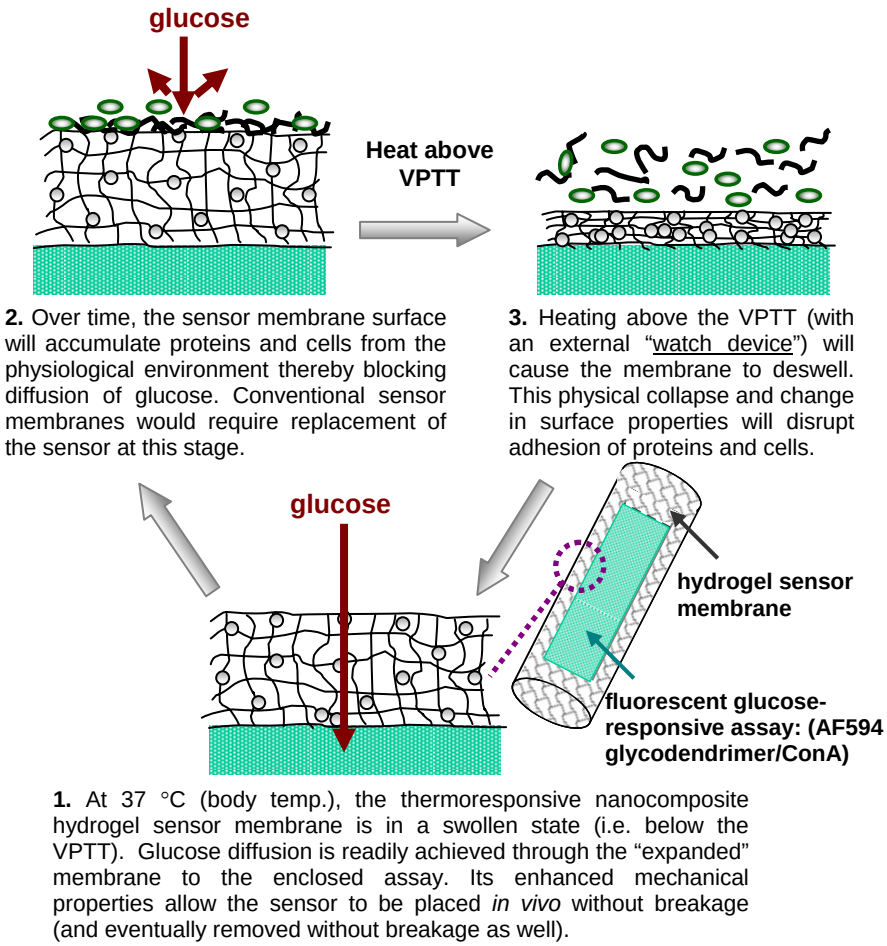

Figure 4.1. Thermal modulation of the thermoresponsive nanocomposite hydrogel sensor membrane will regulate the self-cleaning process.

Transparent thermoresponsive nanocomposite hydrogels were prepared consisting of an organic PNIPAAm hydrogel matrix and variable levels of inorganic polysiloxane nanoparticles (Fig. 4.2). Here, polysiloxane nanoparticles (diameter = ~54 nm) were prepared from anionic emulsion polymerization of octamethyl-cyclotetrasiloxane (D_4) and 1,3,5,7-tetramethyl-1,3,5,7-tetravinylcyclotetrasiloxane (D_4^{Vi}). The resulting nanoparticles were subsequently stabilized by free radical crosslinking the copoly(dimethylsiloxane/methylvinylsiloxane) chains inside the

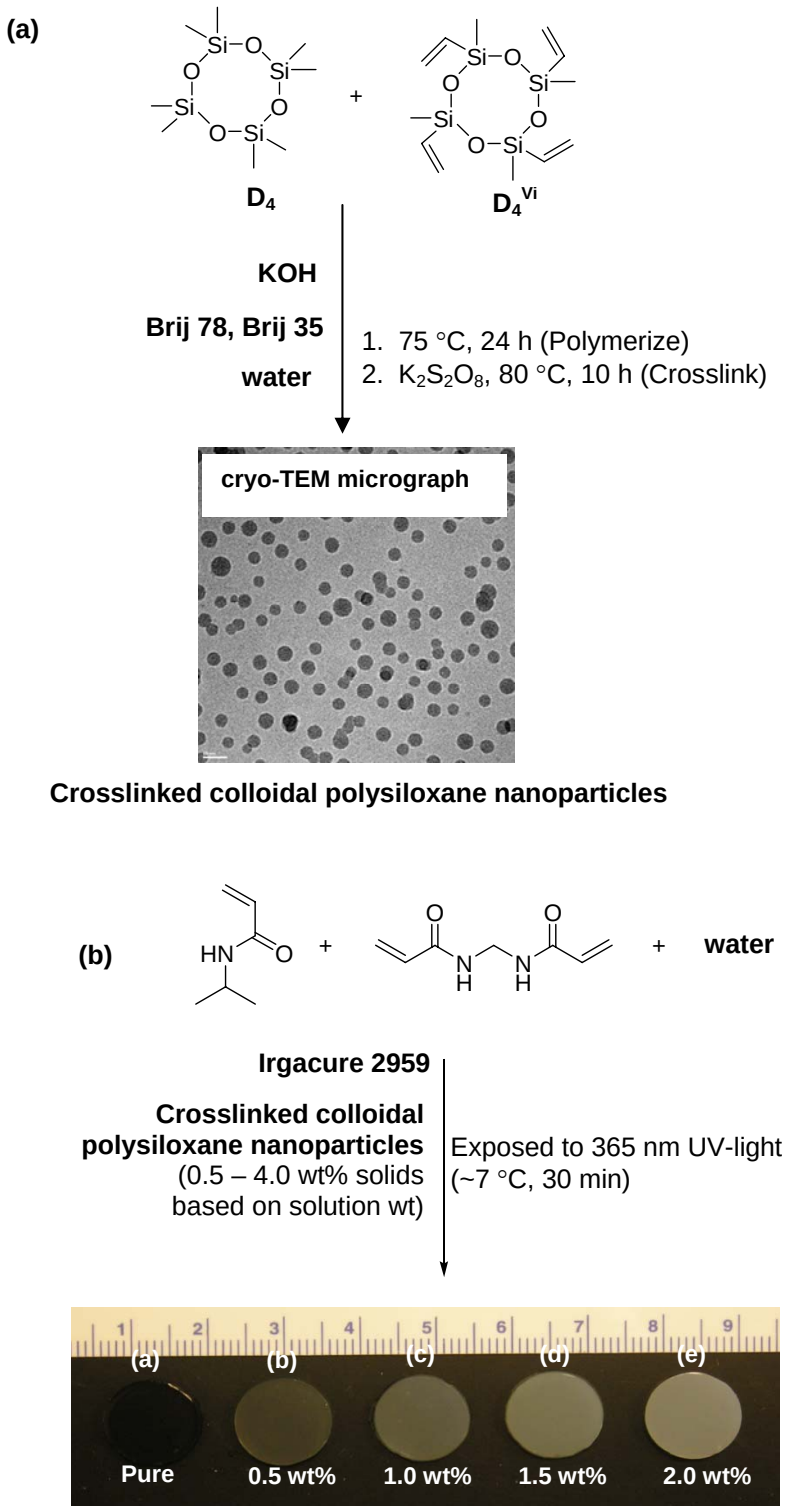

Figure 4.2. **(a)** Preparation of colloidal polysiloxane nanoparticles via emulsion polymerization and subsequent crosslinking and **(b)** preparation of thermoresponsive nanocomposite hydrogels with variable wt% nanoparticles (based on total solution weight).

nanoparticles. Crosslinked polysiloxane nanoparticles (0.5 – 4.0 wt%) were introduced into aqueous solutions of NIPAAm, BIS (crosslinker), and photoinitiator and subsequently photopolymerized at low temperatures (~ 7 °C) to yield thermoresponsive nanocomposite hydrogels. The effect of polysiloxane nanoparticle content on hydrogel morphology, VPTT, mechanical properties as well as temperature-dependent swelling behavior, and cell release behavior are presented.

4.3 Experimental Section

Preparation of Crosslinked Polysiloxane Colloidal Nanoparticles

Polysiloxane colloidal particles were prepared by anionic emulsion olymerization of D_4 and D_4^{Vi} (Fig. 4.2). Into a 500 mL water-jacketed polymerization vessel equipped with a mechanical stirrer and Teflon stirring paddle, reflux condenser, and addition funnel, Brij 35 [$C_{12}H_{25}(OCH_2CH_2)_{23}OH$, Polyoxyethylene (23) lauryl ether] (6 g), Brij 78 [Polyoxyethylene (20) stearyl ether $C_{18}H_{37}(OCH_2CH_2)_{20}OH$] (13.5 g) and Tergitol [Polyglycol ether surfactant] (10.71 g,) were dissolved in deionized (DI) water (146.79 g). A mixture of D_4 (62.4 g, 210 mmol) and D_4^{Vi} (15.6 g, 45 mmol) was added dropwise via the addition funnel to the aqueous solution with constant stirring (300 rpm). Then, KOH aqueous solution (25 wt%) was added dropwise via the addition funnel. The resulting stable emulsion was then heated to 80 °C for 24 h with constant stirring (280 rpm). The final emulsion was cooled, filtered through a 10 μm filter bag, and the pH adjusted to 7 with aqueous acetic acid (25 wt%). The solid content of the emulsion was

determined by weight loss from an aliquot after drying (115 °C, 8 h). Emulsion solid content: 22.2 % (83 % conversion).

These colloidal nanoparticles were subsequently stabilized by crosslinking of the copoly(dimethylsiloxane/methylvinylsiloxane) chains within the nanoparticles via their vinyl groups (Fig. 4.2). The above final emulsion (50 g) was added to a 3-neck round bottom (rb) flask equipped with a Teflon-covered stir bar, reflux condenser, and nitrogen (N_2) inlet. After the addition of $K_2S_2O_8$ (0.5 g), the mixture was reacted at 80 ºC for 10 h under N_2. The emulsion was cooled and filtered through a 10 μm filter bag. The resulting colloidal nanoparticles were purified via dialysis (Slide-A-Lyzer ® Dialysis Cassette, MWCO = 10,000, Pierce Chemical Co.) against daily changes of DI water for 3 days. Emulsion solid content: 10.4%. Dynamic light scattering (DLS): 54 nm (average diameter) and 0.2 (polydispersity, PD).

Characterization of Polysiloxane Colloidal Nanoparticles

Particle size of colloidal nanoparticles was determined by dynamic light scattering (DLS) (Malvern Zetasizer® Nano S) with a detection angle of 90 º. Measurements were carried out at 25 °C. An aliquot of the designated emulsion was highly diluted with DI water just prior to measurement in order to rule out interaction and multiple scattering effects.

Cryogenic transmission electron microscopy (Cryo-TEM) was used to visualize the nanoparticles and confirm their lack of aggregation in water. A FEI-Q20 TEM,

operated at 120 kV and equipped with a Gatan 626 cryo holder, was used for imaging. Further details on sample preparation and imaging analysis were previously described.

Extent of Crosslinking

The amount of uncrosslinked material in select hydrogels was determined by weight loss following Soxhlet extraction. For a given hydrogel, three hydrogel discs (13 mm diameter, 1.5 mm thickness) were punched from a single hydrogel sheet with a die and immediately dried in a vacuum oven (30 in. Hg, 60 ºC, 24 h) and weighed. The dried discs were extracted with dichloromethane in a Soxhlet apparatus for 12 h and weighed after similarly drying in a vacuum oven. The percentage of uncrosslinked material was calculated as the average weight difference of the extracted versus unextracted weight divided by the unextracted weight.

Morphological Characterization

The morphology of hydrogels was studied by scanning electron microscopy (SEM). To retain their morphology, swollen hydrogel specimens were freeze dried in lyophilizer (Labconco CentriVap Gel Dryer System) for 6 h at -40 °C [68]. Cross-sections of the freeze-dried gels were subjected to Pt-sputter coating and viewed with a field emission SEM (Zeiss 1530 VP FE-SEM) at accelerated electron energy of 5 keV and 15 keV.

Kinetic Swelling

For swelling measurements, three hydrogel discs of constant dimension (13 mm diameter, 1.5 mm thickness) were prepared as above. For dynamic deswelling measurements, hydrogel water retention is defined as: $water\ retention = (W_t - W_d)/W_s$, where W_t is the mass of the wet hydrogel at 50 ºC. Each disc, sealed inside a vial containing 20 mL DI water, immersed in water bath for 24 h at 22 °C to get equilibrium. The equilibrated hydrogel discs were then quickly transferred into a 50 °C water bath. At 10, 20, 40 and 80 min, the samples were taken from the water bath and weighed after the excess water on the surfaces blotted with filter paper.

For dynamic swelling measurements, hydrogel water retention is defined as: $water\ uptake = (W_t - W_d)/W_s$, where W_t is the mass of the wet hydrogel at 50 ºC. Each disc was immersed in water bath for 4 h at 50 °C. The partly shrunk hydrogel discs were further dried in a vacuum oven at 60 °C overnight until the hydrogel reached a constant weight. After drying, the discs were then transferred into vials containing 20 ml DI water and placed into a water bath at 22 ºC. At 10, 20, 40, 80, 120, 200, 320, and 450 min, the samples were taken out of the water bath and the masses were recorded after blotting with filter paper.

Volume Phase Transition Temperature (VPTT)

VPTT of swollen hydrogels were determined by differential scanning calorimetry (DSC, TA Instruments Q100). Water-swollen hydrogels were blotted with filter paper and a small piece sealed in a hermetic pan. After cooling to -50 °C, the temperature was

increased to 50 ºC at a rate of 3 ºC/min for 2 cycles. The resulting exothermic phase transition peak is characterized by the initial temperature at which the exotherm starts (T_o), the peak temperature of the exotherm (T_{max}) and the enthalpy change (ΔH) of the phase transition. Data reported is from the 2nd cycle.

Dynamic Mechanical Analysis (DMA)

DMA of hydrogels were measured in the compression mode with a dynamic mechanical analyzer (TA Instruments Q800) equipped with parallel-plate compression clamp with a diameter of 40 mm (bottom) and 15 mm (top). Swollen hydrogel discs of constant dimension (13 mm diameter, 1.5 mm thickness) were punched from a hydrogel sheet and clamped between the parallel plates. Trimethylsiloxy terminated PDMS was then placed around the exposed edges of the hydrogel to prevent dehydration. Following equilibration at the 25 °C (5 min), the samples were tested in a multi-frequency-strain mode (1 to 100 Hz) at the temperature of 25 °C (below the VPTT). Results reported are based on the average of five individual specimens.

Tensile Test

Tensile tests of hydrogels ring specimens were measured on a TA Instruments DMA Q800 operating in the tension mode. Specimens with a ring geometry were prepared by cutting a portion from a hydrogel tube produced from the double wall tubular mold (ID = 3 mm, OD = 7.5 mm). Individual rings (~3 mm width) were cut from the central portion of the appropriate hydrogel tube using a clean razor blade and sample

dimensions measured with an electronic caliper. Each hydrogel ring was blotted with filter paper and loaded onto custom aluminum bars gripped directly into DMA tension clamps so that the upper and lower bars were located inside the ring. Samples were subjected to a constant strain (1 mm/min) until they broke at the center of one side of the ring. Stress was calculated from the measured force divided by the cross-sectional area of two rectangles with sides equal to the width and wall thickness of the ring. The gauge length corresponded to the outer diameter of the ring less the wall thickness. The following parameters were determined: (1) tensile modulus, (2) ultimate tensile strength (UTS), and (3) % strain at break. The tensile modulus was obtained from the slope of the linear part of the stress-strain curve. The UTS represents the maximum stress prior to failure. Strain was calculated from the measured displacement divided by the gauge length. Results reported are the average result of three specimens cut from central portion of the same hydrogel tube.

Temperature-dependent Cell Release

Hydrogel sheets **(a-f)** were prepared as above under sterile conditions. A "PEO-RGDS" hydrogel was prepared from poly(ethylene oxide)-diacrylate (PEO-DA, M_n = 6000 g/mol) containing the acrylate-derivatized cell adhesion peptide RGDS (acryoyl-PEO-RGDS) with standard procedures [191]. Photoinitiator solution (10 μL of 30 wt% solution of DMAP in NVP) was added for every one mL of aqueous solution containing 10 wt% PEO-DA macromers and 1 μmol/mL acryoyl-PEO-RGDS in PBS. The PEO-DA and PNIPAAm-based precursor solutions were each cured between two glass sheets

separated by 0.5 mm polycarbonate spacers by exposure to 365 nm UV light (UV-Transilluminator, 6 mW/cm^2) for 2 min. All hydrogel formulations were permitted to swell for two days in phosphate-buffered saline (PBS; pH = 7.4) with daily PBS changes to remove hydrogel impurities. Swollen hydrogel discs of constant dimension (9 mm diameter, 0.5 mm thickness) were punched from each hydrogel sheet and transferred to a 24 well plate containing media in each well. The plate was then incubated at 37 °C (above VPTT) for 2 h to force PNIPAAm-based hydrogels (**a-e**) into a deswollen, hydrophobic state and to equilibrate the hydrogels with the cell culture media. Mouse smooth muscle precursor cells (10T1/2) were seeded onto each hydrogel surfaces at 25,000 cells/cm^2. After incubation at 37 °C for 4 h, the 24 well plate was transferred to a Zeiss Axiovert A200 microscope and air-cooled to 25 °C (below VPTT) at a rate of ~ 2 ºC/min thereby causing **a-e** to swell. The well plate was then transferred back to a 37 °C incubator for 4 h and a second cooling cycle was similarly performed. For each cooling cycle, images were captured at two second intervals.

4.4 Materials

Octamethylcyclotetrasiloxane (D_4) and 1,3,5,7-tetramethyl-1,3,5,7-tetravinyl-cyclotetrasiloxane (D_4^{Vi}) were purchased from Gelest Inc. Brij 35, Brij 78, Tergitol solution (70% in H_2O), Potassium hydroxide $(KOH)_4$, Potassium persulfate ($K_2S_2O_8$), *N*-isopropylacrylamide (NIPAAm, 97%), 2,2-dimethyl-2-phenyl-acetophenone (DMAP), *N*-vinylpyrrolidone (NVP) were purchased from Aldrich. *N,N'*-methylenebisacrylamide (BIS, 99%) was obtained from Acros Organics. 1-[4-(2-Hydroxyethoxy)-phenyl]-2-

hydroxy-2-methyl-1-propane-1-one (Irgacure® 2959) was obtained from Ciba. Acetic acid was received from Fisher Scientific. All reagents were used as received.

4.5 Preparation of Nanocomposite Hydrogels

Nanocomposite hydrogels were prepared by *in situ* photopolymerization of aqueous precursor solutions containing NIPAAm monomer, BIS crosslinker, Irgacure-2959 photoinitiator, and crosslinked polysiloxane nanoparticles (Fig. 4.1). In a 50 mL rb flask equipped with a Teflon-covered stir bar, NIPAAm (1.0 g, 8.84 mmol), BIS (0.02 g, 0.13 mmol), and Irgacure-2959 (0.08 g, 0.36 mmol) were dissolved in DI water (the total volume equal to 7 mL including the volume of water introduced later by the nanoparticle emulsion) and the solution stirred under N_2 for 15 min. Finally, the appropriate amount of emulsion containing crosslinked colloidal nanoparticles was added and the mixture stirred for 10 min under N_2. In total, four different hydrogel compositions were prepared with varying amounts of colloidal nanoparticles: **(a)** pure NIPAAm (no nanoparticles; a control), **(b)** 0.5 wt%, **(c)** 1.0 wt%, **(d)** 2.0 wt%, **(e)** 3.0 wt%, and **(f)** 4.0 wt% (wt % solids of nanoparticles with respect to total precursor solution wt).

Hydrogel sheets (1.5 or 0.5 mm thick) were prepared by first pipetting a precursor solution between two clamped glass microscope slides (75 x 50 mm) separated by polycarbonate spacers of appropriate thickness (1.5 mm for mechanical test and 0.5 mm for cell release test). The mold was submerged in an ice water bath (~7 °C) and exposed to longwave UV light (UV-Transilluminator, 6 mW/cm^2, 365 nm) for 30 min. After removal from the mold, hydrogel sheet was rinsed with DI water and then soaked

in DI water for 2 days with daily water changes to remove impurities. Hydrogel sheets (1.5 mm thick) were used to prepare samples for morphological, VPTT, swelling, mechanical, and contact angle studies. Hydrogel sheets (0.5 mm thick) were used for cell-release studies.

For tensile tests, hydrogels were prepared with a "ring" geometry. First, hydrogels were prepared in a hollow tube geometry with a double walled tubular mold composed of an inner glass mandrel (diameter = 3 mm) and an outer glass cylinder (diameter = 7.9 mm). The tubular mold was filled with a precursor solution and cured while submerged in an ice water bath (~7 °C) for 30 min under constant rotation such that each surface point of the mold received equal UV intensity and exposure time. The hydrogel tube was removed from the mold and similarly purified as above by rinsing and soaking in DI water. Cutting the resulting hydrogel tube into ~3 mm wide pieces afforded hydrogel ring specimens.

4.6 Results and Discussion

Preparation of Crosslinked Polysiloxane Colloidal Nanoparticles

Polysiloxane colloidal nanoparticles were prepared by anionic ring-opening emulsion polymerization of D_4 and D_4^{Vi} using Brij 35 and Brij 78 as an inisurf (i.e. an initiator and surfactant) (Fig. 4.2) [160]. The colloidal nanoparticles were subsequently crosslinked via free radical reaction between of the vinyl groups. Surfactant and other reaction impurities were removed from the resultant emulsion via dialysis. This process

yielded polysiloxane colloidal nanoparticles having an average diameter of 54 nm (PD = 0.2).

Preparation of Nanocomposite Hydrogels: Crosslinking and Morphology

Nanocomposite hydrogels (**b-f**) were prepared by photopolymerization aqueous mixtures of NIPAAm monomer, BIS crosslinker, Irgacure-2959 photoinitiator, and crosslinked colloidal polysiloxane nanoparticles ~7 °C for 30 min (Fig. 4.3). PNIPAAm hydrogels are typically formed by the free radical crosslinking copolymerization of aqueous solutions of NIPAAm and BIS using redox initiators which typically relies inert environments, elevated temperatures, and/or long reaction times [108, 163-166]. Thus, photopolymerization was utilized herein to prepare PNIPAAm nanocomposite hydrogels more rapidly with a 30 min cure time [167-169]. With increasing PDMS nanoparticle content, resulting hydrogels were substantially more transparent than hydrogels prepared with 220 nm polysiloxane particles [99]. Following Soxhlet extraction, hydrogels containing 4 wt% nanoparticles (**f**) and pure PNIPAAm hydrogel **(a)** both exhibited no detectable weight loss (<0.1 wt%). Thus, photopolymerization effectively produced nanocomposite hydrogels without significant amounts of non-reacted NIPAAm.

The preparation temperatures (T_{prep}) at which PNIPAAm hydrogels are formed has been shown to impact their chemical and physical properties by altering hydrogel morphology [171-176]. Thus, to optimize mechanical strength of the nanocomposite hydrogels, photopolymerization was conducted at ~7 °C to obtain nanocomposite hydrogels consisting of a homogeneous PNIPAAm matrix with embedded nanoparticles.

The homogeneity of the PNIPAAm hydrogel matrix is confirmed by the optically transparent nature of the pure PNIPAAm hydrogel (**a**, no nanoparticles). Freeze-drying (i.e. lyophilization) is known to preserve the structure and volume of swollen hydrogels even after all (or almost all) solvent is removed [177]. SEM micrographs of lyophilized nanocomposite hydrogels revealed that all demonstrated a uniform porous morphology characteristic of homogeneous PNIPAAm hydrogels. Representative SEM images are shown in Fig. 4.3 [176].

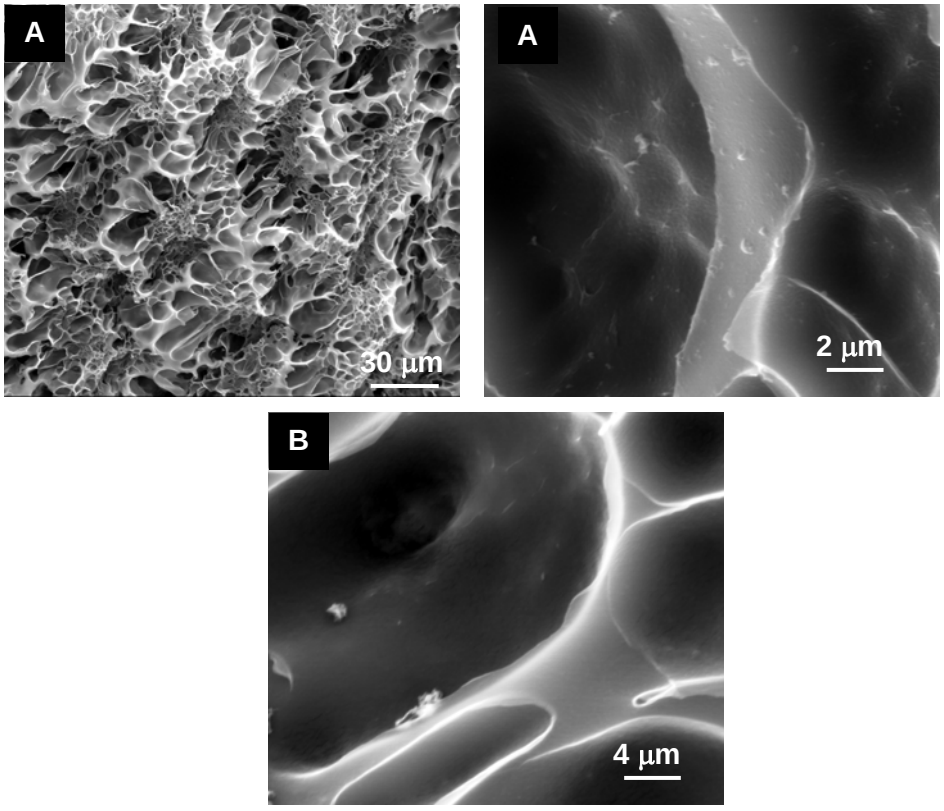

Figure 4.3. SEM micrographs of **(A)** nanocomposite hydrogel **f** (containing 4.0 wt% nanoparticles); **(B)** nanocomposite hydrogel **c** (containing 1.0 wt% nanoparticles).

Kinetic Swelling

At ~ 200 min, all hydrogels reached 80% swelling when cooled from 50 to 22 °C. Swelling was fastest for the hydrogel containing 1 wt% nanoparticles.

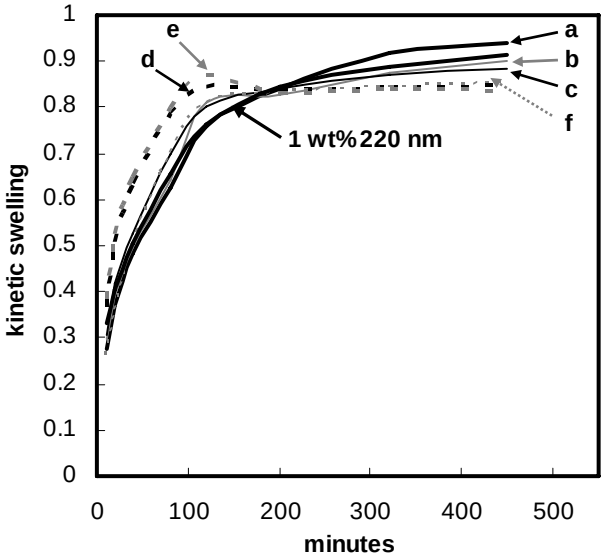

Figure 4.4. Kinetic swelling ratio of nanocomposite hydrogels containing 0.5-2.0 wt% nanoparticles (**b-e**) and pure PNIPAAm hydrogel control (**a**).

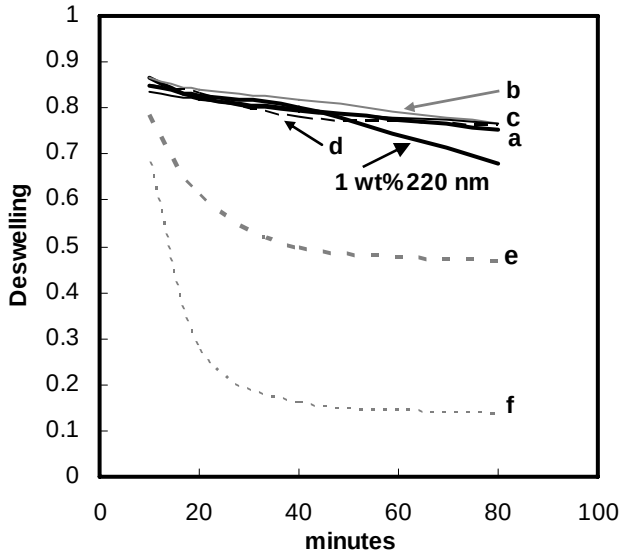

Figure 4.5. Kinetic deswelling ratio of nanocomposite hydrogels containing 0.5-2.0 wt% nanoparticles (**b-e**) and pure PNIPAAm hydrogel control (**a**).

Table 4.1. Composition and thermal transition properties of nanocomposite hydrogels (**b-f**) and pure PNIPAAm hydrogel control (**a**).

	Composition	Volume Phase Transition Temperature (VPTT)		
Hydrogel	Solid wt% nanoparticles	T_o (°C)	T_{max} (°C)	ΔH (J/g)
a	0	32.7	35.4	5.25
b	0.5	33.2	35.9	4.87
c	1.0	32.6	34.9	6.59
d	2.0	32.9	35.3	4.42
e	3.0	32.7	35.2	5.56
f	4.0	32.6	35.1	5.47

PNIPAAm hydrogels exhibit a significant endothermic effect during the volume phase transition due to breaking of hydrogen bonds between water molecules surrounding hydrophobic moieties on the polymer [166, 178]. The VPTT is typically designated by either the onset (T_o) or maximum temperature (T_{max}) of the endothermic peak [167, 179-181]. The VPTT and transition enthalpy (ΔH) values of the nanocomposite hydrogels (**b-f**) and PNIPAAm control (**a**) were determined by their respective DSC thermograms of swollen hydrogel specimens (Fig. 4.6, Table 4.1). T_o values were determined from the intersecting point between two tangent lines from the baseline and slope of the endothermic peak [180]. The VPTT (T_{max} or T_o) of nanocomposite hydrogels (**b-f**) remained essentially unchanged relative to that of the pure PNIPAAm hydrogel (**a**). Similarly, the ΔH values of nanocomposite hydrogels were similar to that of the pure PNIPPAm hydrogel. This indicates that polysiloxane nanoparticles do not interfere with the dissociation of water molecules from hydrophobic groups when heated above the VPTT. The endothermic peak of the nanocomposite hydrogels slightly broadened with increased polysiloxane particle content. Broadening

of the endothermic peak of PNIPAAm-based hydrogels is an indicator of more gradual deswelling above the VPTT [151, 182].

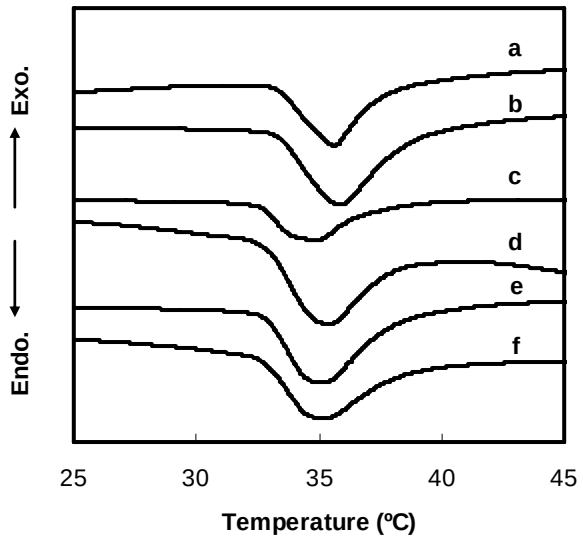

Figure 4.6. DSC thermograms for nanocomposite hydrogels (**b-f**) and pure PNIPAAm hydrogel (**a**).

Tensile Tests and Dynamic Mechanical Analysis

The mechanical properties of biomaterials such as hydrogels directly affect their utility and performance. Because of their frequent use to measure hydrogel mechanical properties, both dynamic mechanical analysis (DMA) and tensile tests were utilized in this study [98, 183, 184]. Mechanical properties of hydrogels in a swollen state are most relevant to their end-use applications. However, mechanical testing of swollen hydrogels is challenging because the difficulty maintaining hydration and their high water content/low polymer mass to unit volume make them mechanically weak and difficult to handle. Thus, during DMA, silicone oil was placed around the hydrogel disc specimen

sandwiched between two compression clamps to inhibit water loss. Tensile testing of flat, rectangular hydrogel specimens with ends secured in tension grips is often complicated by sample slippage from or breakage at the grip. Thus, specimens with a ring geometry were employed to minimize slippage/breakage for improved accuracy [48]. Ring specimens also allowed their rapid mounting on tensile bars so that testing was completed before significant water loss occurred.

In DMA, the measured storage modulus (G') is related to a materials stiffness or resistance to deformation [185]. At all frequencies (1-100 Hz), the G' of the nanocomposite hydrogels (**b-f**) were higher than that of the pure PNIPAAm hydrogel (**a**) and increased with higher levels of polysiloxane nanoparticles (Fig. 4.7). These differences in G' became more pronounced as the frequency was increased. Nanocomposite hydrogels (**b-f**) also showed an increase in tensile modulus and ultimate tensile strength (UTS) with increased polysiloxane nanoparticles content up to 2 wt% (Table 4.2).

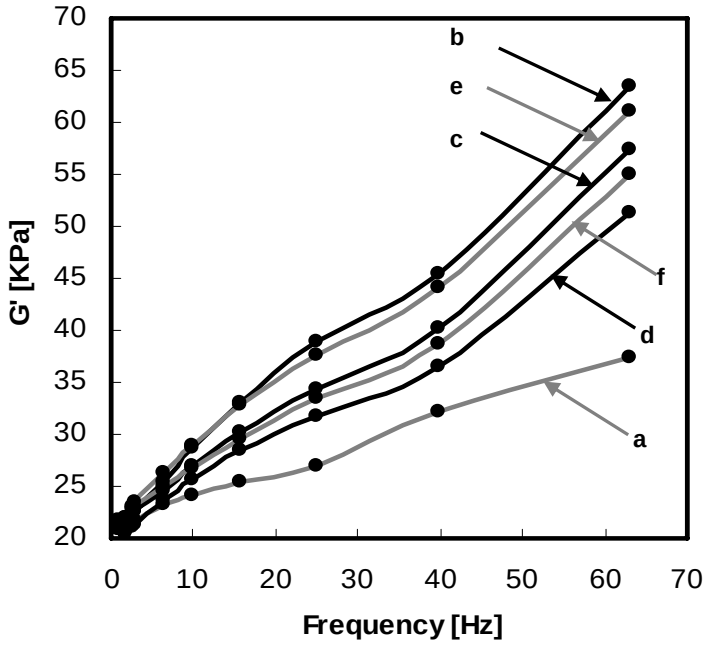

Figure 4.7. Storage modulus (G') of nanocomposite hydrogels (**b-f**) and pure PNIPAAm hydrogel (a) measured in the compression mode.

Table 4.2. Tensile properties of nanocomposite hydrogels (**b-f**) and pure PNIPAAm hydrogel control (**a**).

	Composition	**Tensile Properties**		
Hydrogel	**Solid wt% nanoparticles**	Modulus (kPa)	UTS (kPa)	% strain at break
a	**0**	14.5 ± 1.6	6.7 ± 1.5	50.4 ± 7.7
b	**0.5**	17.1±0.2	7.0±1.3	46.9±8.1
c	**1**	17.5±2.1	8.6±1.1	58.9±8.0
d	**2**	17.2±0.5	8.8±1.0	57.8±5.8
e	**3**	14.2±1.0	7.2±1.0	56.7±6.9
f	**4**	13.8±0.0	6.7±0.9	53.7±7.2
200 nm	**1**	15.6 ± 0.6	9.5 ± 0.5	64.3 ± 1.9

Temperature-Dependent Cell Release Behavior

The ability of nanocomposite hydrogels to release mouse smooth muscle precursor cells (10T1/2) from their surfaces was assessed by examining cell morphology before and after thermal cooling. A PEO-RGDS hydrogel served as a control as it is non-thermoresponsive but cell-adhesive [190]. Since cells grow well on more hydrophobic surfaces, cells were cultured on hydrogels at 37 °C (above the VPTT). It was observed that more cells adhered to the nanocomposite hydrogels (**b-f**) compared to the pure PNIPAAm hydrogel (**a**) which may be explained by the higher hydrophobicity of **b-f** due to the presence of hydrophobic PDMS nanoparticles. Cooling from 37 °C (above VPTT) to 25 °C (below VPTT) forced the PNIPAAm-based hydrogels (**a-f**) to swell and become more hydrophilic. The media within each well containing the hydrogel disc provided water for the swelling process. After the first cooling cycle, a round cell morphology indicative of end stages of cell detachment was observed for cells on **a-f**. Time-lapsed images of cell detachment from nanocomposite hydrogel **c** (containing 1 wt% nanoparticles) are shown in Fig. 4.8. In contrast, cells on the PEO-RGDS hydrogel control maintained an extended morphology indicative of cell adhesion and spreading. Following a subsequent second heating-cooling cycle, the round morphology was even more pronounced on **a-f** (Fig. 4.9).

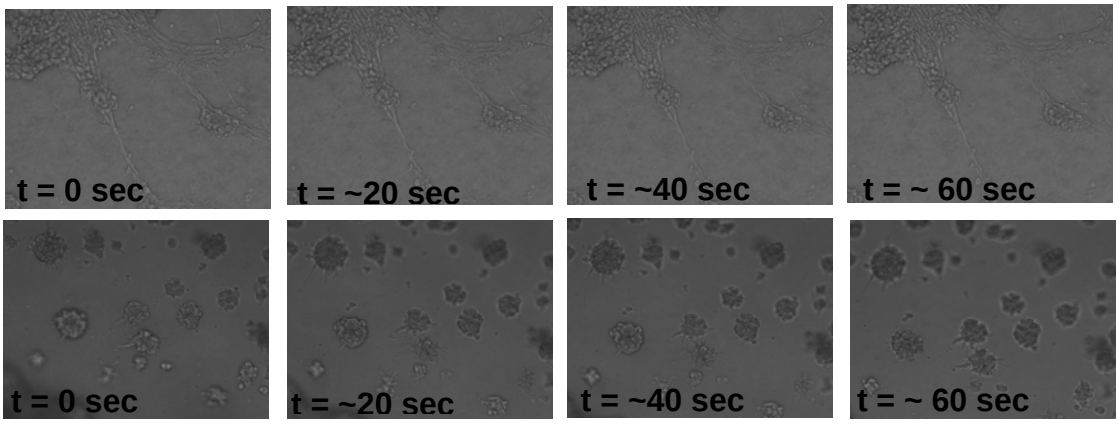

Figure 4.8. Time-lapsed images of a mouse smooth muscle precursor cells (10T1/2) on hydrogel **c** (containing 1 wt%; top row) and hydrogel **d** (2 wt%; bottom row) nanoparticles during first cooling cycle from 37 °C to 25 °C. The cell cluster collapses as individual cells switch from an extended morphology to a round morphology as they detach during the hydrogel swelling induced by cooling.

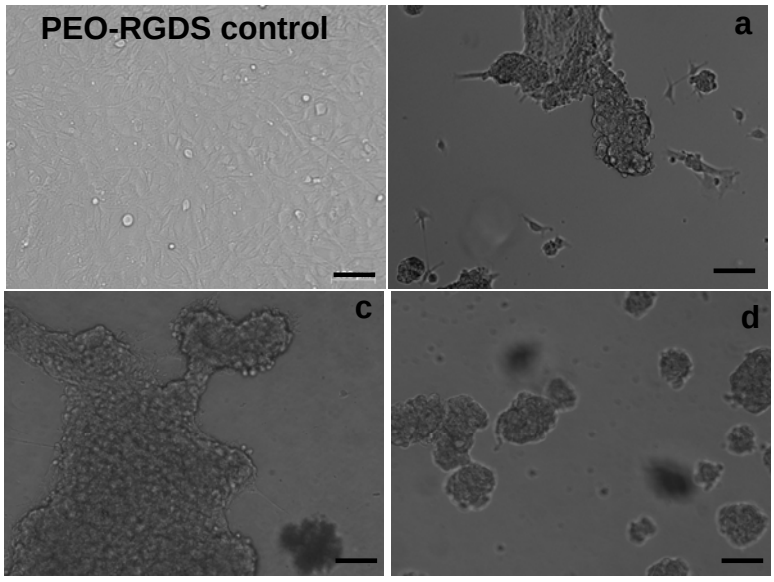

Figure 4.9. Mouse smooth muscle precursor (10T1/2) cells displayed a rounded morphology indicative of detachment on hydrogels **a-f** following two cycles of thermal cooling from 37 °C to 25 °C. A PEO-RGDS hydrogel served as a cell-adhesive but non-thermoresponsive control. All scale bars are 100 μm.

4.7 Conlusions

Transparent thermoresponsive composite hydrogels comprised of a PNIPAAm hydrogel matrix and polysiloxane colloidal nanoparticles (~54 nm ave. diameter) were prepared via *in situ* photopolymerization of aqueous solutions of NIPAAm monomer, BIS crosslinker, photoinitiator and polysiloxane nanoparticles (0.5 to 4.0 wt% based on solution weight) at ~7 °C. Due to the low preparation temperature, the nanocomposite hydrogels exhibited a homogeneous morphology confirmed by SEM analysis. Because the nanoparticles exist as a chemically independent phase, the VPTT of the nanocomposite hydrogels is not altered compared to pure PNIPAAm hydrogels. Increasing the nanoparticle content generally led to an increase in storage modulus (G'), and tensile modulus. When cooled from 37 °C to 25 °C, mouse smooth muscle precursor (10T1/2) cells were shown to effectively detach from nanocomposite hydrogel surfaces.

CHAPTER V

CONCLUSIONS AND FUTURE DIRECTIONS

5.1 Conclusions

In Chapter II, a library of 18 unique $PDMS_{star}$-PEG hydrogels were prepared by photochemical cure of varying weight ratios of $PDMS_{star}$-MA (**A-C**) and PEG-DA (**L** and **H**). Thus, the chemical properties of the hydrogels were switched from a purely organic, PEG to inorganic-organic with increased levels of **A-C**. The morphology of these hydrogels consisted of spherical PDMS-enriched microparticles dispersed throughout a PEG matrix. For hydrogels based on **L**, increased levels of **A-C** systematically decreased tensile modulus and a similar but less substantial decrease was observed for hydrogels based on **H**. For a given hydrogel series based on **L** or **H**, the equilibrium swelling of $PDMS_{star}$-PEG hydrogels were not substantially different from one another or the corresponding pure PEG-DA hydrogel (**L** and **H controls**). Thus, for a given hydrogel series, modulus was independent of hydration. These hydrogels therefore permit the evaluation of the effect of scaffold modulus apart from hydration. The resistance to non-specific protein adhesion as well of non-cytoxicity of PEG-DA hydrogels was maintained for the $PDMS_{star}$-PEG hydrogels. Thus, these inorganic-organic hydrogels with tunable chemical and physical properties are useful to define cell-material interaction relationships in tissue engineering.

In Chapters III and IV, novel thermoresponsive composite hydrogels comprised of a PNIPAAm hydrogel matrix and polysiloxane colloidal nanoparticles (both ~54 nm

and ~220 nm ave. diameter) were prepared via *in situ* photopolymerization. The nanocomposite hydrogels exhibited a homogeneous morphology confirmed by SEM analysis. The VPTT of the nanocomposite hydrogels is not altered compared to pure PNIPAAm hydrogels, since the nanoparticles exist as a chemically independent phase. The dynamic storage modulus (G') in compression and tensile modulus generally increased with nanoparticle content compared with pure PNIPAAm hydrogels. When cooled from 37 to 25°C, mouse smooth muscle precursor (10T1/2) cells were shown to effectively detach from nanocomposite hydrogel surfaces.

5.2 Future Directions

In the future studies, physical properties of $PDMS_{star}$-PEG hydrogels may be altered by systematically tuning total concentration of macromers in the aqueous solution rather than at the same concentration (i.e. 10 wt%) used in Chapter II. These concentrations (5-20 wt%) may be prepared individually or using a gradient maker. Our collaborator, Prof. Mariah Hahn (Texas A&M University) has recently shown that osteoblasts transdifferente into chrondrocyte-like cells as PDMS content increased in $PDMS_{star}$-PEO hydrogels. Thus, these scaffolds merit further study for osteochondral tissue regeneration. The stimulation of hydroxyapatite onto these hydrogels when exposed to simulated body fluid (SBF) is currently being examined in our group. In addition, it was recently observed that organic solvent-based solutions (e.g. dichloromethane) of these macromers results in a homogeneous precursor solutions that upon photocure and hydration with water are notably tougher.

Enhancing the mechanical properties of sensor membrances is valuable to maintain their integrity during insertion and removal from the body. We have recently begun work to improve the mechanical behavior of PNIPAAm nanocomposite hydrogels by changing the PNIPAAm matrix. For instance, interpenetrating polymer networks (IPNs) have been formed with a “tightly” crosslinked and second “loosely” crosslinked PNIPAAm hydrogel. These are sometimes referred to as double network hydrogels. Incorporation of the 220 and 54 nm polysiloxane nanoparticles into these tougher hydrogel matrixes may produce a membrane with excellent mechanical and self-cleaning properties.

REFERENCES

1. Peppas NA, Mikos AG. Preparation methods and structure of hydrogels. Boca Raton, FL: CRC Press, 1986.

2. Lee JH, Khang G, Lee JW, Lee HB. Interaction of different types of cells on polymer surfaces with wettability gradient. J Colloid Interface Sci 1998;205:323-330.

3. Hoffman AS. Hydrogels for biomedical applications. Adv Drug Deliv Rev 2002;54:3-12.

4. Lee KY, Mooney DJ. Hydrogels for tissue engineering Chem Rev 2001;101:1869-1879.

5. Hutmacher DW. Scaffold design and fabrication technologies for engineering tissues-state of the art and future perspectives. J Biomater Sci Polym Ed 2001;12:107-124.

6. Langer R, Vacanti JP. Tissue engineering. Science 1993;260:920-926.

7. Nerem RM. Cellular engineering. Ann Biomed Eng 1991;19:529-545.

8. Stocum DL. Regenerative biology and engineering: strategies for tissue restoration. Wound Repair Regan 1998;6:276-290.

9. Auger FR, M; Goulet, F; Berthod, F.;Moulin; V; Germain, L. Tissue-engineered human skin substitutes developed from collagen-populated hydrated gels: clinical and fundamental applications. Med Biol Engin Comput 1998;36:801-812.

10. Choi YSH, Sung Ran; Lee, Young Moo; Song, Kang Won; Park, Moon Hyang; Nam, Young Soo. Studies on gelatin-containing artificial skin: II. Preparation and characterization of crosslinked gelatin-hyaluronate sponge. J Biomed Mater Res 1999;48:631-639.

11. Oxley HRC, P. H.; Fitton, J. H.; Tighe, B. J. Macroporous hydrogels for biomedical applications: methodology and morphology. Biomaterials 1993;14:1064-1072.

12. Stile RAB, Wesley R.; Healy, Kevin E. Synthesis and characterization of injectable poly(*N*-isopropylacrylamide)-based hydrogels that support tissue formation in vitro macromolecules 1999;32:7370.

13. Gu ZQX, J. M.; Zhang, X. H. The development of artificial articular cartilage--PVA-hydrogel. Biomed Mater Eng 1998;1998:75-81.

14. Muzzarelli RAZ, C.; Ilari, P.; Pugnaloni, A.; Mattioli Belmonte, M.; Biagini, G.; Castaldini, C. Osteoconductive properties of methylpyrrolidinone chitosan in an animal model. Biomaterials 1993;14:925-929.

15. Taguchi TK, Akio; Akashi, Mitsuru. Apatite formation on/in hydrogel matrixes using an alternate soaking process: II. Effect of swelling ratios of poly(vinyl alcohol) hydrogel matrixes on apatite formation. J Biomat Sci Polym Ed 1999;10:331-339.

16. Bellamkonda R, Ranieri JP, Bouche N, Aebischer P. Hydrogel-based 3-dimensional matrix for neural cells. J Biomed Mater Res 1995;29:663-671.

17. Bini TB, Gao SJ, Tan TC, Wang S, Lim A, Hiai LB, et al. Electrospun poly(L-lactide-co-glycolide) biodegradable polymer nanofiber tubes for peripheral nerve regeneration. Nanotechnology 2004;15:1459-1464.

18. Seliktar DB, R.A.; Vito, R. P. Nerem, R.M. Dynamic mechanical conditioning of collagen-gel blood vessel constructs induces remodeling in vitro. Ann Biomed Eng 2000;28:351-362.

19. Ramamurthi A, Vesely I. Evaluation of the matrix-synthesis potential of crosslinked hyaluronan gels for tissue engineering of aortic heart valves. Biomaterials 2004;26:999-1010.

20. Matsters KS, Shah DN, Leinwand LA. Crosslinked hyaluronan scaffolds as a biologically active carrier for valvular interstitial cells. Biomaterials 2005;26:2517-2525.

21. Liu C, Xia Z, Czernuszka JT. Design and development of three-dimensional scaffolds for tissue engineering. Chem Eng Res Design 2007 Jul;85:1051-1064.

22. Frost M, Meyerhoff ME. *In vivo* chemical sensors: tackling biocompatibility. Anal Chem 2006;78:7370-7377.

23. Langer R, Peppas NA. Advances in biomaterials, drug delivery, and bionanotechnology. AIChE J 2003;49:2990-3006.

24. Seal BL, Otero TC, Panitch A. Review: Polymeric biomaterials for tissue and organ regeneration. Mater Sci Eng Rep 2001;34:147-130.

25. Yang S, Leong K-F, Du Z, Chua C-K. The design of scaffolds for use in tissue engineering: Part I. Traditional factors. Tissue Eng 2001;7:679-689.

26. Hollister SJ. Porous scaffold design for tissue engineering. Nat Mater 2005 Jul;4:518-524.

27. Agrawal CM, Robert BR. Biodegradable polymeric scaffolds for musculoskeletal issue engineering. J Biomed Mater Res 2001;55:141-150.

28. Lavik E, Langer R. Tissue engineering: current state and perspectives. Appl Microbiol Biotechnol 2004;65:1-8.

29. Malafaya PB, Silva GA, Reis RL. Natural-origin polymers as carriers and scaffolds for biomolecules and cell delivery in tissue engineering applications. Adv Drug Deliv Rev 2007;59:207-233.

30. Ifkovits JL, Burdick JA. Review: Photopolymerizable and degradable biomaterials for tissue engineering applications. Tissue Eng 2007;13:2369-2385.

31. Drury JL, Mooney DJ. Hydrogels for tissue engineering: scaffold design variables and applications. Biomaterials 2003;24:4337-4351.

32. Cushing MC, Anseth KS. Hydrogel cell cultures. Science 2007;316:1133-1134.

33. Hennink WE, van Nostrum CF. Novel crosslinking methods to design hydrogels. Adv Drug Deliv Rev 2002;54:13-36.

34. Peppas NA, Bures P, Leobandung W, Ichikawa H. Hydrogels in pharmaceutical formulations. Eur J Pharm Biopharm 2000;50:27-46.

35. Nguyen KT, West JL. Photopolymerizable hydrogels for tissue engineering applications. Biomaterials 2002;23:4307-4314.

36. Anseth KS, Metters AT, Bryant SJ, Martens PJ, Elisseeff JH, Bowman CN. In situ forming degradable networks and their application in tissue engineering and drug delivery. J Control Release 2002;78:199-209.

37. Elisseeff J, Anseth K, Sims D, McIntosh W, Randolph M, Langer R. Transdermal photopolymerization for minimally invasive implantation. Proc Natl Acad Sci 1999;96:3104-3107.

38. Nuttelman CR, Rice MA, Rydholm AE, Salinas CN, Shah DN, Anseth KS. Macromolecular monomers for the synthesis of hydrogel niches and their application in cell encapsulation and tissue engineering. Prog Polym Sci 2008;33:167-179.

39. Burdick JA, Anseth KS. Photoencapsulation of osteoblasts in injectable RGD-modified PEG hydrogels for bone tissue engineering. Biomaterials 2002;23:4315-4323.

40. Yang F, Williams CG, Wang D-A, Lee H, Manson PN, Elisseeff J. The effect of incorporating RGD adhesive peptide in polyethylene glycol diacrylate hydrogel on osteogenesis of bone marrow stromal cells. Biomaterials 2005;26:5991-5998.

41. Bryant SJ, Anseth KS. The effects of scaffold thickness on tissue engineered cartilage in photocrosslinked poly(ethylene oxide) hydrogels. Biomaterials 2001;22:619-626.

42. Elisseeff J, McIntosh W, Anseth K, Riley S, Ragan P, Langer R. Photoencapsulation of chondrocytes in poly(ethylene oxide)-based semi-interpenetrating networks. J Biomed Mater Res 2000;51:164-171.

43. Mahoney MJ, Anseth KS. Three-dimensional growth and function of neural tissue in degradable polyethylene glycol hydrogels. Biomaterials 2006;27:2265-2274.

44. Mann BK, Gobin AS, Tsai AT, Schmeldlen RH, West JL. Smooth muscle cell growth in photopolymerized hydrogels with cell adhesive and proteolytically degradable domains: synthetic ECM analogs for tissue engineering. Biomaterials 2001;22:3045-3051.

45. Mann BK, Schmedlen RH, West JL. Tethered-TGF-β-increases extracellula matrix production of vascular smooth muscle cells. Biomaterials 2001;22:439-444.

46. Kraehenbuehl TP, Ferreira LS, Zammaretti P, Hubbell JA. Cell-responsive hydrogel for encapsulation of vascular cells. Biomaterials 2009;30:4318-4324.

47. Beamish JA, Fu AY, Choi A-J, Haq NA, Kottke-Marchant K, Marchant RE. The influence of RGD-bearing hydrogels on the re-expression of contractile vascular smooth muscle cell phenotype. Biomaterials 2009;30:4127-4135.

48. Hahn MS, McHale MK, Wang E, Schmedlen RH, West JL. Physiological pulsatile flow bioreactor conditioning of poly(ethylene glycol)-based tissue engineering grafts. Ann Biomed Eng 2007;35:190-200.

49. Gombotz WR, Guanghui W, Horbett TA, Hoffman AS. Protein adsorption to poly(ethylene oxide) surfaces. J Biomed Mater Res 1991 Dec;25:1547-1562.

50. Hern DL, Hubbell JA. Incorporation of adhesion peptides into nonadhesive hydrogels useful for tissue resurfacing. J Biomed Mater Res 1998;39:266-276.

51. Halstenberg S, Panitch A, Rizzi S, Hall H, Hubbell JA. Biologically engineered protein-*graft*-poly(ethylene glycol) hydrogels: a cell adhesive and plasmin-degradable biosynthetic material for tissue repair. Biomacromolecules 2002;3:710-723.

52. West JL, Hubbell JA. Polymeric biomaterials with degradation sites for proteases involved in cell migration. Macromolecules 1999;32:241-244.

53. Sawhney AS, Pathak CP, Hubbell JA. Bioerodible hydrogels based on photopolymerized poly(ethylene glycol)-*co*-poly(α–hydroxy acid) diacrylate macromers. Macromolecules 1993;26:581-587.

54. Martens PJ, Bryant SJ, Anseth KS. Tailoring the degradation of hydrogels formed from multivinyl poly(ethylene glycol) and poly(vinyl alcohol) macromers for cartilage tissue engineering. Biomacromolecules 2003;2003:283-292.

55. Bryant SJ, Durand KL, Anseth KS. Manipulations in hydrogel chemistry control photoencapsulated chondrocyte behavior and their extracellular matrix production. J Biomed Mater Res 2003;67A:1430-1436.

56. Bryant SJ, Anseth KS. Controlling the spatial distribution of ECM components in degradable PEG hydrogels for tissue engineering of cartilage. J Biomed Mater Res 2003;64A:70-79.

57. Metters AT, Anseth KS, Bowman CN. Fundamental studies of a novel, biodegradable PEG-*b*-PLA hydrogel. Polymer 2000;41:3993-4004.

58. Kleinman HK, Philp D, Hoffman MP. The role of the extracellular matrix in morphogenesis. Curr Opin Biotechnol 2003;14:526-532.

59. Lutolf MP, Hubbell JA. Synthetic biomaterials as instructive extracellular microenvironments for morphogensis in tissue engineering. Nature Biotech 2005;23:47-55.

60. Causa F, Netti PA, Ambrosio L. A multi-functional scaffold for tissue regeneration: the need to engineer a tissue analogue. Biomaterials 2007;28:5093-5099.

61. Dado D, Levenberg S. Cell-scaffold mechanical interplay within engineered tissues. Sem Cell Dev Biol 2009;20:656-664.

62. Dutta RC, Dutta AK. Cell-interactive 3D-scaffold; advances and applications. Biotech Adv 2009;27:334-339.

63. Kim B-S, Nikolovski J, Bonadio J, Smiley E, Mooney DJ. Engineered smooth muscle tissues: regulating cell phenotype with the scaffold. Exp Cell Res 1999;251:321-328.

64. Benoit DSW, Schwartz MP, Durney AR, Anseth KS. Small functional groups for controlled differentiation of hydrogel-encapsulated human mesenchymal stem cells. Nature Mater 2008;7:816-823.

65. Chaterji S, Gemeinhart RA. Enhanced osteoblast-like cell adhesion and proliferation using sulfonate-bearing polymeric scaffolds. J Biomed Mater Res 2007;83A:990-998.

66. Escobar-Ivirico JL, Salmeron-Sanchez M, Gomez-Ribelles JL, Monleon-Pradas M, Soria JM, Gomes ME, et al. Proliferation and differentiation of goat bone marrow stromal cells in 3D scaffolds with tunable hydrophilicity. J Biomed Mater Res 2009;91B:277-286.

67. Simon CG, Yang Y, Vinoy T, Dorsey SM, Morgan AW. Cell interactions with biomaterials gradients and arrays. Comb Chem High Throughput Screen 2009;12:544-553.

68. Lin NJ, Hu H, Sung L, Lin-Gibson S. Quantification of cell response to polymeric composites using a two-dimensional gradient platform. Comb Chem High Throughput Screen 2009;12:619-625.

69. Lin NJ, Lin-Gibson S. Osteoblast response to dimethacrylate composites varying in composition, conversion and roughness using a combinatorial approach. Biomaterials 2009;30:4480-4487.

70. Jansen EJP, Sladek REJ, Bahar H, Yaffe A, Gijbels MJ, Kuijer R, et al. Hydrophobicity as a design criterion for polymer scaffolds in bone tissue engineering. Biomaterials 2005;26:4423-4431.

71. Ren L, Tsuru K, Hayakawa S, Osaka A. Novel approach to fabricate porous gelatin-siloxane hybris for bone tissue engineering. Biomaterials 2002;23:4765-4773.

72. Song J-H, Yoon B-H, Kim Y-E, Kim H-W. Bioactive and degradable hybridized nanofibers of gelatin-siloxane for bone regeneration. J Biomed Mater Res 2008;84:875.

73. Ning CQ, Mehta J, El-Ghannam A. Effect of silica on the bioactivity of calcium phosphate composites *in vitro*. J Mater Sci Mater Med 2005;16:355-360.

74. McGlohorn JB, W.D. Holder J, Grimes LW, Thomas CB, Burg KJL. Evaluation of smooth muscle cell response using two types of porous polylactide scaffolds with differing pore topography. Tissue Eng 2004;10:505-514.

75. Kim EJ, Boehm CA, Fleischman AJ, Muschler GF, Kostov YV, Roy S. Modulating human connective tissue progenitor cell behavior on cellulose acetate scaffolds by surface microtextures. J Biomed Mater Res 2009;90A:1198-1205.

76. Crouch AS, Miller D, Luebke KJ, Hu W. Correlation of anisotropic cell behaviors with topographic aspect ratio. Biomaterials 2009;30:1560-1567.

77. Mattioli-Belmonte M, Vozzi G, Kyriakidou K, Pulieri E, Lucarini G, Vinci B, et al. Rapid-prototype and salt-leached PLGA scaffolds condition cell morpho-functional behavior. J Biomed Mater Res 2008;85A:466-476.

78. Sarkar S, Dadhania M, Rourke P, Desai TA, Wong JY. Vascular tissue engineering: microtextured scaffold templates to control organization of vascular smooth muscle cells and extracellular matrix. Acta Biomaterialia 2005;1:93-100.

79. Glawe JD, Hill JB, Mills DK, McShane MJ. Influence of channel width on alignment of smooth muscle cells by high-aspect-ratio microfabricated elastomeric cell culture scaffolds. J Biomed Mater Res 2005;75A:106-114.

80. Khetan S, Katz JS, Burdick JA. Sequential crosslinking to control cellular spreading in 3-dimensional hydrogels. Soft Matter 2009;5:1601-1606.

81. Engler AJ, Sen S, Sweeney HL, Discher DE. Matrix elasticity directs stem cell lineage specification. Cell 2006;126:677-689.

82. Discher DE, Janmey P, Wang Y-l. Tissue cells feel and respond to the stiffness of their substrate. Science 2005;310:1139-1143.

83. Choquet D, Felsenfeld DP, Sheetz MP. Extracellular matrix rigidity causes strengthening of integrin-cytoskeleton linkages. Cell 1997;88:39-48.

84. Gray DS, Tien J, Chen CS. Repositioning of cells by mechanotaxis on surfaces with micropatterned Young's modulus. J Biomed Mater Res 2003;66A:605-614.

85. Stegemann JP, Hong H, Nerem RM. Mechanical, biochemical, and extracellular matrix effects on vascular smooth muscle cell phenotypes. J Appl Physiol 2005;98:2321-2327.

86. Peyton SR, Raub CB, Keschrumrus VP, Puttman AJ. The use of poly(ethylene glycol) hydrogels to investigate the impact of ECM chemistry and mechanics on smooth muscle cells. Biomaterials 2006;27:4881-4893.

87. Liao H, Munoz-Pinto D, Qu X, Hou Y, Grunlan MA, Hahn MS. Influence of hydrogel mechanical properties and mesh size on vocal fold fibroblast extracellular matrix production and phenotype. Acta Biomaterialia 2008;4:1161-1171.

88. Bryant SJ, Anseth KS. Hydrogel properties influence ECM production by chondrocytes photoencapsulated in poly(ethylene glycol) hydrogels. J Biomed Mater Res 2002;59:63-72.

89. Munoz-Pinto DJ, Bulick AS, Hahn MS. Uncoupled investigation of scaffold modulus and mesh size on smooth muscle cell behavior. J Biomed Mater Res Part A 2009;90A:303-316.

90. Van-Dyke ME, Clarson SJ, Arshady R. Silicone biomaterials. In: Arshady R, editor. Introduction to polymeric biomaterials. London: Citus Books, 2003. p. 109-135.

91. Gobin AS, West JL. Effects of epidermal growth factor on fibroblast migration through biomimetic hydrogels. Biotechnol Prog 2003;19:1781-1785.

92. Cai G, Weber WP. Synthesis of terminal Si-H irregular tetra-branched star polysiloxanes. Pt-catalyzed hydrosilylation with unsaturated epoxides. Polysiloxane films by photo-acid catalyzed crosslinking. Polymer 2004;45:2941-2948.

93. Grunlan MA, Lee NS, Mansfeld F, Kus E, Finlay JA, Callow JA, et al. Minimally adhesive polymer surfaces prepared from star oligosiloxanes and star oligofluorosiloxanes. J Polym Sci Part A: Polymer Chem 2006;44:2551-2566.

94. Boutevin B, Guida-Pietrasanta F, Ratsimihety A. Synthesis of photocrosslinkable fluorinated polydimethylsiloxanes: direct introduction of acrylic pendant groups via hydrosilylation. J Polym Sci, Part A: Polym Chem 2000;38:3722-3728.

95. Hahn MS, Taite LJ, Moon JJ, Rowland MC, Ruffino KA, West JL. Photolithographic patterning of polyethylene glycol hydrogels. Biomaterials 2006;27:2519-2524.

96. Chojnowske J. Polymerization. In: Clarson SJ, Semlyen JA, editors. Siloxane polymers. PTR Prentice Hall: Englewood Cliffs, JJ, 1993. p. 19-22.

97. Ford MC, Bertram JP, Hynes SR, Michaud M, Li Q, Young M, et al. A macroporous hydrogel for the coculture of neural progenitor and endothelial cells to form functional vascular networks *in vivo*. Proc Natl Acad Sci 2006;103:2512-2517.

98. Anseth KS, Bowman CN, Brannon-Peppas L. Mechanical properties of hydrogels and their experimental determination. Biomaterials 1996;17:1647-1657.

99. Hou Y, Matthews AR, Smitherman AM, Bulick AS, Hahn MS, Hou H, et al. Thermoresponsive nanocomposite hydrogels with cell-releasing behavior Biomaterials 2008;29:3175-3184.

100. Anderson JM, Ziats NP, Azeez A, Brunstedt MR, Stack S, Bonfield TL. Protein adsorption and macrophage activation on polydimethylsiloxane and silicone rubber. J Biomater Sci Polym Ed 1995;7:159-169.

101. Ju H, McCloskey BD, Sagle AC, Kusuma VA, Freeman BD. Preparation and characterization of crosslinked poly(ethylene glycol) diacrylate hydrogels as fouling-resistant membrane coatings. J Mem Sci 2009;330:180-188.

102. Renner K, Amberger A, Konwalinka G, Kofler R, Gnaiger E. Changes of mitochondrial respiration, mitochondrial content and cell size after induction of apoptosis in leukemia cells. Biochim Biophys Acta 2003;1642:115-123.

103. Wu XY, Zhang Q, Arshady R. Stimuli Sensitive Hydrogels. In: Arshady R, editor. The PBM Series: Introduction to Polymeric Biomaterials. London: Citrus Books, 2003. p. 162-163.

104. Schild HG. Poly(*N*-isopropylacrylamide): Experiment, theory, and application. Prog Polym Sci 1992;17:163-249.

105. Heskins M, Guillet JE. Solution properties of poly(*N*-isopropylacrylamide). J Macromol Sci Chem Part A 1968;2:1441-1455.

106. Hirokawa Y, Tanaka T. Volume phase transition in a nonionic gel. J Chem Phys 1984;81:9379-9380.

107. Hoffman AS, Afrassiabi A, Dong LC. Thermally reversible hydrogels: II. Delivery and selective removal of substances from aqueous solution. J Controlled Release 1986;4:213-222.

108. Zhang J, Pelton R, Deng Y. Temperature-dependent contact angles of water on poly(*N*-isopropylacrylamide) gels. Langmuir 1995;11:2301-2302.

109. Yakushiji T, Sakai K, Kikuchi A, Aoyagi T, Sakurai Y, Okano T. Effect of cross-linked structure on temperature-responsive hydrophobic interaction of poly(*N*-isopropylacrylamide) hydrogel-modified surfaces with steroids. Anal Chem 1999;71:1125-1130.

110. Kikuchi A, Okano T. Temperature-responsive, polymer-modified surfaces for green chromatography. Macrmol Symp 2004;207:217-227.

111. Takei YG, Aoki T, Sanui K, Ogata N, Sakurai Y, Okano T. Dynamic contact angle measurement of temperature-responsive surface properties for poly(*N*-isopropylacrylamide) grafted surfaces. Macromolecules 1994;27:6163-6166.

112. Yakushiji T, Sakai K, Kikuchi A, Aoyagi T, Sakurai Y, Okano T. Graft architectural effects on thermoresponsive wettability changes of poly(*N*-isopropylacrylamide)-modified surfaces. Langmuir 1998;14:4657-4662.

113. Yamato M, Akiyama Y, Kobayashi J, Yang J, Kikuchi A, Okano T. Temperature-responsive cell culture surfaces for regenerative medicine with cell sheet engineering. Prog. Polym. Sci. 2007;32:1123-1133.

114. Kumar A, Srivastava A, Galaev IY, Mattiasson B. Smart polymers: physical forms and bioengineering applications. Prog Polym Sci 2007;32:1205-1237.

115. Yang J, Yamato M, Nishida K, Ohki T, Kanzaki M, Sekine H, et al. Cell delivery in regenerative medicine: the cell sheet engineering approach. J Controlled Release 2006;116:193-203.

116. Ratner BD, Horbett T, Hoffman AS. Cell adhesion to polymeric materials: implications with respect to biocompatibility. J Biomed Mater Res 1975;9:407-422.

117. Groth T, Altankov G, Klosz K. Adhesion of human peripheral blood lymphocytes is dependent on surface wettability and protein preadsorption. Biomaterials 1994;15:423-428.

118. Wan Y, Yang J, Yang J, Bei J, Wang S. Cell adhesion on gaseous plasma modified poly(L-lactide) surface under shear stress field. Biomaterials 2003;24:3757-3764.

119. Khorasani MT, Mirzadeh H, Irani S. Plasma surface modification of poly(L-lactic acid) and poly(lactic-co-glycolic acid) films for improvement of nerve cell adhesion. Radiat Phys Chem 2008;77:280-287.

120. Wachem PBv, Beugeling T, Feijen J, Bantjes A, Detmers JP, Aken WGv. Interaction of cultured human endothelial cells with polymeric surfaces of different wettabilities. Biomaterials 1985;6(403-408).

121. Wachem PBv, Hogt AH, Beugeling T, Feijen J, Bantjes A, Detmers JP, et al. Adhesion of cultured human endothelial cells onto methacrylate polymers with varying surface wettability and charge. Biomaterials 1987;8:323-328.

122. Tamada Y, Ikada Y. Effect of preadsorbed proteins on cell adhesion to polymer surfaces. J Colloid Interface Sci 1993;155:334-339.

123. Tamada Y, Ikada Y. Cell adhesion to plasma-treated polymer surfaces. Polymer 1993;34:2208-2212.

124. Arima Y, Iwata H. Effect of wettability and surface functional groups on protein adsorption and cell adhesion using well-defined mixed self-assembled monolayers. Biomaterials 2007;28:3074-3082.

125. Sangermano M, Bongiovanni R, Malucelli G, Priola A, Pollicino A, Recca A. Fluorinated epoxides as surface modifying agents of UV-curable systems. J Appl Polym Sci 2003;89:1524-1529.

126. Yamada N, Okano T, Sakai H, Karikusa F, Sawasaki Y, Sakurai Y. Thermo-responsive polymeric surfaces: control of attachment and detachment of cultured cells. Makromol Chem Rapid Commun 1990;11:571-576.

127. Okano T, Yamada N, Sakai H, Sakurai Y. A novel recovery system for cultured cells using plasma-treated polystyrene dishes grafted with poly(N-isopropylacrylamide). J Biomed Mater Res 1993;27:1243-1251.

128. Okano T, Yamada N, Okuhara M, Sakai H, Sakurai Y. Mechanism of cell detachment from temperature-modulated, hydrophilic-hydrophobic polymer surfaces. Biomaterials 1995;16:297-303.

129. Okano T, Kikuchi A, Sakurai Y, Takei Y, Ogata N. Temperature-responsive poly(*N*-isopropylacrylamide) as a modulator for alteration of hydrophilic/hydrophobic surface properties to control activation/inactivation of platelet. J Controlled Release 1995;36:125-133.

130. Morikowa N, Matsuda T. Thermoresponsive artificial extracellular matrix: N-isopropylacrylamide-graft-copolymerized gelatin. J Biomat Sci Polym Ed 2002;13:167-183.

131. Recum HAv, Kim SW, Kikuchi A, Okuhara M, Sakurai Y, Okano T. Novel thermally reversible hydrogel as detachable cell culture substrate. J Biomed Mater Res 1998;40:631-639.

132. Takezawa T, Mori Y, Yoshizato K. Cell culture on a thermo-responsive polymer surface. Bio/technology 1990;8:854-856.

133. Ista L, Lopez G. Lower critical solubility temperature materials as biofouling release agents. J Indust Mircrobiol Biotech 1998;20:121-125.

134. Cunliffe D, Smart CA, Tsibouklis J, Young S, Alexander C, Vulfson EN. Bacterial adsorption to thermoresponsive polymer surfaces. Biotechnol Lett 2000;22:141-145.

135. Callwaert M, Rouxhet PG, Boulange-Petermann L. Modifying stainless steel surfaces with responsive polymers: effect of PS-PAA and PNIPAAM on cell adheshion and oil removal. J Adhesion Sci Technol 2005;19:765-781.

136. Guenther M, Gerlach G, Kuckling D, Kretschmer K, Corten C, Weber J, et al. Chemical sensors based on temperature-responsive hydrogels. Proc SPIE Int Soc Opt Eng 2006;6167:61670T/61671-61670T/61611.

137. Chen J, Yoshida M, Maekawa Y, Tsubokawa N. Temperature-switchable vapor sensor materials based on *N*-isopropylacrylamide and calcium chloride. Polymer 2001;42:9361-9365.

138. Judeinstein P, Sanchez C. Hybrid organic-inorganic materials: a land of multidisplinarity. J Mater Chem 1996;6:511-525.

139. Meyer T, Hellweg T, Spange S, Hesse S, Jager C, Bellmann C. Synthesis and properties of crosslinked polyvinylformamide and polyvinylamine hydrogels in conjunction with silica particles. J Polym Sci Part A: Polym Chem 2002;40:3144-3152.

140. Fichet O, Vidal F, Laskar J, Teyssie D. Polydimethylsiloxane-cellulose acetate butyrate interpenetrating polymer networsk synthesis and kinetic study. Part I. Polymer 2005;46:37-47.

141. Park JH, Bae YH. Hydrogels based on poly(ethylene oxide) and poly(tetramethyloxide) or poly(dimethyl siloxane): synthesis, characterization, and in vitro protein adsorption and platelet adhesion. Biomaterials 2002;23:1797-1808.

142. Stone DA, Allcock HR. A new polymeric intermediate for the synthesis of hybrid inorganic-organic polymers. Macromolecules 2006;39:4935-4937.

143. Bae YH, Okano T, Kim SW. "On-Off" thermocontrol of solute transport. I: temperature dependence of swelling of *N*-isopropylacrylamide networks modified with hydrophobic components in water. Pharm Res 1991;8:531-537.

144. Yoshida R, Sakai K, Okano T, Sakurai Y. Modulating the phase transition temperature and thermosensitivity in N-isopropylacrylamide copolymer gels. J Biomat Sci Polym Ed 1994;6:585-598.

145. Geever LM, Devine DM, Nugent MJD, Kennedy JE, Lyons JG, Higginbotham CL. The synthesis, characterisation, phase behaviour and swelling of temperature sensitive physically crosslinked poly(1-vinyl-2-pyrrolidinone)/poly(*N*-isopropylacrylamide) hydrogels. Eur Polym J 2006;42:69-80.

146. Dong L-C, Hoffman AS. Synthesis and application of thermally reversible heterogels for drug delivery. J Controlled Release 1990;13:21-31.

147. Liu L, Sheardown H. Glucose permeable poly(dimethyl siloxane) poly(*N*-isopropylacrylamide) interpenetrating networks as opthalmic biomaterials. Biomaterials 2005;26:233-244.

148. Erbil C, Kazancioglu E, Uyanik N. Synthesis, characterization and thermoreversible behaviours of poly(dimethyl siloxane)/poly(*N*-isopropyl acrylamide) semi-interpenetrating networks. Eur Polym J 2004;40:1145-1154.

149. Kurihara S, Minagoshi A, Nonaka T. Preparation of poly(*N*-isopropylacrylamide)-SiO_2 hybrid gels and their thermosensitive properties. J Appl Polym Sci 1996;62:153-156.

150. Zhang X-Z, Zhuo R-X. Synthesis and characterization of a novel thermosensitive gel with fast response. Colloid Polym Sci 1999;277:1079-1082.

151. Zhang X-Z, Zhuo R-X. Dynamic properties of temperature-sensitive poly(*N*-isopropylacrylamide) gel cross-linked though siloxane linkage. Langmuir 2001;17:12-16.

152. Imai Y, Yoshida N, Naka K, Chujo Y. Thermoresponsive organic-inorganic polymer hybrids from poly(*N*-isopropylacrylamide). Polym J 1999 31:258-262.

153. Loos W, Prez FD. The sol-gel approach towards thermo-responsive poly(*N*-isopropylacrylamide) hydrogels with improved mechanical properties. Macromol Symp 2004;210:483-491.

154. Soppimath KS, Aminabhavi TM, Kulkarni AR, Rudzinski WE. Biodegradable polymeric nanoparticles as drug delivery devices. J Controlled Release 2001;70:1-20.

155. Brigger I, Dubernet C, Couvreur P. Nanoparticles in cancer therapy and diagnosis. Adv Drug Deliv Rev 2002;54:631-651.

156. Tsuda Y, Kikuchi A, Yamato M, Nakao A, Sakurai Y, Umezu M, et al. The use of patterned dual thermoresponsive surfaces for the collective recovery as co-cultured cell sheets. Biomaterials 2005;26:1885-1893.

157. Hatakeyama H, Kikuchi A, Yamato M, Okano T. Patterned biofunctional designs of thermoresponsive surfaces for spatiotemporally controlled cell adhesion, growth, and thermally induced detachment. Biomaterials 2007;28:3632-3643.

158. Beebe DJ, Moore JS, Bauer JM, Yu Q, Liu RH, Devadoss C, et al. Functional hydrogel structures for autonomous flow control inside microfluidic channels. Nature 2000;404:568-590.

159. Harmon ME, Tang M, Frank CW. A microfluidic actuator based on thermoresponsive hydrogels. Polymer 2003;44:4545-4556.

160. Lin M, Chu F, Bourgeat-Lami E, Guyot A. Particle size in emmulsion polymerization of octamethyltetrasiloxane. J Dispersion Sci Tech 2004;25:827-835.

161. Zhang D, Jiang X, Yang C. Microemulsion polymerization of siloxane with nonionic surfactants as emulsifiers. J Appl Polym Sci 2003;89:3587-3593.

162. Abbas S, Li Z, Hassan H, Lodge TP. Thermoreversible morphology transitions of poly(styrene-*b*-dimethylsiloxane) diblock copolymer micelles in dilute solution. Macromolecules 2007;40:4048-4052.

163. Kato E, Kitada T, Nakamoto C. Anomalous compressibility of *N*-isopropylacrylamide gels near the volume phase transition temperature. Macromolecules 1993;26:1758-1760.

164. Palasis M, Gehrke SH. Permeability of responsive poly(*N*-isopropylacrylamide) gel to solutes. J Controlled Release 1992;18:1-12.

165. Park TG, Hoffman AS. Deswelling characteristics of poly(*N*-isopropylacrylamide) hydrogels. J Appl Polym Sci 1994;52:85-89.

166. Shibayama M, Morimoto M, Nomura S. Phase separation induced mechanical transition of poly(*N*-isopropylacrylamide)/water isochore gels. Macromolecules 1994;27:5060-5066.

167. Singh D, Knuckling D, Choudhary V, Adler H-J, Koul V. Synthesis and characterization of poly(*N*-isopropylacrylamide) films by photopolymerization. Polym Adv Technol 2006;17:186-192.

168. Liang L, Feng Z, Peurrung L, Viswanathan V. Temperature-sensitive membranes prepared by UV photopolymeriztion of *N*-isopropylacrylamide on surfaces of porous hydrophilic polypropylene membranes. J Membrane Sci 1999;162:235-246.

169. Fisher JP, Dean D, Engel PS, Mikos AG. Photoinitiated polymerization of biomaterials. Annu Rev Mater Res 2001;31:171-181.

170. Kubota H, Fukuda A. Photopolymerization synthesis of poly(*N*-isopropylacrylamide) hydrogels. J Appl Polym Sci 1997;65:1313-1318.

171. Takata S-i, Norisuye T, Shibayama M. Preparation temperature dependence and effects on hydrolysis on static inhomogeneities of poly(acrylamide) gels. Macromolecules 1999;32:3989-3993.

172. Yan Q, Hoffman AS. Synthesis of macroporous hydrogels with rapid swelling and deswelling properties for delivery of macromolecules. Polymer 1995;36:887-889.

173. Rathjen CM, Park C-H, Goodrich PR, Walgenbach DD. The effect of preparation temperature on some properties of a temperature-sensitive hydrogel. Polym Gels Networks 1995;3:101-115.

174. Sayil C, Okay O. The effect of preparation temperature on the swelling behavior of poly(*N*-isopropylacrylamide) gels. Polym Bull 2000;45:175-182.

175. Kayaman N, Kazan D, Erarslan A, Okay O, Baysal BM. Structure and protein separation efficiency of poly(*N*-isopropylacrylamide) gels: effect of synthesis conditions. J Appl Polym Sci 1998;67:805-814.

176. Ju S-J, Chu L-Y, Zhu Z-L, Hu L, Song H, Chen W-M. Effects of internal microstructures of poly(*N*-isopropylacrylamide) hydrogels on thermo-responsive volume phase-transition and controlled-release characteristics. Smart Mater Struct 2006;15:1767-1774.

177. Bekiari V, Lianos P. Photophysical behavior of terpyridine-lanthanide ion complexes incorporated in a poly(*N*,*N*-dimethylacrylamide) hydrogel. Langmuir 2006;22:8602-8606.

178. Shibayama M, Mizutani S-y, Nomura S. Thermal properties of copolymer gels containing *N*-isopropylacrylamide. Macromolecules 1996;29:2019-2024.

179. Feil H, Bae YH, Feijen J, Kim SW. Effect of comonomer hydrophilicity and ionization on the lower critical solution temperature of *N*-isopropylacrylamide copolymers. Macromolecules 1993;26:2496-2500.

180. Otake K, Inomata H, Konno M, Saito S. Thermal analysis of the volume phase transition with *N*-isopropylacrylamide gels. Macromolecules 1990;23:283-289.

181. Kaneko T, Asoh T-a, Akashi M. Ultrarapid molecular release from poly(*N*-isopropylacrylamide) hydrogels perforated using silica nanoparticle networks. Macromol Chem Phys 2005;206:566-574.

182. Bae YH, Okano T, Kim SW. Temperature dependence of swelling of crosslinked poly(*N*,*N*'-alkyl substituted acrylamides) in water. J Polym Sci Part B: Polym Phys 1990;28:923-936.

183. Jones DS. Dynamic mechanical analysis of polymeric systems of pharmaceutical and biomedical significance. Int J Pharm 1999;179:167-178.

184. Meyvis TKL, Stubbe BG, Stennbergen MJV, Hennink WE, Smedt SCD, Demeester J. A comparison between the use of dynamic mechanical analysis and oscillatory shear rheometry for the characterisation of hydrogels. Int J Pharm 2002;244:163-168.

185. Wicks ZW, Jones FN, Pappas SP, editors. Organic coatings science and technology. 2nd ed. New York: John Wiley & Sons, 1999.

186. Haraguchi K, Takehisa T. Nanocomposite hydrogels: a uniques organic-inorganic network strcture with extrordinary mechanical, optical, and swelling/de-swelling properties. Adv Mater 2002;14:1120-1124.

187. Liu W, Zhang B, Lu WW, Li Z, Zhu D, Yao KD, et al. A rapid temperture-responsive sol-gel reversible poly(*N*-isopropylacrylamide)-*g*-methylcellulose copolymer hydrogel. Biomaterials 2004;25:3005-3012.

188. Alarcon CdlH, Twaites B, Cunliffe D, Smith JR, Alexander C. Grafted thermo- and pH responsive copolymers: surface properties and bacterial adsorption. Int J Pharm 2005;295:77-91.

189. Tamirisa PA, Koskinen J, Hess DW. Plasma polymerized hydrogel thin films. Thin Solid Films 2006;515:2618-2624.

190. Mann BK, Tsai AT, Scott-Burden T, West JL. Modification of surfaces with cell adhesion peptides alters extracellular matrix deposition. Biomaterials 1999;20:2281-2286.

191. Mann BK, Tsai AT, Scott-Burden T, West JL. Modification of surfaces with cell adhesion pepetides alters extracellular matrix deposition. Biomaterials 1999;20:2281-2286.

APPENDIX A

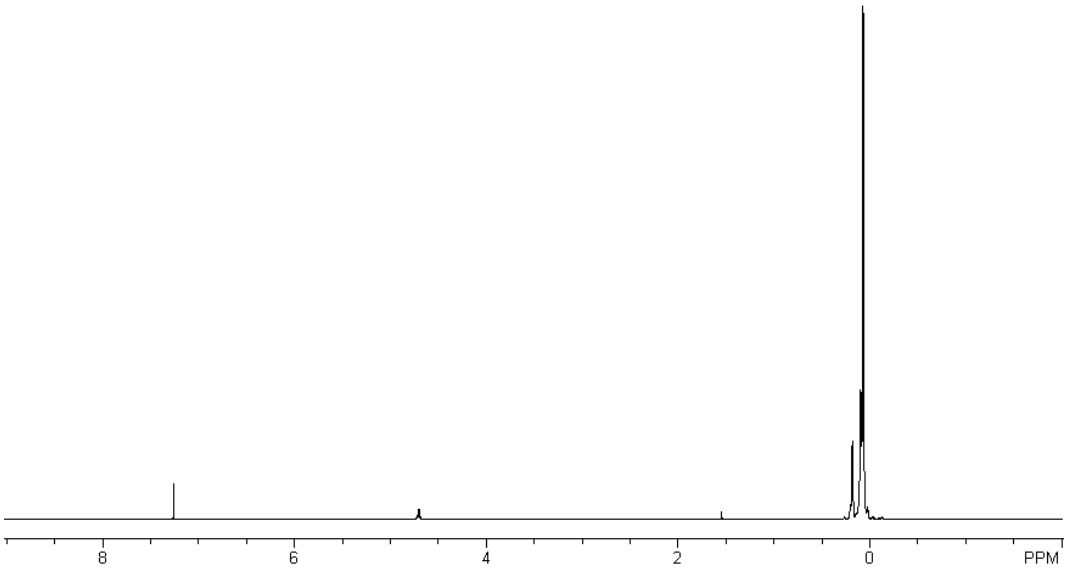

^{1}H NMR of PDMS$_{star}$-Si-H (**a**).

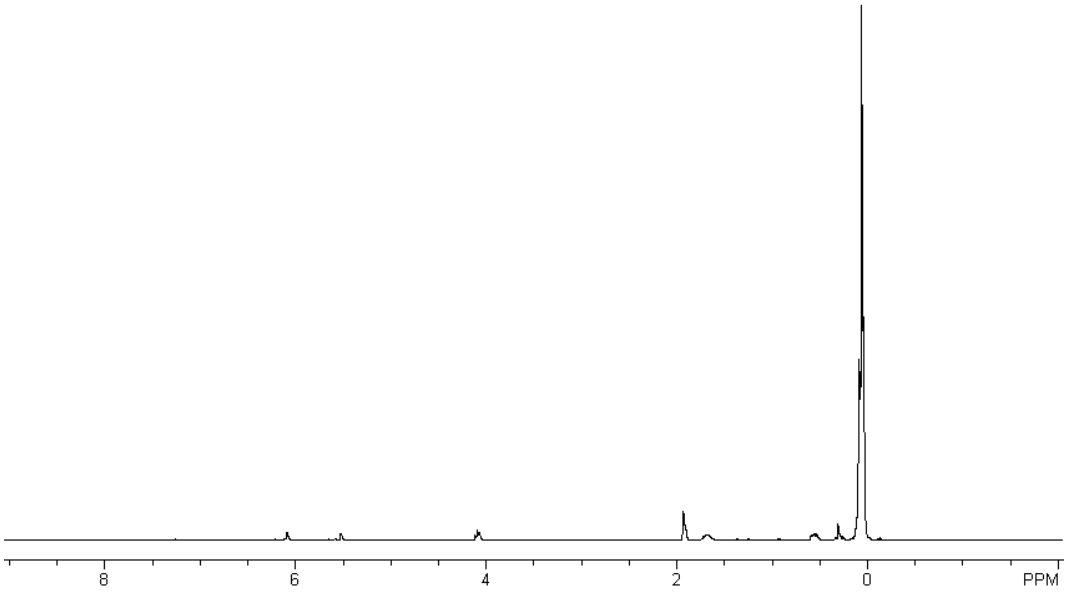

^{1}H NMR of PDMS$_{star}$-MA (**A**).

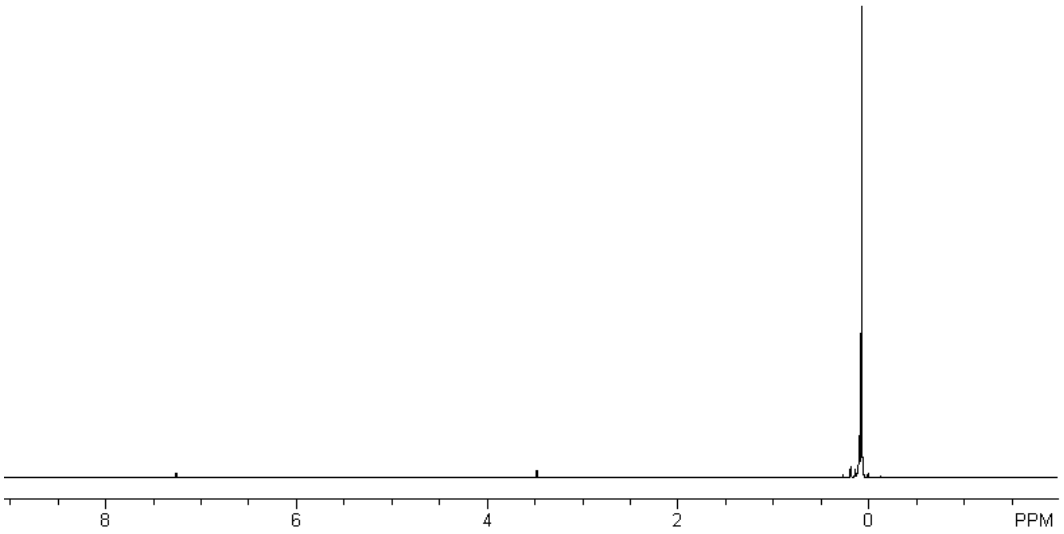

^{1}H NMR of PDMS$_{star}$-Si-H (**b**).

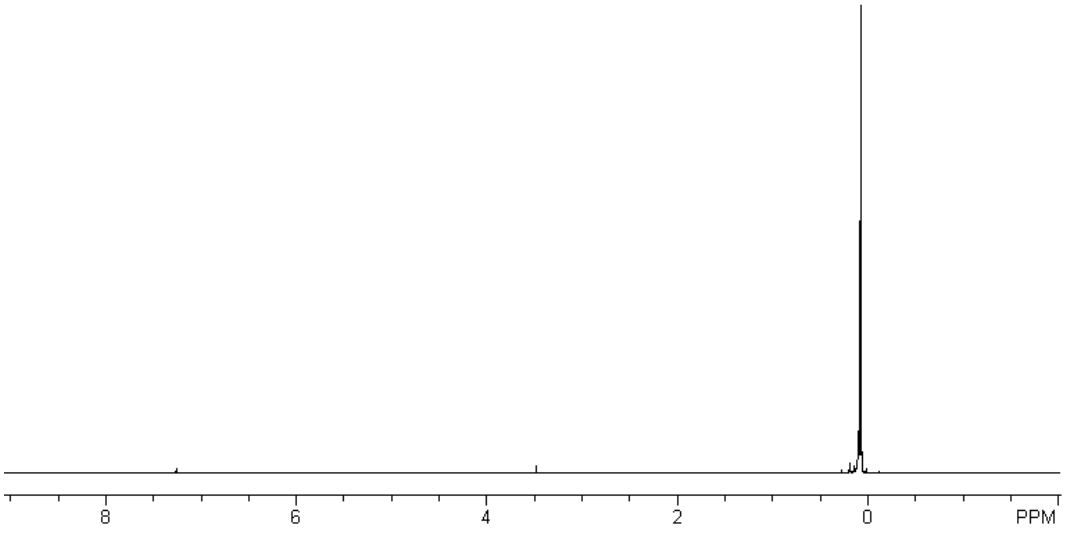

^{1}H NMR of PDMS$_{star}$-MA (**B**).

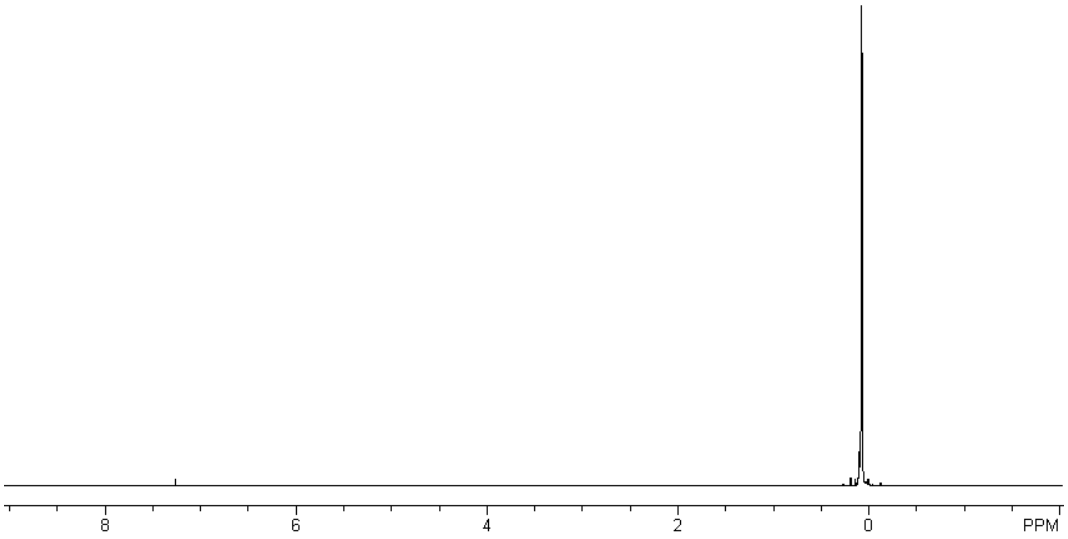

^{1}H NMR of PDMS$_{star}$-Si-H (**c**).

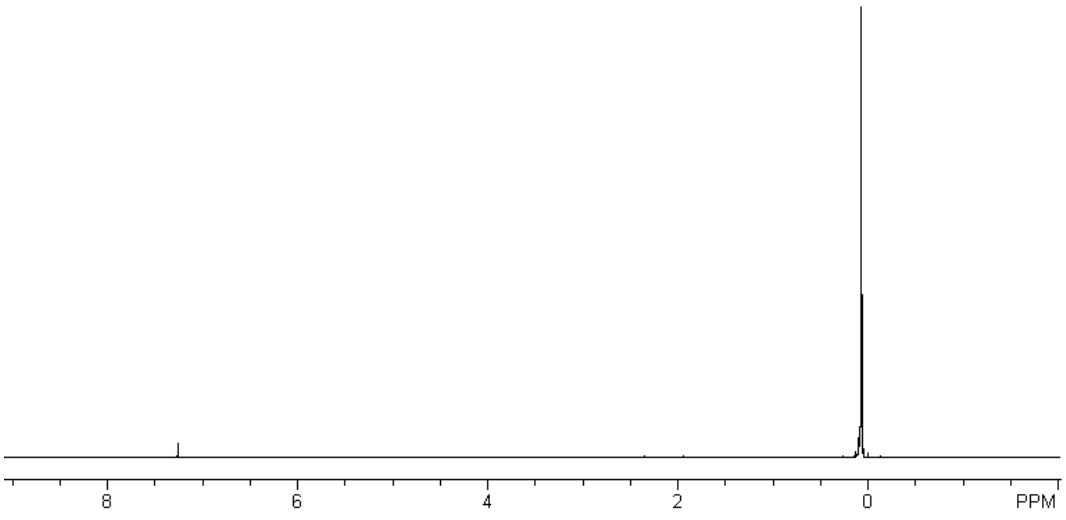

^{1}H NMR of PDMS$_{star}$-MA (**C**).

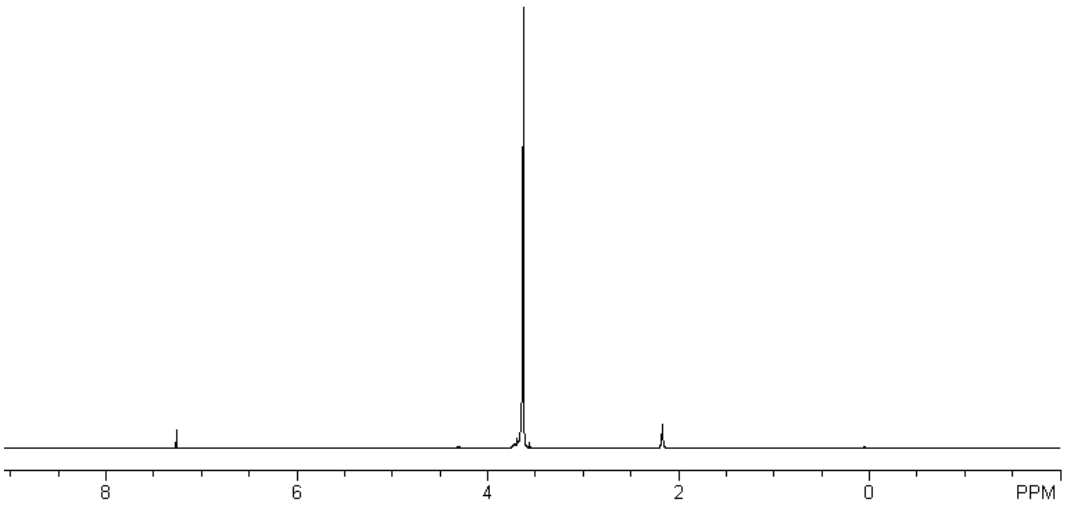

^{1}H NMR of PEG-DA (**L**).

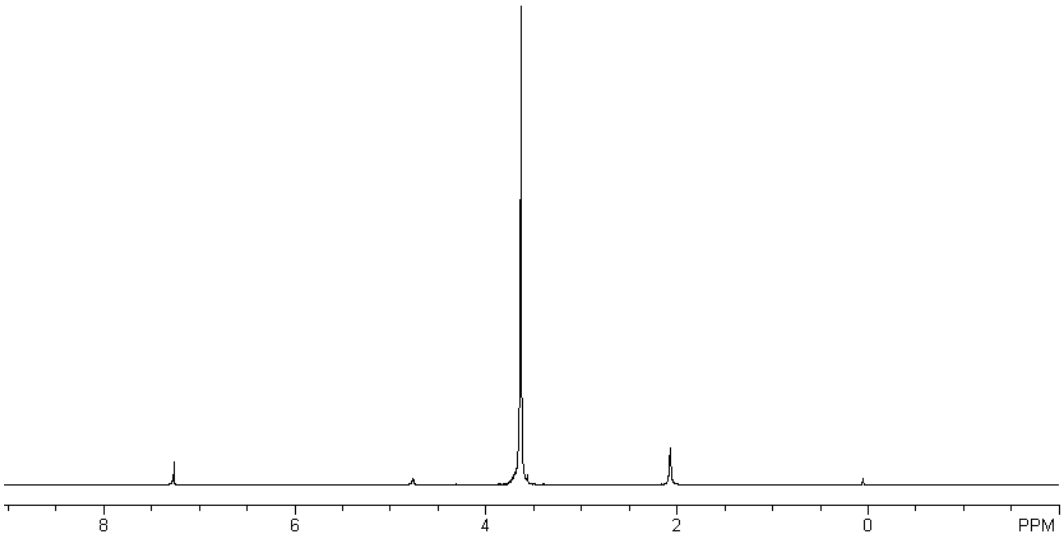

^{1}H NMR of PEG-DA (**H**).

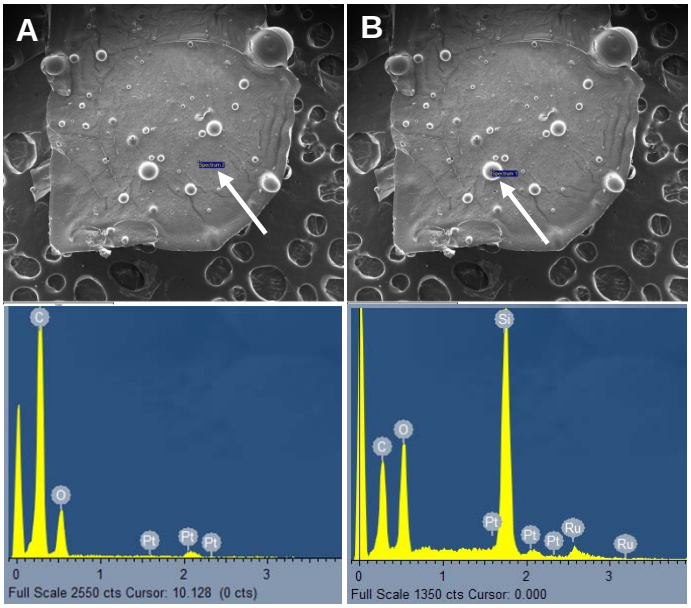

SEM images and corresponding EDS spectra of $C_{20}H_{80}$ **(A)** bulk matrix **(B)** a microparticle. The presence of Si in the microparticle and not the surrounding area indicates that they are Si-enriched and formed from $PDMS_{star}$-MA.

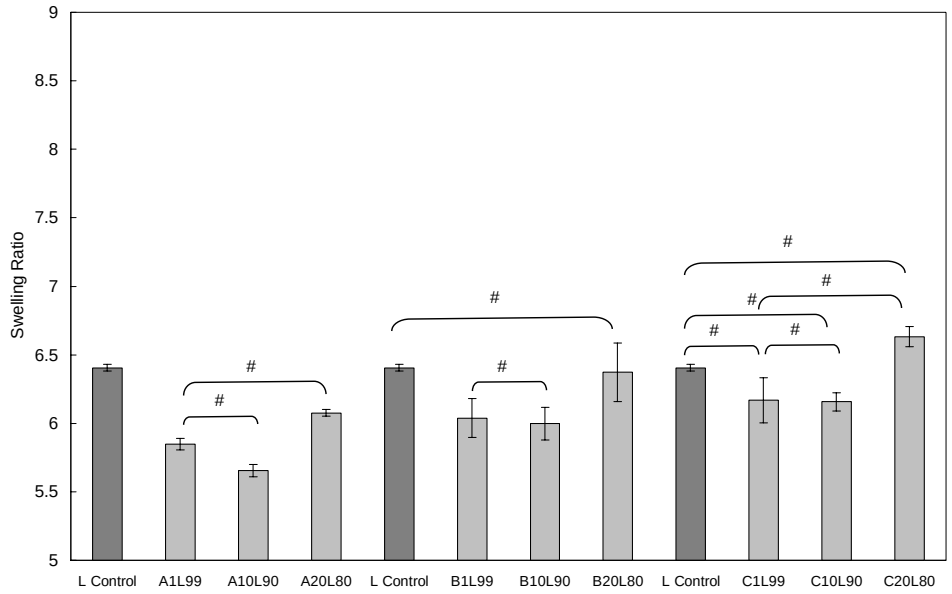

Swelling ratio of **L** series hydrogel at 37 ºC. Statistical significance within a given series (i.e. A, B and C) was determined by one-way analysis of variance (Holm-Sidak method where $p = 0.05$. (#) indicates $p > 0.05$.).

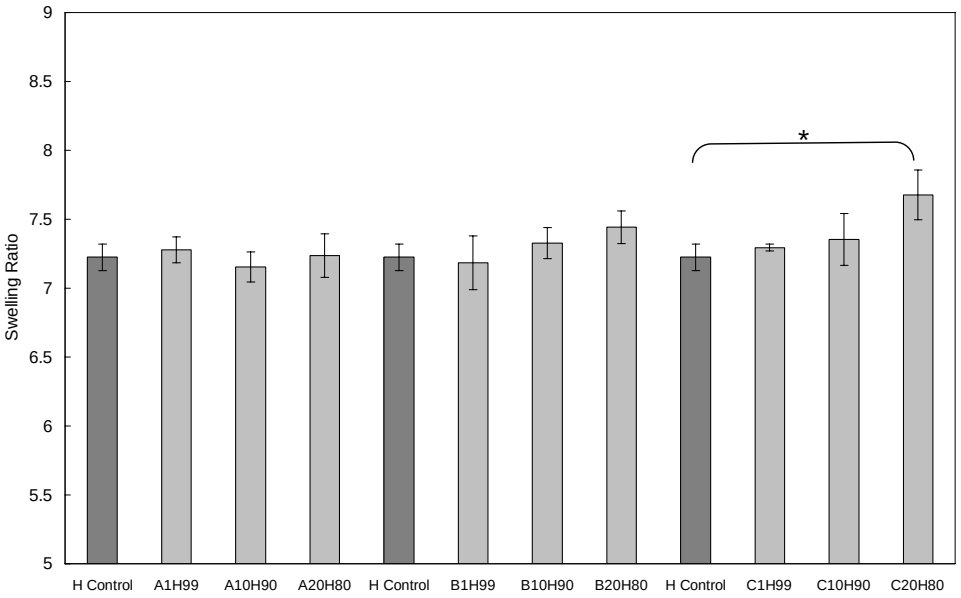

Swelling ratio of **H** series hydrogel at 37 ºC. Statistical significance within a given series (i.e. A, B and C) was determined by one-way analysis of variance (Holm-Sidak method where $p = 0.05$. (*) indicates $p < 0.05$). Remaining compositions are all statistically similar.

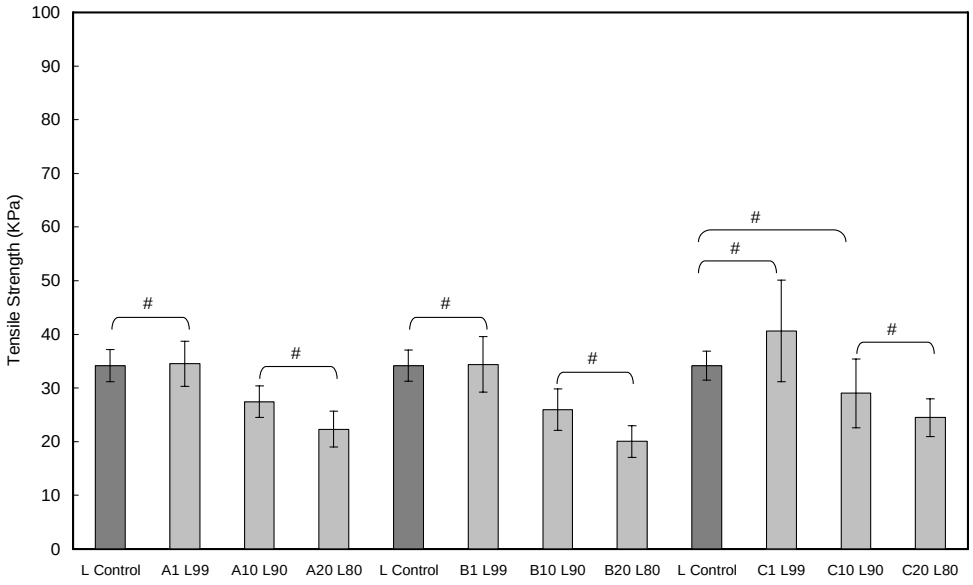

Tensile strength of **L** series hydrogels. Statistical significance within a given series (i.e. A, B and C) was determined by one-way analysis of variance (Holm-Sidak method where p = 0.05. (#) indicates p>0.05).

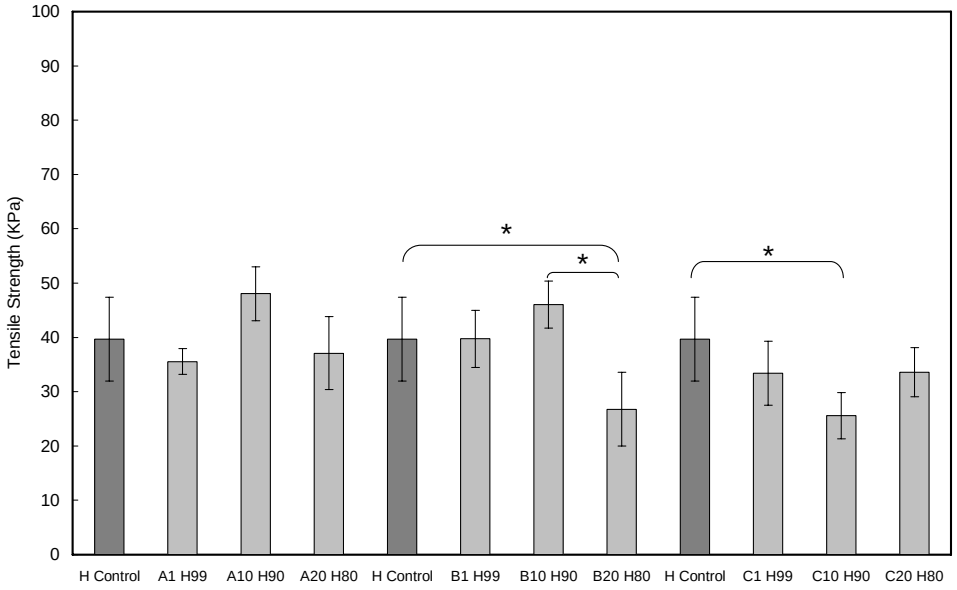

Tensile strength of **H** series hydrogels. Statistical significance within a given series (i.e. A, B and C) was determined by one-way analysis of variance (Holm-Sidak method where p = 0.05. (*) indicates p<0.05).

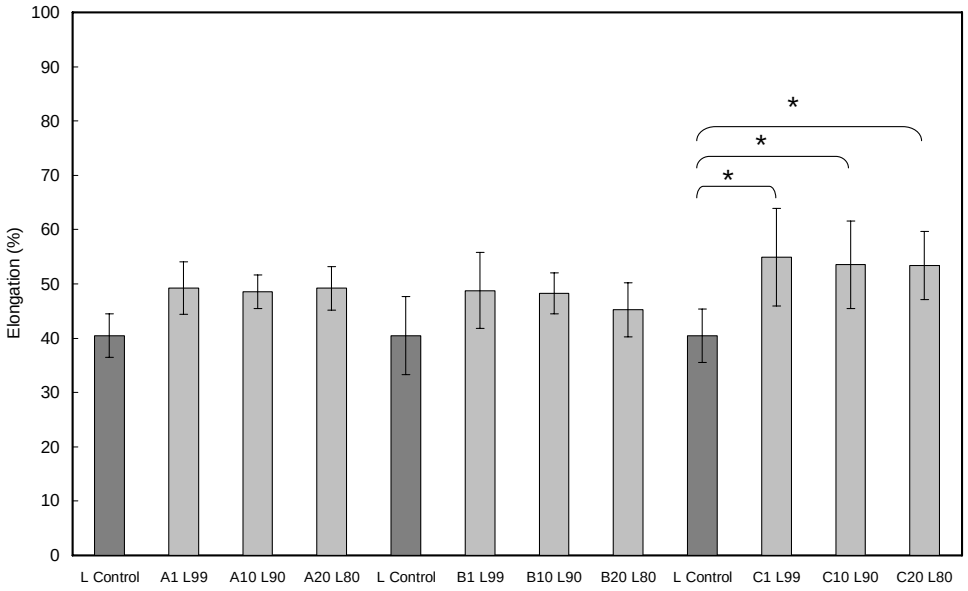

Elongation% of **L** series hydrogels. Statistical significance within a given series (i.e. A, B and C) was determined by one-way analysis of variance (Holm-Sidak method where p = 0.05. (*) indicates $p < 0.05$).

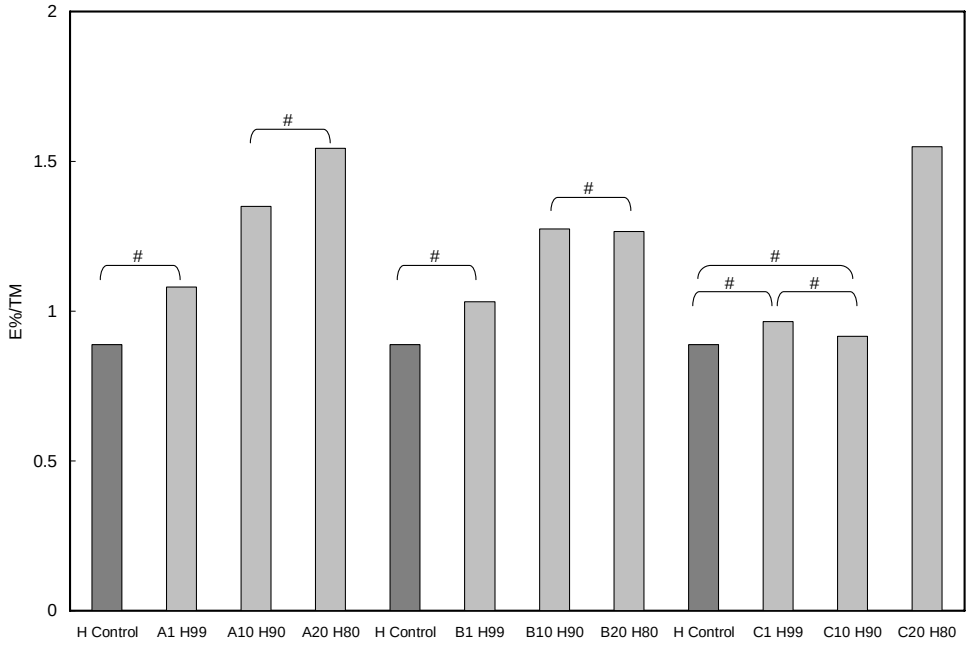

Elongation% of **H** series hydrogels. Statistical significance within a given series (i.e. A, B and C) was determined by one-way analysis of variance (Holm-Sidak method where p = 0.05. (*) indicates $p<0.05$).

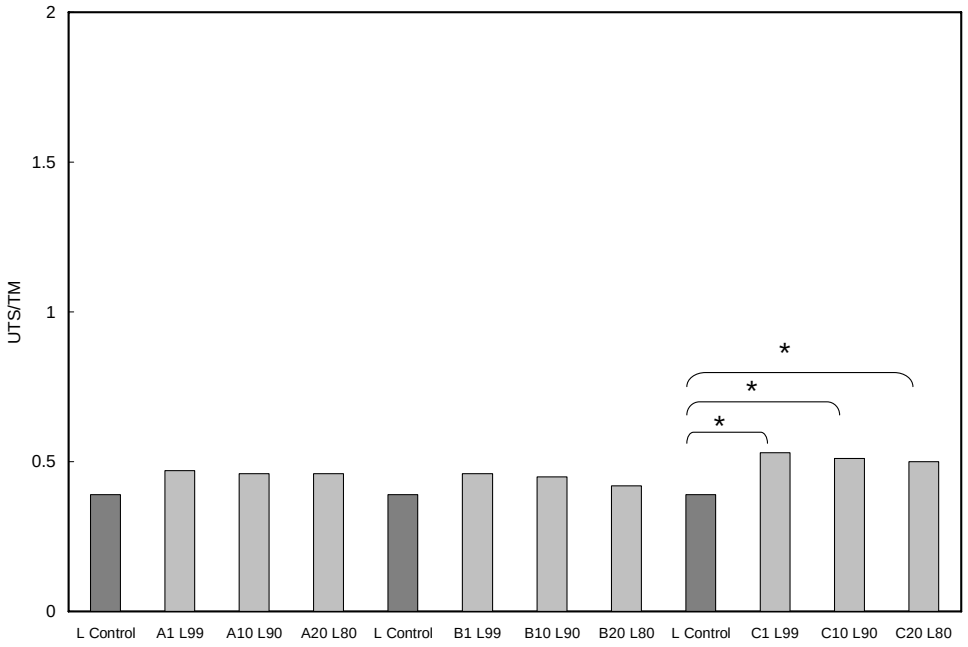

UTS/TM of **L** series hydrogels. Statistical significance within a given series (i.e. A, B and C) was determined by one-way analysis of variance (Holm-Sidak method where p = 0.05. (*) indicates $p < 0.05$).

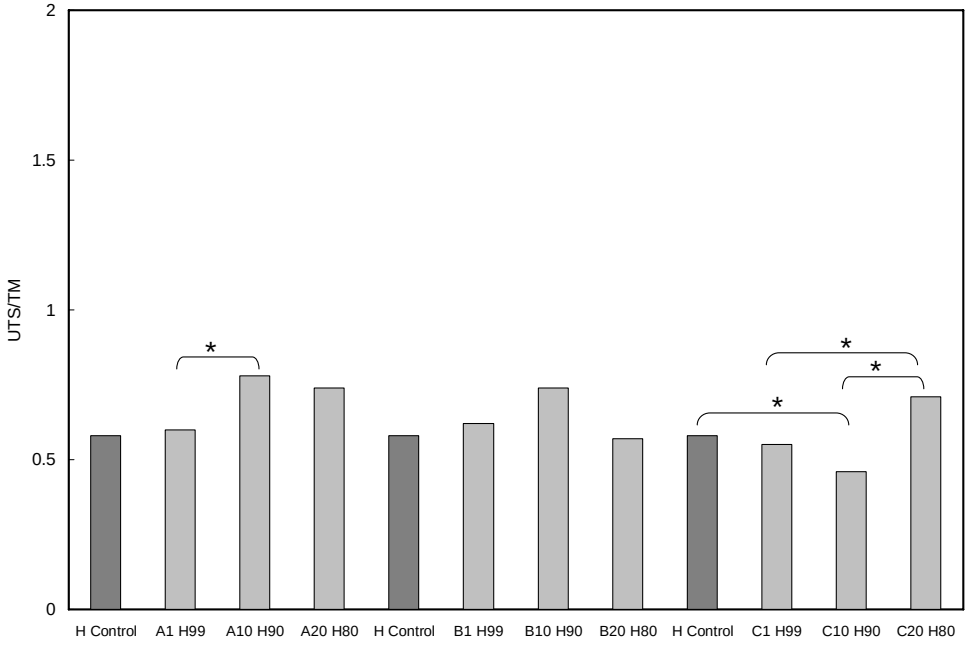

UTS/TM of **H** series hydrogels. Statistical significance within a given series (i.e. A, B and C) was determined by one-way analysis of variance (Holm-Sidak method where p = 0.05. (*) indicates $p < 0.05$).

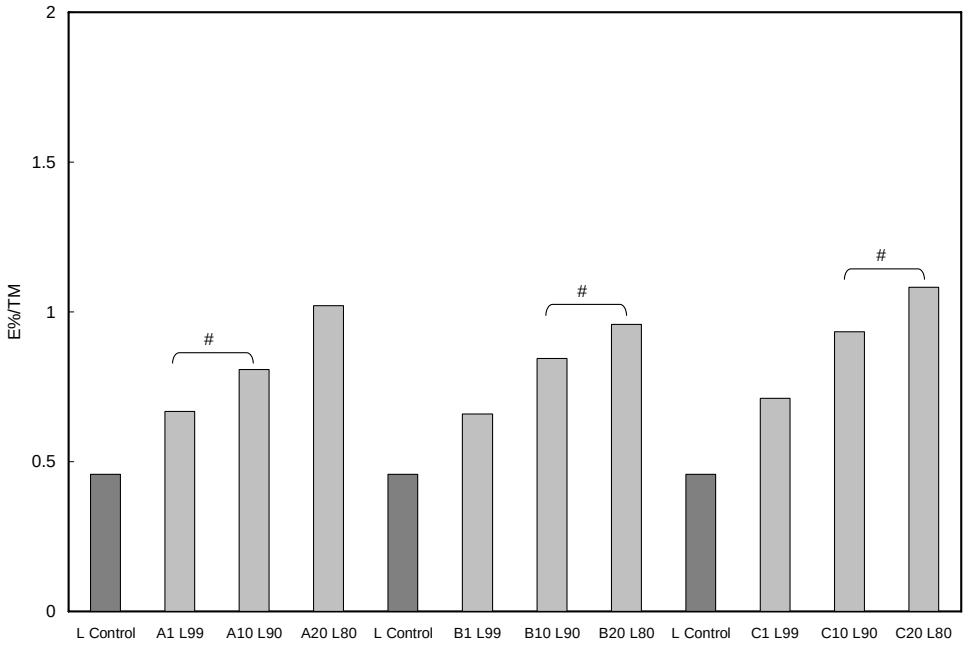

E%/TM of **L** series hydrogels. Statistical significance within a given series (i.e. A, B and C) was determined by one-way analysis of variance (Holm-Sidak method where p = 0.05. (#) indicates p > 0.05).

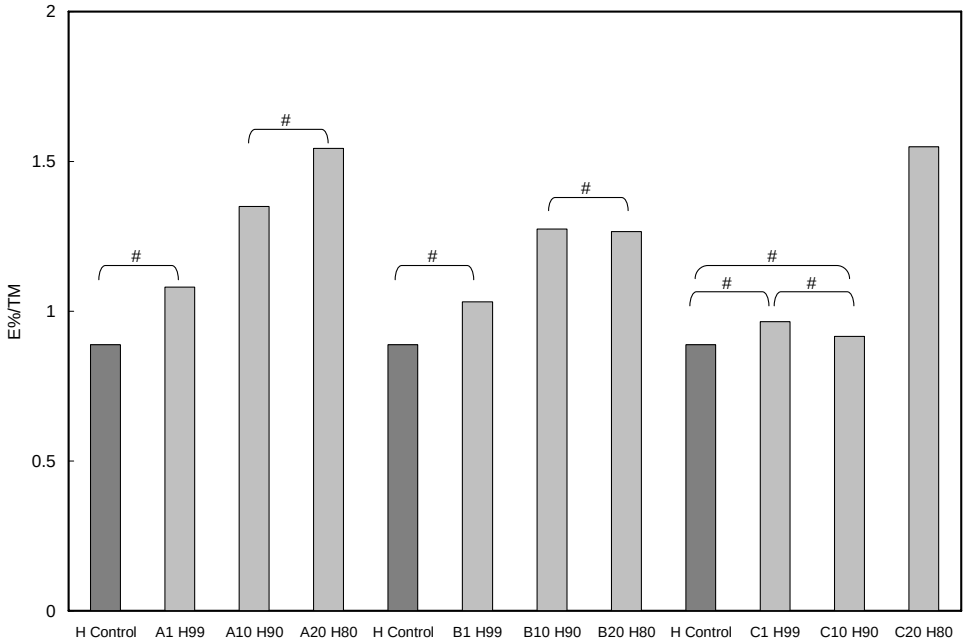

E%/TM of **H** series hydrogels. Statistical significance within a given series (i.e. A, B and C) was determined by one-way analysis of variance (Holm-Sidak method where p = 0.05. (#) indicates p > 0.05).

APPENDIX B

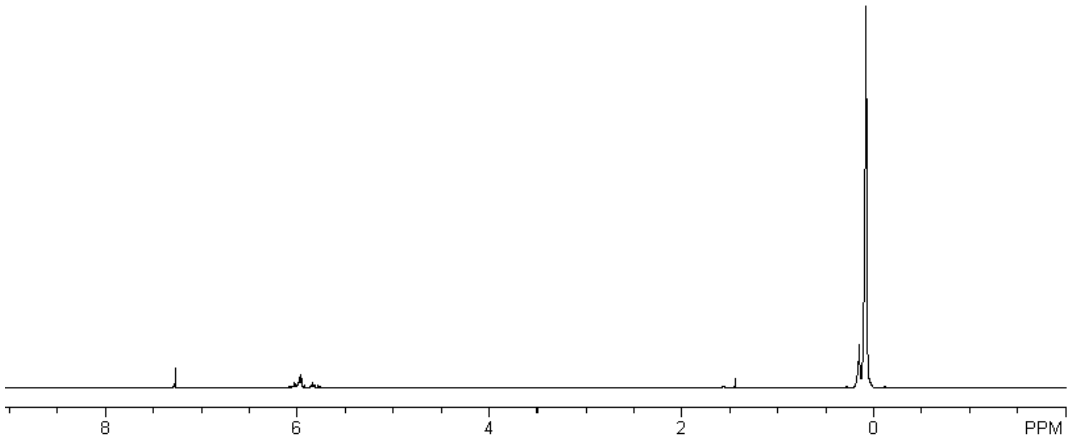

^{1}H NMR of polysiloxane nanoparticles (~ 220 nm ave. diameter).

APPENDIX C

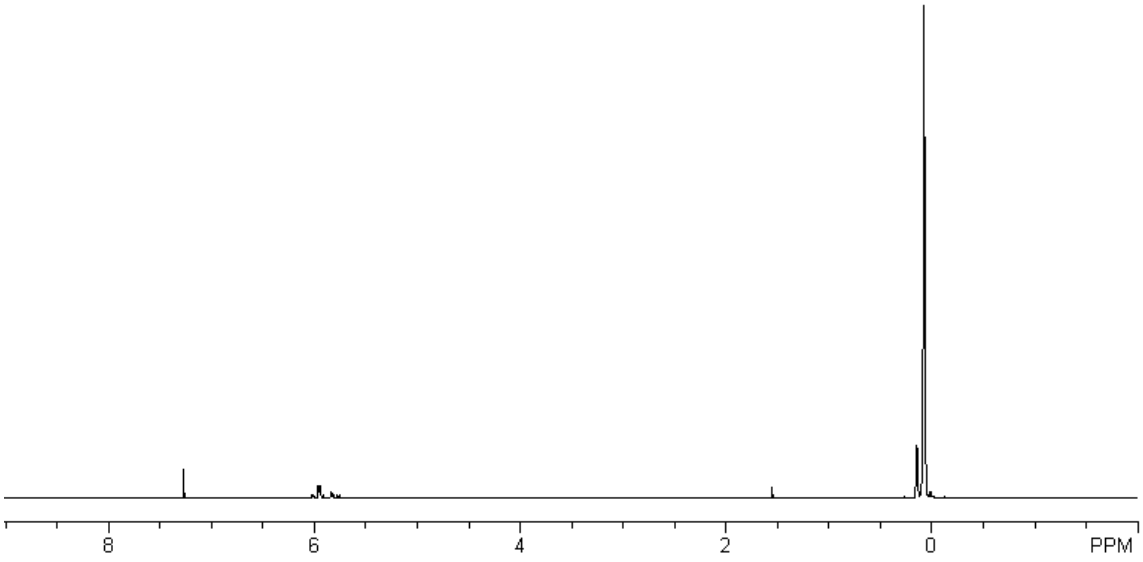

^{1}H NMR of polysiloxane nanoparticles (~ 54 nm ave. diameter).

VITA

Yaping Hou received her Bachelor of Engineering degree in materials science and engineering from Beijing University of Aeronautics and Astronautics, Beijing, China in 2001. She entered the Materials Science and Engineering program at Texas A&M University, College Station, TX in 2005 and received her Doctor of Philosophy degree in December 2009. Her research interests include design of thermoresposive PDMS/PNIPAAm nanocomposite hydrogels with cell-releasing behavior and design of PDMSstar-PEO hydrogels as tissue engineering scaffolds with tunable properties. Her expertise is in: (1) Differential Scanning Calorimetry (DSC), (2) Dynamic Mechnical Analysis (DMA), (3) Thermal Gravity Analysis (TGA), (4) Scanning Electron Microscopy (SEM), (5) Environmental Scanning Electron Microscopy (ESEM), (6) Transmission Electron Microscopy (TEM), (7) Cryo-Transmission Electron Microscopy (Cryo-TEM), (8) Confocal Laser Scanning Microscopy (CLSM), (9) Dynamic light scattering (DLS), (10) Fourier-Transform Infrared Spectroscopy (FTIR), (11) Gel Permeation Chromatography (GPC) and (12) Goniometer.

Yaping Hou may be reached by contacting Prof. Melissa A. Grunlan at the Biomedical Engineering Department, Texas A&M University, College Station, TX 77840-3120. Her email is: yaping.hou@tamu.edu.